



**Politecnico  
di Torino**

**Politecnico di Torino**

Corso di Laurea Magistrale in  
Ingegneria Energetica e Nucleare  
A.a. 2020/2021  
Sessione di Laurea Ottobre 2021

# **Analysis of a LOFA in EU DEMO Breeding Blanket**

Relatore:

Dr. Antonio Froio

Candidato:

Fabrizio Lisanti



# Abstract

In the next decades, in order to address climate change, the electricity generation sector needs to definitely abandon fossil fuels and rely on sustainable and carbon-free energy sources. In view of this, fusion energy represents, in the long-term, a clean and predictable energy source, useful to handle and balance the well-known intermittency of the wind and solar electricity production. In the framework of the European roadmap for the realization of fusion energy, a key step is the realization of the EU DEMO fusion reactor, the first fusion device to produce electricity and to exploit a closed-fuel cycle, demonstrating tritium self-sufficiency.

To produce the tritium fuel needed for the fusion reactions, DEMO will be the first fusion reactor to have a Breeding Blanket (BB); the BB, in fact, contains lithium-based materials (called *breeding materials*) which, interacting with the neutron flux coming from the plasma, produce the tritium needed to sustain the fusion reactions. Among the concepts proposed during the years for the EU DEMO BB, one of the most promising ones is the Helium Cooled Pebble Bed (HCPB). This concept involves the use of gaseous helium at 80 bars as a coolant, ceramic pebbles made by a mixture of  $\text{Li}_4\text{SiO}_4$  and  $\text{Li}_2\text{TiO}_3$  as breeding material, beryllium ceramic pebbles as Neutron Multiplying Material (NMM), and the EUROFER97 low-activation stainless steel as structural material. Since the BB is directly exposed to the heat load coming from the plasma, its cooling is of huge importance to avoid excessive overheating of the solid structures which can lead to structural failure; moreover, the cooling scheme must be optimized to maximize the heat removal and, hence, deliver more heat to the Power Conversion System (PCS).

The thermal-hydraulic design of the BB concepts must be studied under both operational and accidental conditions. Being the design of EU DEMO reactor at a pre-conceptual stage, preliminary studies using numerical tools are needed to give useful feedbacks for future detailed studies and experiments. In this work a model of the of the Primary Heat Transfer System (PHTS) of the HCPB BB is developed, starting from the already existing GETTHEM code developed at Politecnico di Torino, to perform parametric analyses regarding the accidental scenario of a Loss of Flow Accident (LOFA). The model, written with the Modelica modelling language, aims to be a system-level, fast-running tool useful to simulate the global thermal-hydraulic behavior of the HCPB BB under the above-mentioned accidental scenario, with a particular focus on the temperatures reached inside the solid structures of the First Wall (FW), as it is the region directly exposed to the plasma. Three different initiating events are considered for the onset of a LOFA: (i) the complete loss of the circulating power of the cooling loop, which leads to the most severe scenario, (ii) the failure of one of the two circulators feeding the cooling loop, and (iii) the obstruction of a single FW channel. Moreover, each scenario has been tested with and without the intervention of the emergency plasma shutdown system, which, if activated soon enough, has shown that it can effectively mitigate the consequences of the accident.

# Contents

List of figures .....	4
Nomenclature .....	8
1. Introduction .....	11
1.1. The EU DEMO plant.....	11
1.1.2. EU DEMO tokamak functioning principle and components.....	12
1.2. Aim of the work .....	17
2. EU DEMO Helium-Cooled Pebble Bed Breeding Blanket and PHTS system.....	18
2.1. HCPB design description .....	18
2.1.1. Enhanced HCPB general architecture.....	19
2.2. The HCPB cooling scheme and Primary Heat Transfer System .....	22
2.2.1. The HCPB BB cooling scheme .....	22
2.2.2. HCPB Primary Heat Transfer System architecture .....	24
3. Computational tools and overview of the model .....	26
3.1. Modeling environment .....	26
3.1.1. The Modelica language.....	26
3.2. Description of the GETTHEM code for the HCPB PHTS .....	28
3.2.1 Introduction to the GETTHEM code .....	28
3.2.2. GETTHEM code assumptions.....	30
3.2.3. GETTHEM code equations .....	31
3.2.4. GETTHEM model components.....	33
3.3. Description of the model used for this thesis work .....	39
4. Simulation scenarios and results .....	42
4.1. Introduction.....	42
4.1.1. Input data .....	43
4.2. LOFA scenarios .....	46
4.2.1. Normal operating conditions .....	47
4.2.2. Total LOFA .....	53
4.2.2.1. Case I: no intervention of the mitigation system .....	53

4.2.2.2. Case II: intervention of the mitigation system .....	57
4.2.3. Partial LOFA: failure of one circulator.....	61
4.2.3.1. Case I: no intervention of the mitigation system .....	61
4.2.3.2. Case II: intervention of the mitigation system .....	64
4.2.4. Obstruction of a FW channel.....	67
4.2.4.1. Case I: no intervention of the mitigation system .....	68
4.2.4.2. Case II: intervention of the mitigation system .....	71
5. Conclusions .....	74
References .....	77

# List of figures

Figure 1.1: EU DEMO design stages [1].....	11
Figure 1.2: General layout of EU DEMO tokamak. Main components and their operating temperatures are highlighted. [32] .....	13
Figure 1.3: View of the superconducting magnets system and the resulting helical path of charged particles inside the plasma.[9].....	14
Figure 2.1: HCPB design stages during DEMO pre-conceptual design and advantages and drawbacks of each design w.r.t. the starting design [13].....	18
Figure 2.2: HCPB-BL2017 BB system. Left: view of all the toroidally arranged sectors; right: detailed view of a single sector and its segments [15].....	19
Figure 2.3: HCPB-BL2017 detail view. a) 3D view of the COB11 BZ region, b) poloidal-toroidal cross section of the fuel-breeder pin, c) radial poloidal view of the pin [15] .....	20
Figure 2.4: Radial-toroidal cross section of the HCPB segment [15] .....	21
Figure 2.5: Simplified view of the DEMO BoP layout [5] .....	22
Figure 2.6: HCPB blanket cooling [15].....	23
Figure 2.7: Schematic flow path of the HCPB [15].....	23
Figure 2.8: View of the BB PHTS layout (case II) [16].....	25
Figure 3.1 Examples of several object diagrams on Modelica. [19] .....	27
Figure 3.2: Sketch of the model for the WCLL loop (FW: First Wall object; BZ: Breeding Zone object; IM: Inlet Manifold; OM: Outlet Manifold; ID: Inlet Distributor; MIX: Mixer; HX/SG: Heat eXchanger/Steam Generator) [24].....	29
Figure 3.3: Cross-sectional view of a CP. The division of solid wall objects between adjacent channels is highlighted [29].....	33
Figure 3.4: BM object for the HCPB-I cooling scheme (adapted from [23]). .....	34
Figure 3.5: BM object for the HCPB-S cooling scheme: a) BZ and caps cooling loops; b) FW cooling loop, with ex-vessel components (heat exchanger and circulator) [23].....	34
Figure 3.6: schematic view of a FW channel object; the orange rectangles are the connectors for thermal coupling with neighboring channels, and blue circles are the heat loads input connectors.[23].....	35
Figure 3.7: FW solid object: interface between neighboring channels; heat transfer mechanisms between solid- solid and solid-fluid are highlighted. [22] .....	36

Figure 3.8: View of the GETTHEM HCPB cooling model. The blue and red arrows highlight the counter-current flow path between the twin circuits at the BM level (adapted from [23]). .....	38
Figure 3.9: Sketch of the Dymola diagram view of the HCPB cooling loop model; IFP/OFP: Inner/Outer Fuel Pin; HX: Heat eXchanger; MVI/MVO: Inlet/Outlet Mixing Volume; MI/MO: Inlet/Outlet Manifold; A/B: branches A and B. ....	40
Figure 4.1: Heat load pulsed profile (1 period) applied to the FW object solid walls. [23].....	46
Figure 4.2: Helium mass flow rate time evolution in the front part of each FW channel; Normal Operating Conditions (NOC).....	47
Figure 4.3: Helium temperature distribution along the FW channel length at time $t=350$ s (in NOC); the squares represent the values computed in each fluid node; Inlet/Front/Outlet sides are separated by dashed red lines. ....	48
Figure 4.4: EUROFER97 temperature distribution along the FW channel length at time $t=350$ s (in NOC); squares represent the value computed in each solid volume; Inlet/Front/Outlet sides are separated by dashed red lines. ....	49
Figure 4.5: Temperature evolution in time (9600 s period) of the helium in the 5 <sup>th</sup> node of the front part (NOC).....	50
Figure 4.6: Temperature evolution in time (9600 s period) of EUROFER97 in the 3 <sup>rd</sup> volume of the front part (NOC). ....	51
Figure 4.7: Channel 1 helium temperature evolution; each curve represents a different fluid node of the front part (NOC). ....	52
Figure 4.8: Channel 1 EUROFER temperature evolution; each curve represents a different FV of the front part (NOC). ....	52
Figure 4.9: Helium mass flow rate time evolution in the front part of each FW channel; case of a total LOFA without plasma shutdown. ....	54
Figure 4.10: Helium temperature evolution in a FW channel; each curve represents a different fluid node of the front part; case of a total LOFA without plasma shutdown.....	54
Figure 4.11: EUROFER temperature evolution in a FW channel; each curve represents a different fluid node of the front part; case of a total LOFA without plasma shutdown. ....	55
Figure 4.12: Helium temperature distribution along the FW channel length at time $t=2461$ s; the squares represent the values computed in each fluid node; case of a total LOFA without plasma shutdown. ....	56
Figure 4.13: EUROFER temperature distribution along the FW channel length at time $t=2236$ s; squares represent the value computed in each solid volume; case of a total LOFA without plasma shutdown. ....	56

Figure 4.14: Helium mass flow rate time evolution in a FW channel.: three hypotheses on the mitigation system intervention; case of a total LOFA with plasma shutdown; in the blue box: magnified view of the curves around 2120 s.....	57
Figure 4.15: Helium temperature time evolution in the 5th node of the FW channel front part: three hypotheses on the mitigation system intervention; case of a total LOFA with plasma shutdown; a) view of the whole period, b) post-accident detail (1980 s – 4000 s).....	59
Figure 4.16: EUROFER97 temperature time evolution in the 3rd node of the FW channel front part: three hypotheses on the mitigation system intervention; case of a total LOFA with plasma shutdown; a) view of the whole period, b) post-accident detail (1980 s – 4000 s).....	60
Figure 4.17: EUROFER temperature distribution along the FW channel length at time $t=2060$ s; squares represent the value computed in each solid volume; case of a total LOFA with plasma shutdown after 60 s from the accident. ....	60
Figure 4.18: Helium mass flow rate time evolution in the front part of each FW channel; case of a partial LOFA without plasma shutdown. ....	62
Figure 4.19: Helium temperature evolution in a FW channel; each curve represents a different fluid node of the front part; case of a partial LOFA without plasma shutdown. ....	63
Figure 4.20: EUROFER temperature evolution in a FW channel; each curve represents a different fluid node of the front part; case of a partial LOFA without plasma shutdown.....	63
Figure 4.21: EUROFER temperature distribution along the FW channel length at time $t=2851$ s; squares represent the value computed in each solid volume; case of a partial LOFA without plasma shutdown.....	64
Figure 4.22: EUROFER97 temperature time evolution in the 3rd node of the FW channel front part: three hypotheses on the mitigation system intervention; case of a partial LOFA with plasma shutdown; a) view of the whole period, b) post-accident detail (1980 s – 2200 s). ....	65
Figure 4.23: EUROFER temperature distribution along the FW channel length at time $t=2060$ s; squares represent the value computed in each solid volume; case of a partial LOFA with plasma shutdown after 60 s. ....	66
Figure 4.24: Helium mass flow rate time evolution in the front part of each FW channel; case of a channel obstruction without plasma shutdown.....	68
Figure 4.25: Temperature evolution in time of helium in the 5th node of the FW front channel part; case of a channel obstruction without plasma shutdown; in the blue box: magnified view of the channel 4 curve around 2000 s. ....	69
Figure 4.26: Temperature evolution in time of EUROFER97 in the 3rd solid volume of the FW front channel part; case of a channel obstruction without plasma shutdown.....	69

Figure 4.27: Helium temperature evolution in a non-obstructed FW channel; each curve represents a different fluid node of the front part; case of a channel obstruction without plasma shutdown..... 70

Figure 4.28: EUROFER temperature distribution along channel 1 (blue line) and the obstructed channel (red line); squares represent the value computed in each solid volume; case of a channel obstruction without plasma shutdown. .... 71

Figure 4.29: EUROFER97 temperature time evolution in the 3rd node of the obstructed channel front part: three hypotheses on the mitigation system intervention; case of a channel obstruction with plasma shutdown; a) view of the whole period, b) post-accident detail (1980 s – 2200 s)..... 72

Figure 4.30: EUROFER temperature distribution along channel 1 (blue line) and the obstructed channel (red line); squares represent the value computed in each solid volume; case of a channel obstruction with plasma shutdown after 60 s..... 73

# Nomenclature

<b>EU DEMO</b>	European Demonstration Power Plant
<b>ITER</b>	International Thermonuclear Experimental Reactor
<b>FPP</b>	Fusion Power Plant
<b>BoP</b>	Balance of Plant
<b>PCS</b>	Power Conversion System
<b>ESS</b>	Energy Storage System
<b>IHTS</b>	Intermediate Heat Transfer System
<b>PHTS</b>	Primary Heat Transfer System
<b>BB</b>	Breeding Blanket
<b>TFC</b>	Toroidal Field Coils
<b>CS</b>	Central Solenoid
<b>PFC</b>	Poloidal Field Coils
<b>VV</b>	Vacuum Vessel
<b>DTT</b>	Divertor Tokamak Test
<b>BZ</b>	Breeding Zone
<b>BM</b>	Breeding Module
<b>TBR</b>	Tritium Breeding Ratio
<b>NMM</b>	Neutron Multiplying Material
<b>HCPB</b>	Helium-Cooled Pebble Bed
<b>HCLL</b>	Helium-Cooled Lithium-Lead
<b>WCLL</b>	Water-Cooled Lithium-Lead
<b>DCLL</b>	Dual Cooled Lithium-Lead
<b>GETTHEM</b>	General Tokamak THERmal-hydraulic Model
<b>LOFA</b>	Loss Of Flow Accident
<b>FW</b>	First Wall
<b>PCD</b>	Pre-Conceptual Design
<b>CB</b>	Ceramic Breeder
<b>SMS</b>	Single Module Segment

<b>MMS</b>	Multi Module Segment
<b>OB</b>	OutBoard
<b>IB</b>	InBoard
<b>BSS</b>	Back Supporting Structure
<b>IHX</b>	Intermediate Heat eXchanger
<b>DBTT</b>	Ductile-to-Brittle Transition Temperature
<b>LOCA</b>	Loss Of Coolant Accident
<b>MSL</b>	Modelica Standard Library
<b>OMSC</b>	Open Source Modelica Consortium
<b>CFD</b>	Computational Fluid Dynamics
<b>FV</b>	Finite Volumes
<b>SG</b>	Steam Generator
<b>CP</b>	Cooling Plate
<b>HTC</b>	Heat Transfer Coefficient
<b>NOC</b>	Normal Operating Conditions



# Chapter 1

## 1. Introduction

### 1.1. The EU DEMO plant

The development of the European Demonstration Fusion Power Plant (DEMO) is one of the main goals of EUROfusion, the European Consortium for the development of fusion energy [1]. It lies between ITER, the world's largest fusion experiment which is currently under construction, and the first commercial fusion power plant, with the aim of generating several hundreds of MW of net electricity and operating with a closed tritium fuel-cycle by the middle of the century.

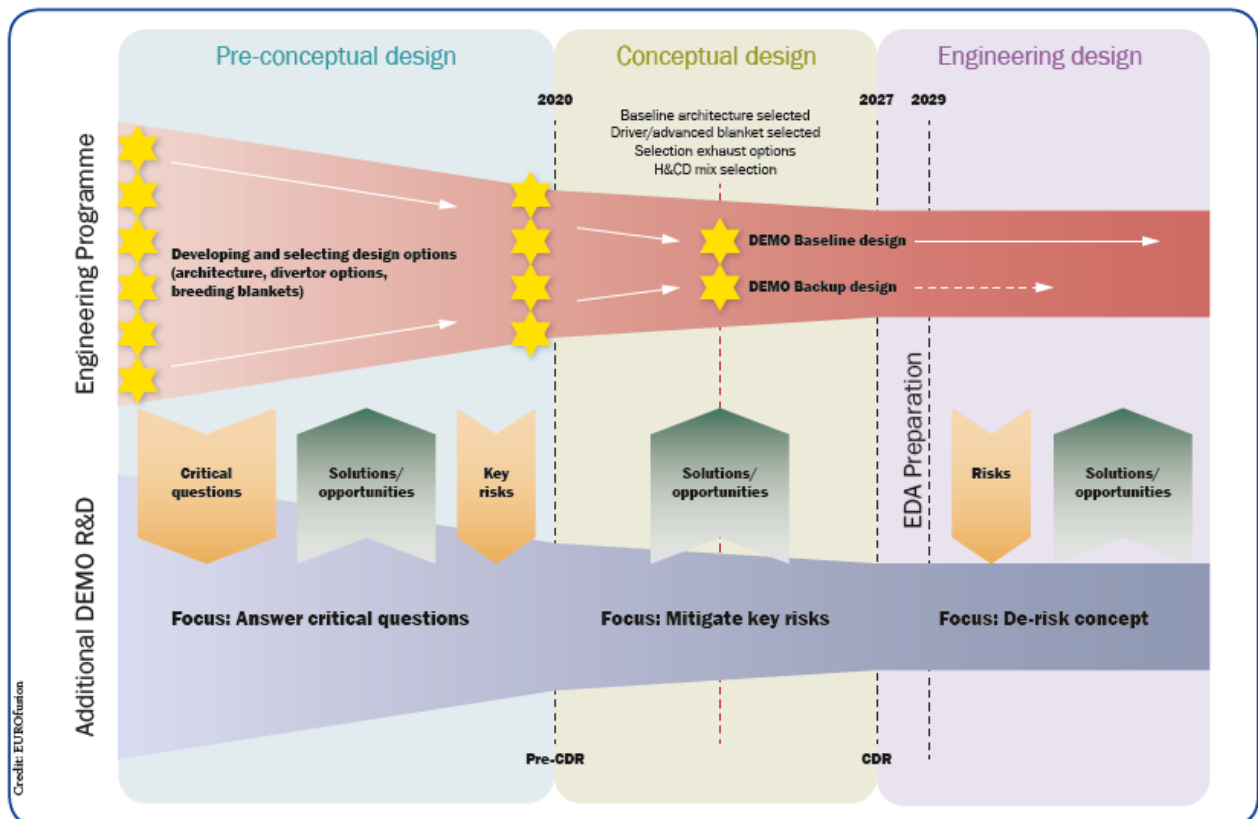


Figure 1.1: EU DEMO design stages [1]

DEMO is currently at a pre-conceptual design phase, meaning that the selection of the technologies and design principles of the main tokamak components (which will be presented

in section 1.2) are still under investigation; in this sense, DEMO design should be based as much as possible on the ITER operation experience [2], which will hopefully demonstrate robust burning D-T plasma regimes and provide useful info about materials and technologies (e.g., vacuum vessel, magnets, cryostat). At the moment, due to the uncertainties regarding the technological solutions to be adopted, it's been considered undesirable for the initial study effort to focus on developing a detailed design and therefore some flexibility in the approach to the conceptual design is needed.

The main goals [1,3,4] DEMO must achieve are:

1. Produce a net electricity output of about 500 MW achieving long plasma pulses (> 2h),
2. Tritium self-sufficiency, minimizing T inventories,
3. Demonstrate all the technologies for the construction of a Fusion Power Plant (FPP),
4. Ensure an adequate level of reliability and availability and demonstrate safety and sustainability of the plant,
5. Prepare the ground for an assessment of the feasibility and economic viability of a future commercial FPP.

Since the device aims to produce net electric power, it will be the first FPP to exploit a complete Balance of Plant (BoP), including a heat transfer system and a Power Conversion System (PCS) to generate electricity [5]. The BoP, especially the turbine, requires steady thermal operating conditions while the tokamak operation will be pulsed; that is the reason why an Energy Storage System (ESS) is needed. Thus far, the most promising option for the ESS is the Intermediate Heat Transfer System (IHTS), making use of molten salts to store energy, which receives the heat from the Primary Heat Transfer System (PHTS) and delivers it to the steam generator of the PCS that, in turn, is based on a Rankine cycle. The component that interfaces the EU DEMO machine with the BoP system is the so-called Breeding Blanket (BB). It is the plasma-facing component exposed to the largest heat deposition inside the tokamak and, as a result, the cooling of the BB through the PHTS will have a key role in the production of electricity. Also, the EU DEMO BB will have the function of producing Tritium, the fuel needed for fusion reactions together with Deuterium, in order to achieve fuel self-sufficiency (i.e., goal 2). This is necessary because Tritium is poorly available in nature, given that it is a radioactive isotope with short half-life, and therefore EU DEMO must demonstrate the capability of exploiting a closed fuel-cycle, minimizing the fuel inventories required, and eventually produce a sufficient surplus of Tritium needed for the startup of a new FPP.

### **1.1.2. EU DEMO tokamak functioning principle and components**

EU DEMO tokamak is a complex device that generates thermal power through nuclear fusion reactors between two isotopes of hydrogen, namely Deuterium (D) and Tritium (T). These two isotopes, in order to undergo a fusion reaction, must be heated to extremely high temperatures (in the order of magnitude of hundreds of millions of Kelvins) at which they ionize and

become plasma. After these D-T reactions, Helium particles and neutrons are emitted as products:



Neutrons carry most of the energy generated, 14.1 MeV, heating up the BB, while the remaining energy of the Helium is used to keep the plasma hot. Unlike fission, fusion reaction does not need neutrons to take place; this means that fusion chain reactions cannot happen, avoiding the possibility of an uncontrolled growth of power and making the fusion technology intrinsically safe.

Since the plasma is ionized, the D-T mixture must be confined inside a doughnut-shaped chamber called torus thanks to a combination of magnetic fields, generated by different sets of superconducting magnets. Figure 1.2 shows the EU DEMO layout.

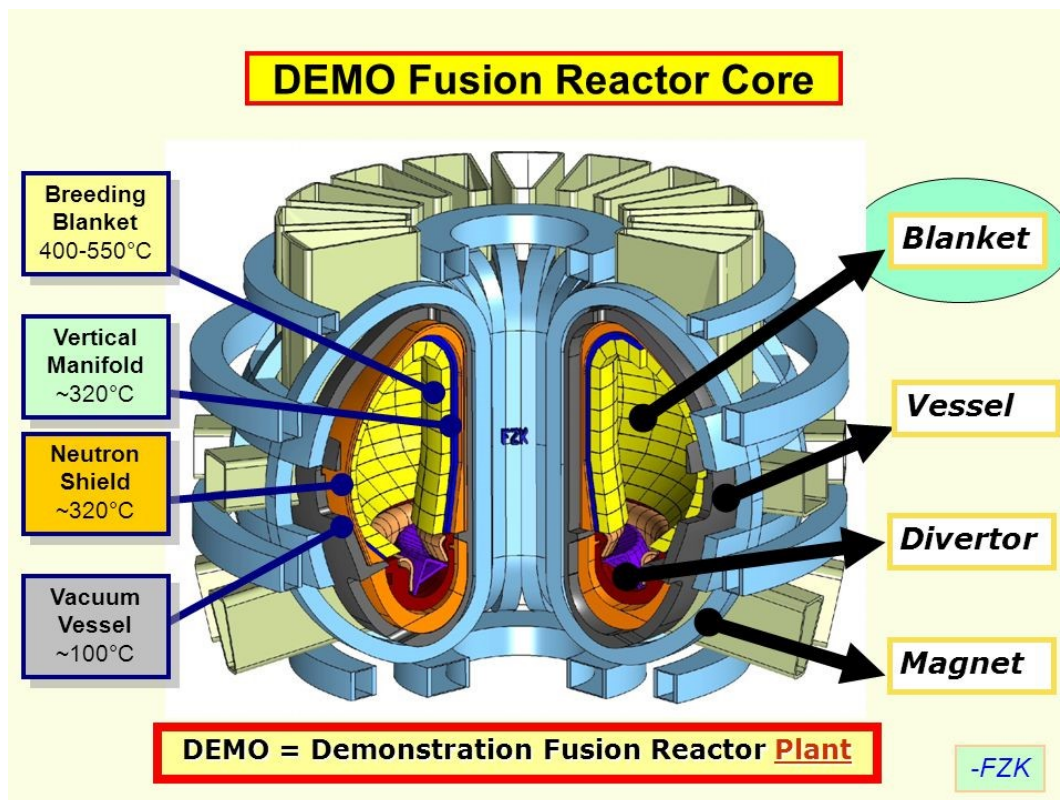


Figure 1.2: General layout of EU DEMO tokamak. Main components and their operating temperatures are highlighted. [32]

The DEMO **superconducting magnet system** will be the largest magnet system ever made, reaching higher currents and magnetic fields (up to 13 T) than any other counterpart on Earth. The magnetic field needed for plasma confinement and stability has field lines following an helicoidal path around the torus, which are actually the resultant of three different magnetic field components: (i) a toroidal field component produced by D-shaped Toroidal Field Coils (TFCs), (ii) a poloidal component given by a strong electric current flowing inside the plasma which, in turn, is induced by the AC current flowing inside the Central Solenoid (CS), and (iii) a vertical field component generated by six ring-shaped Poloidal Field Coils

(PFCs) placed outside of the toroidal ones [6]. While the first two components of the field (i.e., toroidal and poloidal) provide the confinement for the plasma, the vertical component contribute to its stability and gives a particular shape to the plasma useful to reach the so-called “divertor configuration”. Because of the great currents they will carry, the magnets must be manufactured from superconducting materials with zero electric resistivity, to avoid a massive heat deposition due to Joule effect. The materials selected for EU DEMO are Niobium3-Tin ( $Nb_3Sn$ ) for the TFCs and the CS, and Niobium-Titanium ( $NbTi$ ) for the PFCs, both superconducting when cooled with supercritical helium at 4.5 K.

It is interesting noticing that, inside the same machine, there will be a 100 million K plasma just few meters away from the superconducting magnets operating at 4.5 K; for this reason, DEMO, just like ITER, will need a **cryostat**. This component is a huge stainless-steel chamber which provides the high-vacuum, ultra-cool environment for the superconducting magnets and for the thermal shield operating at 80 K, as well as serving as a structural support for the tokamak [7]. It has some penetrations to allow access for maintenance and several accesses for cooling systems, magnet feeders, auxiliary heating, and diagnostics.

Inside the cryostat, DEMO features the **Vacuum Vessel (VV)**, a stainless-steel toroidal chamber that provides an ultra-high vacuum environment needed for the plasma [8]. It houses and supports the plasma-facing components and acts as a first safety barrier/shield for radioactivity.

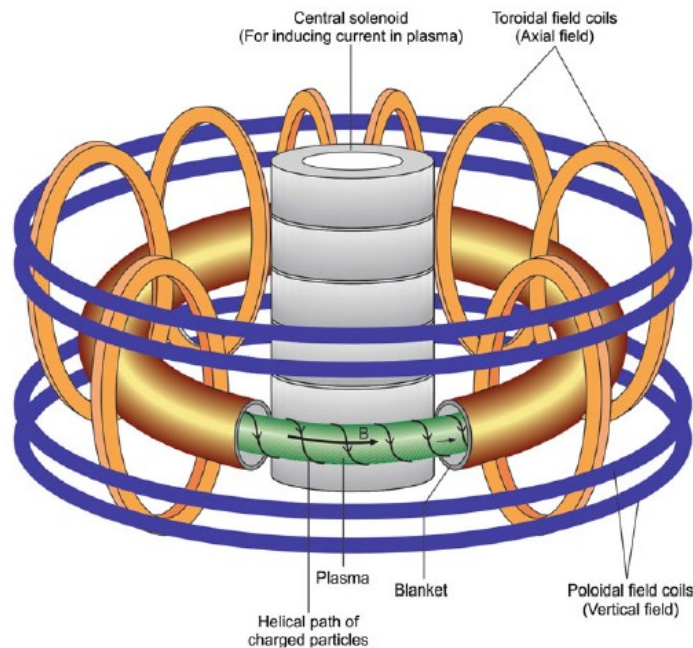


Figure 1.3: View of the superconducting magnets system and the resulting helical path of charged particles inside the plasma.[9]

The two in-vessel components directly facing the plasma which are exposed to the highest heat deposition inside the tokamak are the divertor and the breeding blankets. The **divertor**, placed at the bottom of the VV, is the target of the Helium ashes and other charged particles escaping from the plasma boundary along the so-called Separatrix, an open magnetic field line which separates the toroidally confined region from the region where field lines

connect to material surfaces. This component serves the dual function of extracting the huge heat load carried by plasma particles and pumping the impurities out of the VV, preventing them to reenter the plasma. Currently, the most mature divertor technology, already selected for ITER, is a solid and modular structure, made by several cassette assemblies with toroidally symmetrical geometry [10]. These cassettes, actively cooled by water, have a stainless-steel body covered by a tungsten armor, chosen following an international R&D effort because of its high melting point. However, the power to be exhausted in DEMO is about six times larger with respect to ITER, this means that the heat flux hitting the divertor plates will be larger than  $40 \text{ MW}/\text{m}^2$  (compared to the  $10 \text{ MW}/\text{m}^2$  predicted for ITER steady state operation), definitely too high to withstand, given the maximum heat flux presently limited to  $20 \text{ MW}/\text{m}^2$  by materials technology. To overcome this issue, several other options are being investigated in parallel to ITER operation, for instance by the Divertor Tokamak Test (DTT) facility in the ENEA Frascati Research Center, supported by EUROfusion, which aims to explore and qualify alternative power exhaust solutions for DEMO. Three different strategies are being followed: (i) increase the fraction of energy exhausted by radiation channel using impurity seeding, (ii) exploring liquid metal divertors, which could bear up to  $100 \text{ MW}/\text{m}^2$  thanks to the latent heat of vaporization, and (iii) increase of the flux expansion to distribute the strike-point heat flux over a larger area of the target (Super-X configuration).

Last but not least, EU DEMO will have a **Breeding Blanket**, covering the interior of the VV torus in a modular layout. Other than shielding for radiation-sensitive components and personnel from neutron and heat fluxes, the BB, as mentioned previously, has two primary roles. First, it must extract the neutrons power, by mean of a suitable coolant flow, to avoid failures of the structural materials and to heat up another fluid, leading to electricity production in the PCS. An adequate design of the cooling system is required in order to maximize the net efficiency of the plant. On the other hand, the BB must breed and extract enough tritium for the plant self-sufficiency. Tritium production take place in the so-called Breeding Zone (BZ), where a material (thereby called *breeder*) enriched in Lithium is invested by the neutron flux coming from the plasma, giving nuclear reactions which produce tritium. Lithium has two different isotopes in nature, with different abundance on earth, each of them interacting with neutrons as follows:



Where  $n'$  is a thermal neutron and  $n$  a fast one. Reaction (2) is triggered by a fast neutron coming from the plasma, producing a thermal neutron that, reacting with Li-6, gives another Tritium atom (reaction (1.2)). An important parameter for the assessment of the plant self-sufficiency regarding the fuel is the Tritium Breeding Ratio (TBR), the ratio between Tritium produced in the blanket and Tritium burnt in the plasma. The additional neutron produced by reaction (1.3) helps meeting DEMO requirement for a TBR larger than 1, but it is not enough; due to parasite neutron absorptions and leakages, also a Neutron Multiplying Material (NMM) is needed inside the blanket. The BB has also a third role: it acts as a first barrier

er against high-energy neutrons coming from the fusion reactions inside the plasma. It reduces the neutron irradiation that hits the VV and, along with the VV itself, protects the most radiation-susceptible components of the tokamak, which are the superconducting magnets operating at the extremely low temperature of 4.5 K.

Several options for the design of the BB are currently being studied for implementation in DEMO plant by research activities coordinated by the EUROfusion consortium, involving different choices for breeder material, NMM and coolant [11,12]. The most promising concepts are:

- *Helium-Cooled Pebble Bed (HCPB)*: this concept has gaseous helium coolant, a mixture of  $\text{Li}_4\text{SiO}_4$  and  $\text{Li}_2\text{TiO}_3$ , in form of ceramic pebbles, as breeder, and beryllium pebbles as NMM. Tritium is extracted by means of a helium purge flow. The selected structural material, chosen also for the other three concepts, is a ferritic-martensitic stainless steel named EUROFER, which guarantees low levels of neutron-induced activation.
- *Helium-Cooled Lithium-Lead (HCLL)*: this concept has a helium-cooled structure made of EUROFER steel, and a liquid PbLi eutectic flow, enriched to 90% in Li-6 to ensure the target TBR, serves as both tritium breeder and neutron multiplier. The main drawback of a liquid metal breeder is the interaction with the magnetic fields, leading to MHD pressure losses. Since liquid metal does not play the role of coolant, its velocity inside the blanket can be minimized to reduce the electromagnetic pressure losses.
- *Water-Cooled Lithium-Lead (WCLL)*: this concept too uses liquid PbLi eutectic as breeder and neutron multiplier material, whereas the role of coolant is fulfilled by pressurized water. As it happens for the HCLL concept, the presence of liquid metal induces MHD pressure losses which should be minimized. Structural material is EUROFER steel.
- *Dual Cooled Lithium-Lead (DCLL)*: as suggested by the name, this concept make use of two coolants. Helium cools the FW and module box, while liquid PbLi eutectic, with a Li-6 enrichment of 90%, self-cools the BZ while acting, at the same time, as breeding material and NMM. Liquid metal flows with high velocities to fulfil his role as coolant leading to relevant MHD losses, hence the design should account for this issue.

This thesis work will focus on the HCPB concept, which will be addressed more in detail in chapter 2.

## 1.2. Aim of the work

The EU DEMO HCPB blanket, like other concepts, is still at a pre-conceptual design stage, making it difficult and pointless to implement a detailed model for the dynamic simulation of the thermal-hydraulic behavior of the BB cooling loop, which can be very expensive from a computational point of view, given that data and design choices may change within a short period of time.

For this reason, this thesis uses as numerical tool the GETTHEM (General Tokamak THERmal-hydraulic Model) code, a system-level code developed at Politecnico di Torino for the thermal-hydraulic modeling of the EU DEMO PHTS and BoP, which allows to run fast simulations and get useful results on the global behavior of the components involved, both during nominal transients and accidental scenarios.

The scope of the thesis is to parametrically analyze the consequences of a Loss-of-Flow Accident (LOFA) inside the HCPB breeding blanket. This accident may be caused by different initiating events such as circulator trip, loss of offsite power or channel obstruction, and can result in excessive overheating of the BB segments and, eventually, the failure of the materials if the accident is not readily detected, delaying the plasma shutdown. Different simulations will be performed considering both partial and total LOFA and making different assumptions on the plasma shut down system intervention, highlighting the maximum temperature reached inside the blanket for each scenario. In particular, the model will have a higher level of detail for the First Wall (FW) with respect to other regions of the blanket, because that is the region in which the most critical conditions are expected.

# Chapter 2

## 2. EU DEMO Helium-Cooled Pebble Bed Breeding Blanket and PHTS system

### 2.1. HCPB design description

In the framework of the EU Roadmap to Fusion Energy, the EUROfusion Consortium started in 2014 the Pre-Conceptual Design (PCD) phase of DEMO reactor, at first indicating four BB concepts to be explored and then focusing on the two most promising: WCLL and HCPB. As already said above, this work will focus on the latter.

The starting point for the HCPB was the ITER HCPB TBM “act-alike” [13] (shown in figure 2.1 below), organized in horizontal and vertical grids joined to the U-shaped, actively cooled FW. The so-called Breeder Units, containing  $\text{Li}_4\text{SiO}_4$  and the NMM, were placed inside cubicles between two parallel cooling plates. Due to the complex geometry and large amount of steel, this concept showed poor results regarding the assessment of the tritium self-sufficiency, which could not be ensured.

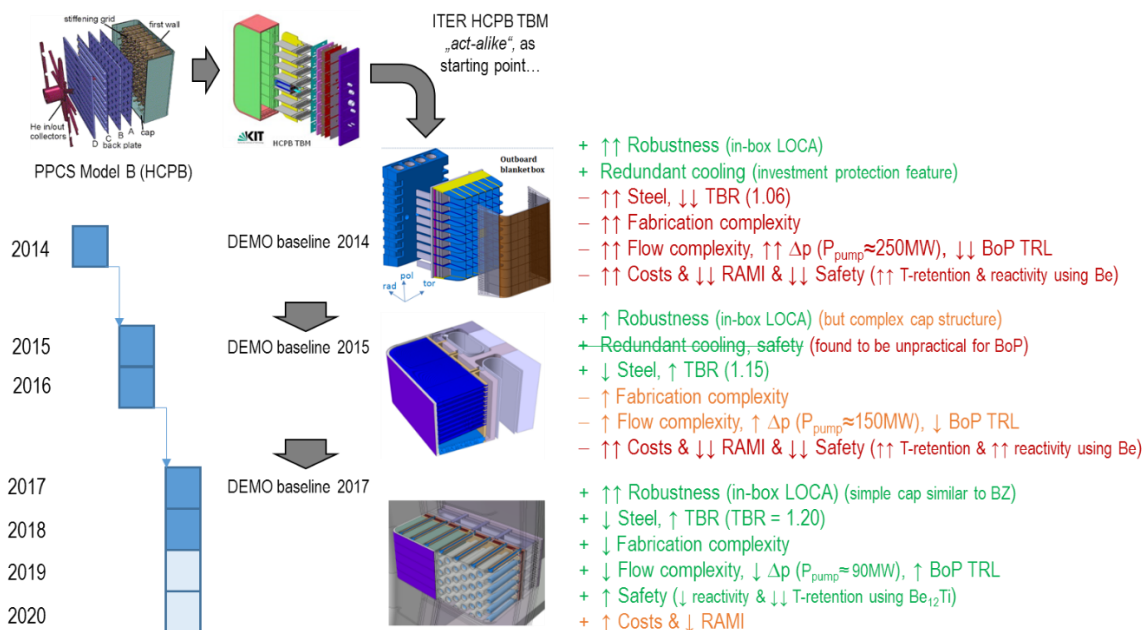


Figure 2.1: HCPB design stages during DEMO pre-conceptual design and advantages and drawbacks of each design w.r.t. the starting design [13].

With the release of the new DEMO baseline (BL) of 2015, a new revision of the BB was carried out to reduce both the complexity of the box and the coolant pressure losses (hence the circulating power too), revealing good breeding performances with a TBR near to 1.15 and good thermo-hydraulic performances; nevertheless, the improved knowledge on reactor integration, plasma physics and reliability, and the new requirements of DEMO BL2017, revealed the necessity to focus on a near-term solution with more technology readiness and a simpler and more reliable cooling scheme for the PHTS.

To cope with these requirements, a new different design was proposed in 2017, then improved in 2018 and 2019, which is based on a fission-like arrangement of fuel-breeder pins filled by Ceramic Breeder (CB) and oriented along the radial direction of the blanket [14]. This enhanced concept, the HCPB-BL2017-v1/v2, is considered to be the reference design for the conceptual design phase of EU DEMO; in the following section a summary of its design will be presented, based on the detailed report available on [15].

### 2.1.1. Enhanced HCPB general architecture

Since the DEMO BL2017 foresees a reduction of the radial thickness of the blanket from 1.3 to about 1 meter, it is considered to be more adequate to adopt a Single Module Segment (SMS) architecture, compared to the previous Multi Module Segment (MMS), in order to make the segment more robust against large forces that can arise from a plasma disruption event. The BB system is divided in 16 toroidally arranged sectors (see figure 2.2), each of them have been divided in 3 Outboard (OB) and 2 Inboard (IB) segments; the IB segments consists of 12 BZ regions and the OB ones of 17.

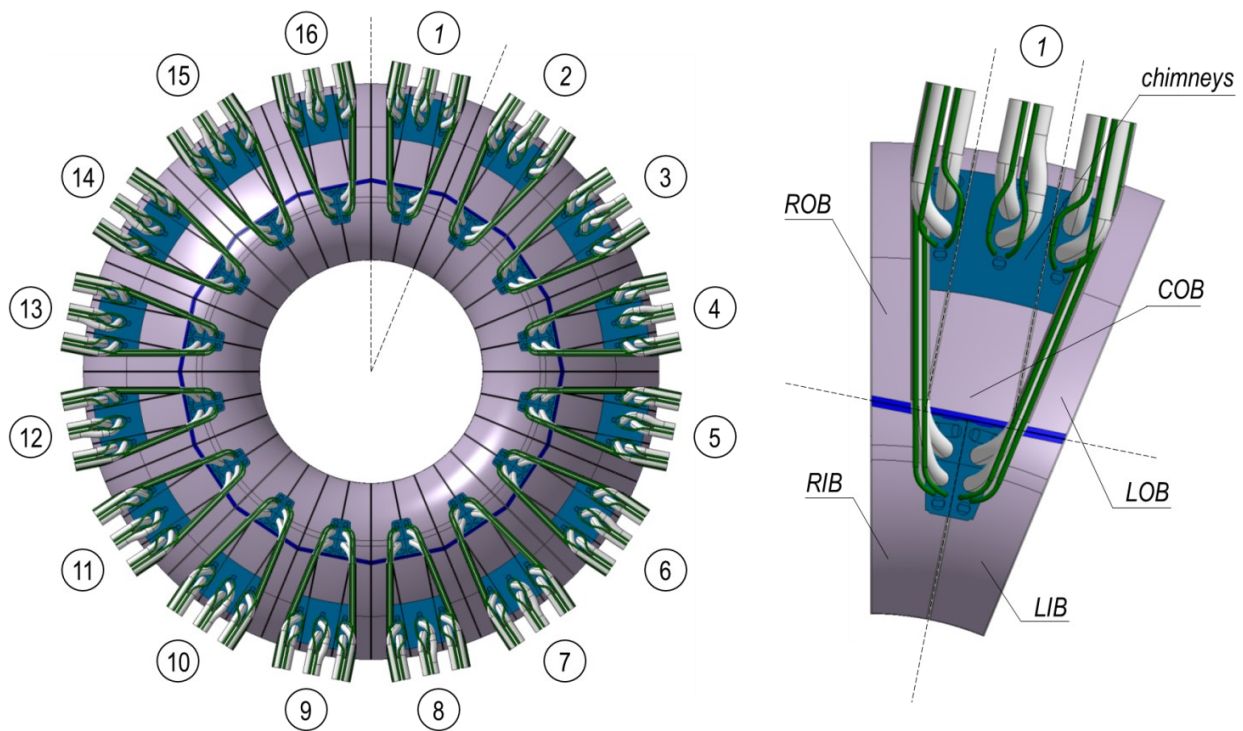


Figure 2.2: HCPB-BL2017 BB system. Left: view of all the toroidally arranged sectors; right: detailed view of a single sector and its segments [15]

The fuel-breeder pin is the key element of this concept: it consists of two concentric tubes with a circular cross section, forming the inner and outer cladding of the pin (Figure 2.3). Inner and outer cladding join at the front side of the blanket and the space between them is filled with an advanced CB called KALOS, a solid solution of  $\text{Li}_4\text{SiO}_4$  with  $\text{Li}_2\text{TiO}_3$  in form of pebbles. The pin is inserted inside a pressure tube, attached to the BZ backplate, which are structural elements acting against accidental over-pressurization; also, the annulus between pressure tube and outer cladding represents the return of the coolant that comes from BZ inlet manifold, passing first through the inner cladding.

The neutron multiplier element, surrounding the pressure tube, is a hexagonal matrix containing  $\text{Be}_{12}\text{Ti}$  pebbles (as shown in Figure 2.3b), filling the front of the blanket between the FW and the BZ backplate. A purge gas, mainly helium plus a small fraction of  $\text{H}_2$ , flows through the NMM and CB extracting the tritium produced by the blanket.

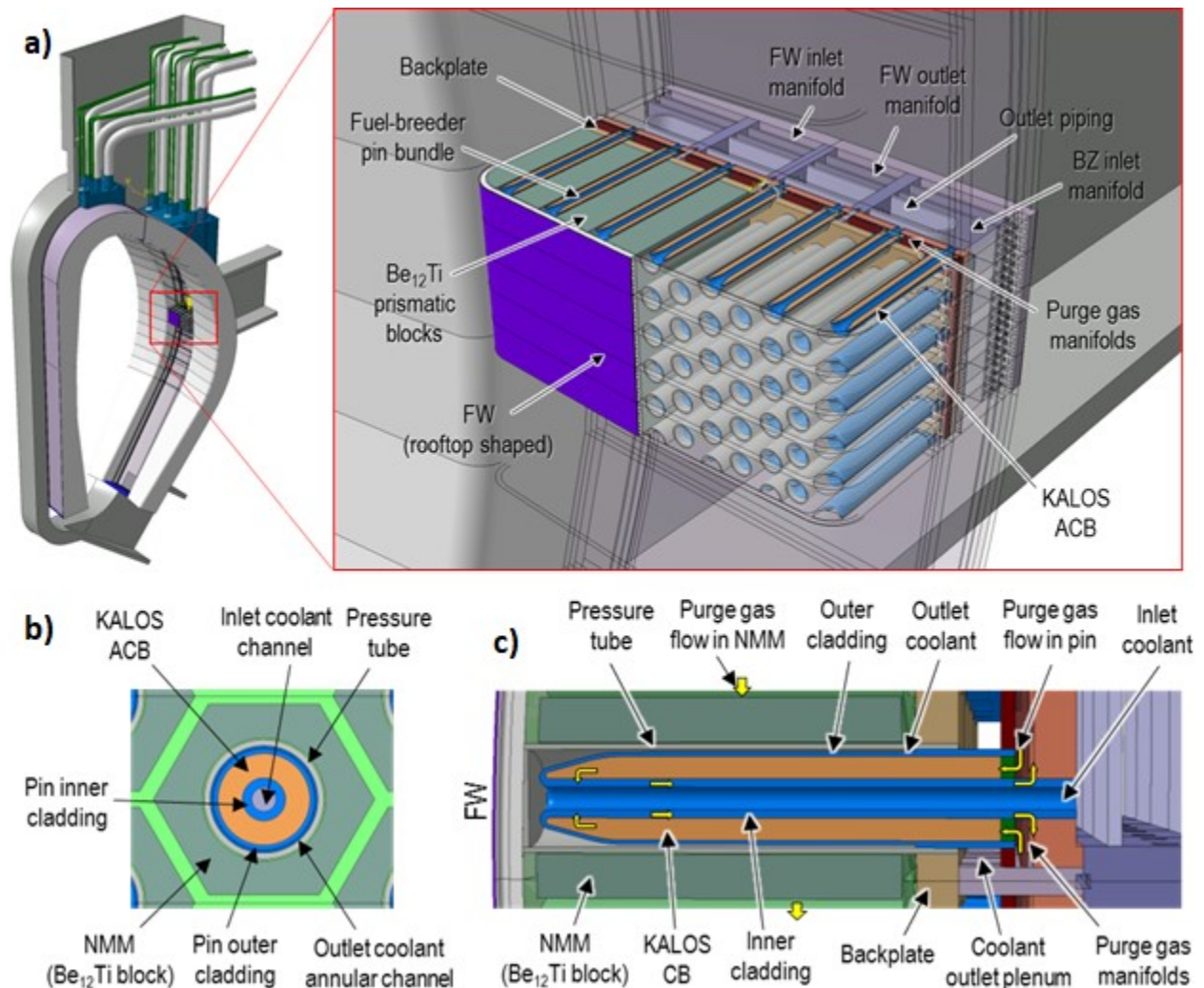


Figure 2.3: HCPB-BL2017 detail view. a) 3D view of the COB11 BZ region, b) poloidal-toroidal cross section of the fuel-breeder pin, c) radial poloidal view of the pin [15]

Figure 2.4 shows a radial-toroidal view of the BB, in which are indicated all the manifold volumes, behind the BZ, collecting inlet and outlet purge gas and coolant flows. A set of three different plates behind the BZ backplate form the inlet and outlet purge gas manifold. The segment is closed by a thick Back Supporting Structure (BSS) plate, which enclose, to-

gether with the purge gas backplate, two volumes for the coolant FW and fuel-breeder pin inlet.

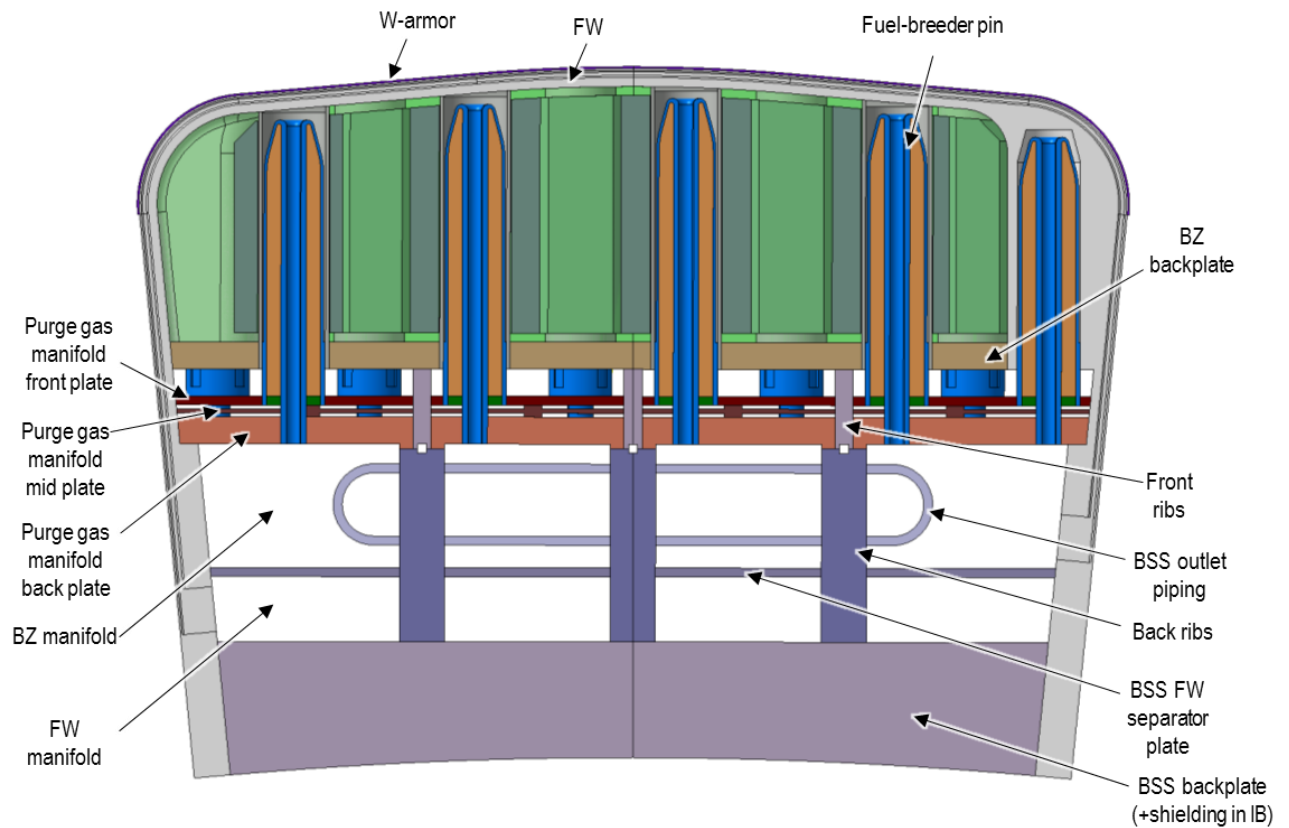


Figure 2.4: Radial-toroidal cross section of the HCPB segment [15]

Like previous designs, the FW is a U-shaped actively cooled plate facing the plasma, coated by a protecting armor of tungsten against plasma particles erosion. The FW is cooled by helium (inlet temperature and pressure of 300 °C and 80 bars respectively) flowing in parallel rectangular-shaped channels, which run toroidally inside the FW plate in counter-current flow with their neighbors. Also, to widen the impact area of fast particles coming from the plasma, the FW will have a rooftop shaping with a slightly tilted surface.

## 2.2. The HCPB cooling scheme and Primary Heat Transfer System

As already said, EU DEMO will have a pulsed cycle during normal operating condition. These oscillating conditions would have negative effects on the main components of the PCS, that are steam generators and turbine, affecting their lifetime. To cope with this issue, the DEMO BoP will be designed in a way that the PHTS and PCS are thermally decoupled, interposing between them an IHTS, which uses molten salts, collecting part of the thermal energy coming from the PHTS during a plasma pulse, and releasing it to the PCS during the dwell time. Figure 2.5 show a simplified view of the BoP. The PHTS will hence feature an Intermediate Heat Exchanger (IHX), having hot helium on the primary side and molten salts on the secondary.

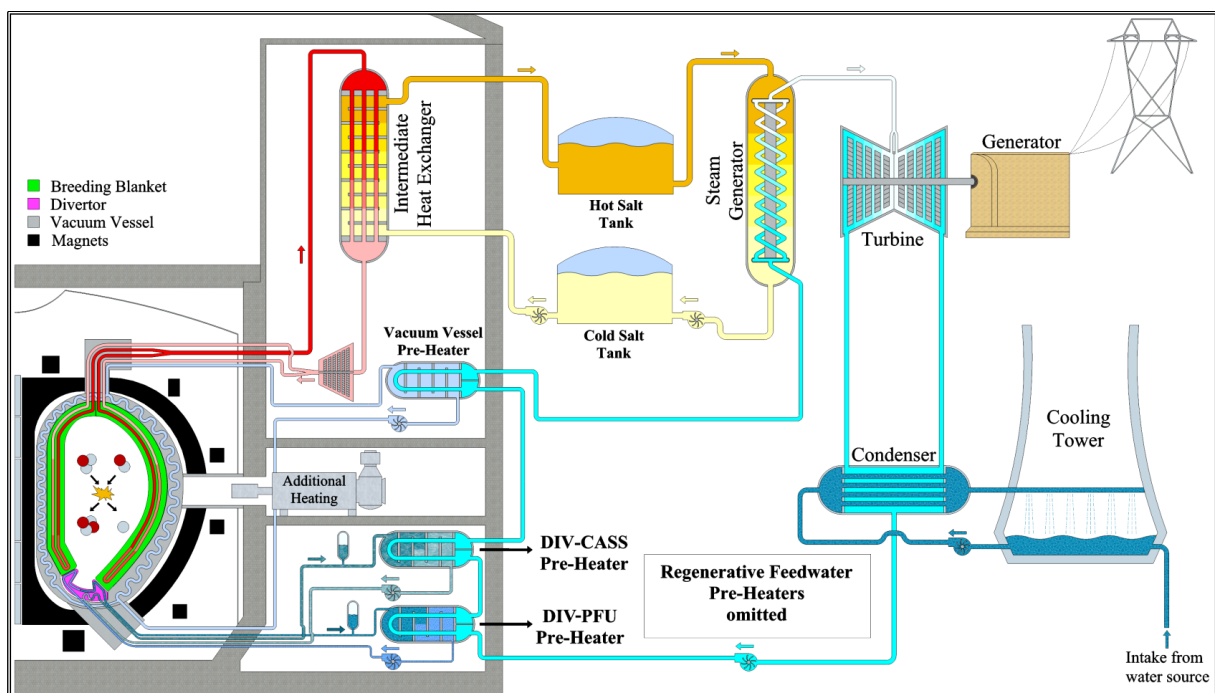


Figure 2.5: Simplified view of the DEMO BoP layout [5]

### 2.2.1. The HCPB BB cooling scheme

The coolant selected for HCPB concept is fluid helium, as the name suggests. This choice has been made because of several reasons: (i) helium has nearly no interactions with the neutron flux, allowing good tritium breeding performances, (ii) it does not undergo phase changes, giving the possibility to operate at high temperatures, (iii) it has good heat conduction properties with respect to other gases, and (iv) it is chemically inert, avoiding unwanted reactions with structural and functional materials. The main drawback of helium as a coolant is represented by its low density, which can result in large circulating power. The coolant, at a pressure of 80 bars, enters the BB with a temperature of 300 °C, heating up to 520 °C at the outlet (Figure 2.6) [15]. This temperature window is set by the structural material, EUROFER97, having as lower bound its Ductile-to-Brittle Transition Temperature (DBTT) and as upper bound the temperature at which it starts showing a large loss of creep strength, i.e., 550 °C.

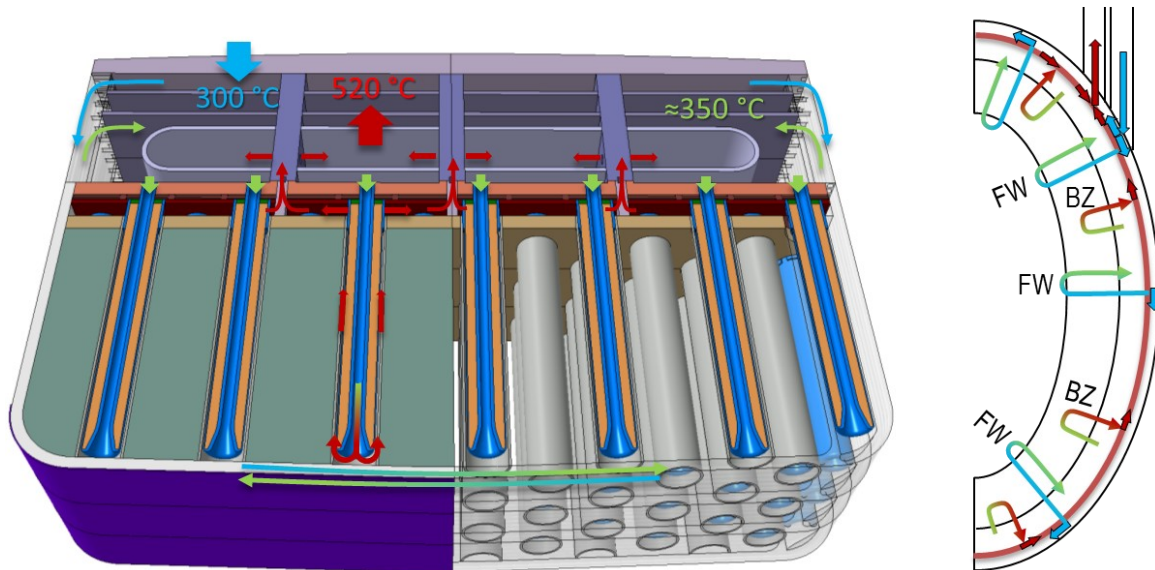


Figure 2.6: HCPB blanket cooling [15]

Helium enters the segment at the FW inlet manifold, from where it flows through the FW channels reaching a temperature of about 350 °C, depending on the poloidal position. Indeed, different poloidal positions have different heat loads coming from the plasma, meaning that the coolant outlet temperature from the FW varies poloidally and, in the most critical regions, it could reach too high values causing problems in the BZ. For this reason, the fluid is then collected in the BZ inlet manifold, where it is mixed with helium coming from all poloidal regions reaching a homogeneous temperature, and then it is sent into the fuel pins and recollected by the outlet manifold at a mixed temperature of 520 °C. Figure 2.7 gives a more intuitive view of the HCPB BB flow scheme, including two FW channels cooled in counter-current flow.

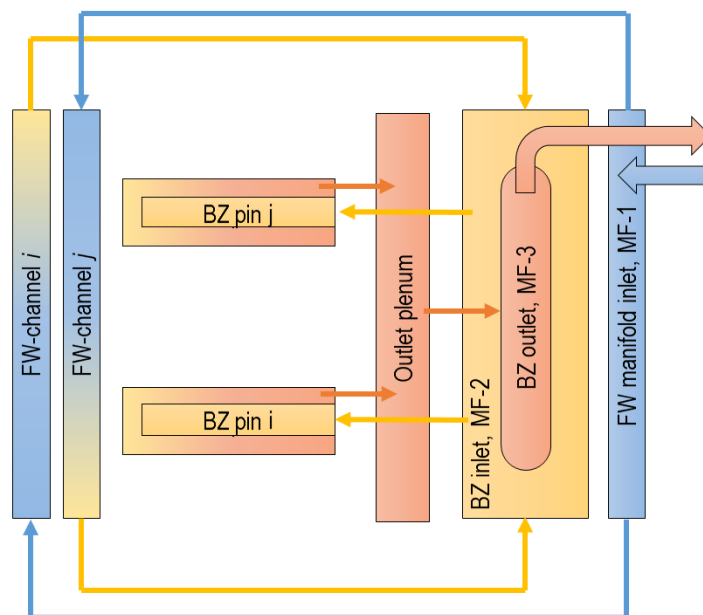


Figure 2.7: Schematic flow path of the HCPB [15]

## 2.2.2. HCPB Primary Heat Transfer System architecture

The HCPB BB PHTS [16] is designed to extract about 200 MW from the in-vessel components and transfer it to the ESS by mean of the Intermediate Heat Exchanger. It has a quite complex architecture, since it must feed each segment of the BB system, weighting the coolant mass flow rates to be delivered to different segments in function of their heat removal requirements. Table 2.1 shows the main input data for the PHTS, helium side.

Table 2.1: PHTS helium cooling loop input data (adapted from [16]).

<b>HELIUM COOLING LOOP</b>	
<i>N° of IB segments [-]</i>	32
<i>N° of OB segments [-]</i>	48
<i>IB segments power [MW]</i>	575.4
<i>OB segments power [MW]</i>	1453.7
<i>BB inlet pressure [bar]</i>	80
<i>BB inlet temperature [°C]</i>	300.0
<i>BB Outlet temperature [°C]</i>	520.0
<i>BB Pressure drop [kPa]</i>	79.9

The idea for the implementation of the HCPB PHTS cooling loops follows some initial criteria for the general safety and integration. For instance, to mitigate the consequences of a Loss of Coolant Accident (LOCA), DEMO must have more than one cooling loop, and every cooling loop must have redundancy of the circulators to limit the effects of a LOFA. The importance of redundancy of circulators will be assessed later in this thesis. Moreover, the design should follow a trade-off between limited costs, high efficiency of the plant and minimization of coolant inventories and radioactive materials.

Two layouts for the PHTS have been studied: the first one has separate loops for IB and OB segments (case I), while for the second one each loop collects helium from both IB and OB segments (case II). Regarding the number of loops, it should be a submultiple of 16 (i.e., the number of sectors of the tokamak) and, due to the need to contain costs and to integrate the PHTS's components inside the reactor building, it should be smaller than 12. A parametric study has been made by Moscato et al. [17], taking into account additional requirements such as maximum pipe diameter, maximum coolant speed in hot and cold legs etc.; as a result, two choices for case I and II have been identified, respectively made by 2 IB loops plus 8 OB loop for case I, and 8 loops for case II. At the end, the layout corresponding to case II seemed to be the most promising one.

Thus, the design chosen for the PHTS features 8 separate cooling loops, evenly distributed on two opposite sides of the reactor building. Each loop provides pressurized helium to both IB and OB BB segments of two tokamak sectors (see figure 2.8) and extracts a thermal power of 254 MW.

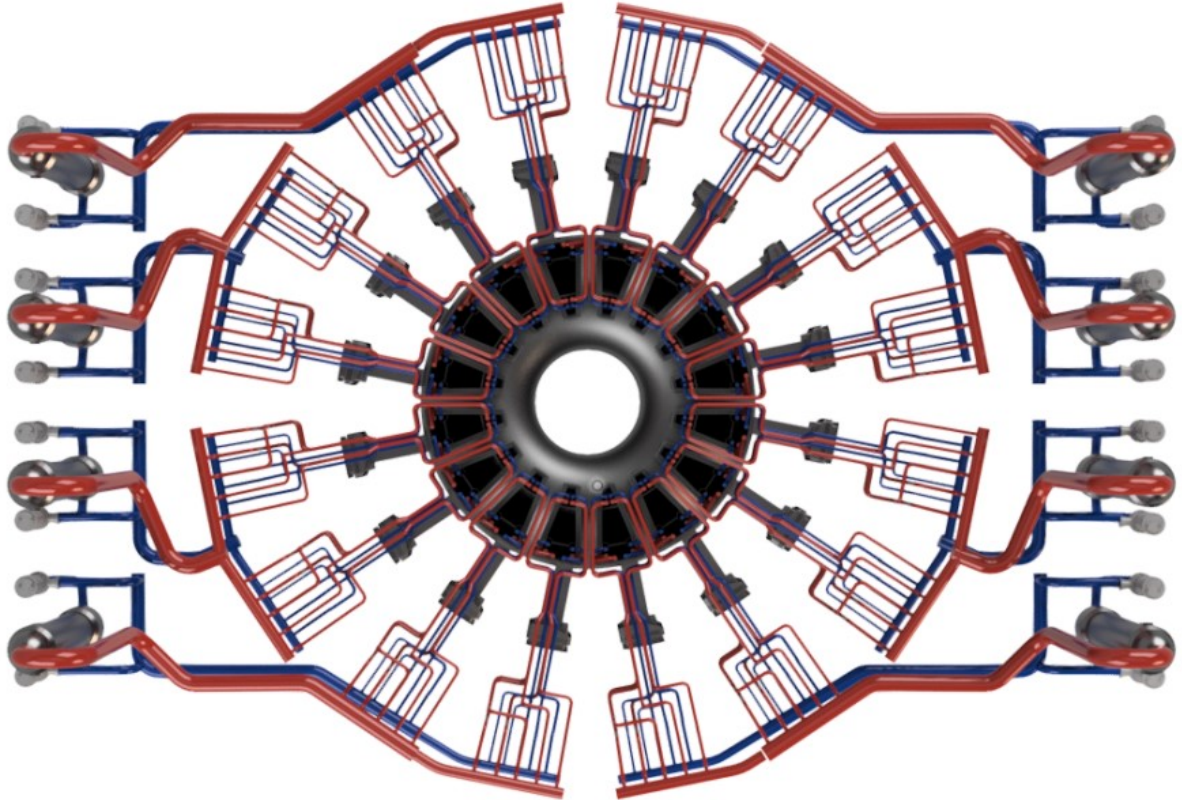


Figure 2.8: View of the BB PHTS layout (case II) [16]

Each cooling loop is completed by the heat exchanger, with molten salts on the secondary side, and two circulators. For the IHX the shell and tube technology has been adopted, due to strong prior knowledge on this kind of exchangers, having HITEC salt on the shell side because of its low pressure (hence reduced costs of manufacturing) and helium on the tube side. Helium enters the exchanger from the top head and flows downward, while molten salts have an ascending motion crossing the plates inside the shell (see figure 2.9) and exits from the top. Cold helium is collected at the bottom of the IHX and sent to the circulators' suctions through two pipes.

Two circulators are placed near the bottom of the heat exchanger, ensuring redundancy criteria to mitigate the effects of a LOFA due to a single circulator failure. Circulators should continuously deliver the adequate coolant flow to the blankets during pulse and dwell phases.

# Chapter 3

## 3. Computational tools and overview of the model

### 3.1. Modeling environment

The starting point of this thesis work is to have a simple model able to represent the PHTS of the HCPB blanket. As already anticipated, since the scope of this work is to make a preliminary system-level analysis of the global thermal-hydraulic behavior of the BB (under the accidental scenario of a LOFA), without going into too much detailed studies, the model should be written in a simple and intuitive way, allowing fast-running simulations to get global results (but still maintaining a decent degree of detail for the coolant and solid thermal behavior) for different scenarios with different sets of parameters. For this purpose, the Modelica language was chosen.

#### 3.1.1. The Modelica language

Modelica is a freely available, object-oriented, equation-based, acausal modeling language, useful for modeling large and complex physical systems which can be made by components of different nature (e.g., thermal, electrical, mechanical, electronic, hydraulic, or control components) [18, 19,20]. For this multi-domain nature, the Modelica language is used in a wide range of applications, such as, for instance, fluid systems, automotive systems or mechanical systems. Recently, it has also been used for nuclear fusion applications regarding the cooling of the superconducting magnets and the development of the GETTHEM code, for the thermal-hydraulic transient modeling of the EU DEMO PHTS.

One of the features that distinguishes Modelica from most of the other programming languages is its declarative and acausal nature. Although some classes (e.g., functions) are described by algorithms, all other objects are described simply by sets of equations and not by assignments statements. This allows an acausal modeling where the order in which equations are stated is not important. Moreover, Modelica is “built” as a dynamic modeling language, so models and simulations are implicitly time dependent, and a pre-defined variable ‘time’ is used to plot results. The equations defining the model can be algebraic or differential in time, since it is possible to use the operator `der` to perform time derivatives. For space derivatives, instead, the derivative must be simplified with discretization methods (e.g., finite differences, finite volumes etc.), leading to algebraic expressions.

Since Modelica is an object-oriented language, each component of the physical system to represent is modeled through a different object. A model is described by schematics, also known as object diagrams, in which several objects are linked to each other thanks to some elements called connectors, which are the interface between the component and the external world. Moreover, each component is internally defined by another schematic or, on “bottom” level (or layer), by a set of equations that describes the model in Modelica syntax [19]. In this way, models of different objects can be contained in other models on a broader scale, having a modular architecture made by layers, which ensure a more user-friendly layout. Figure 3.1 gives some examples of object diagrams.

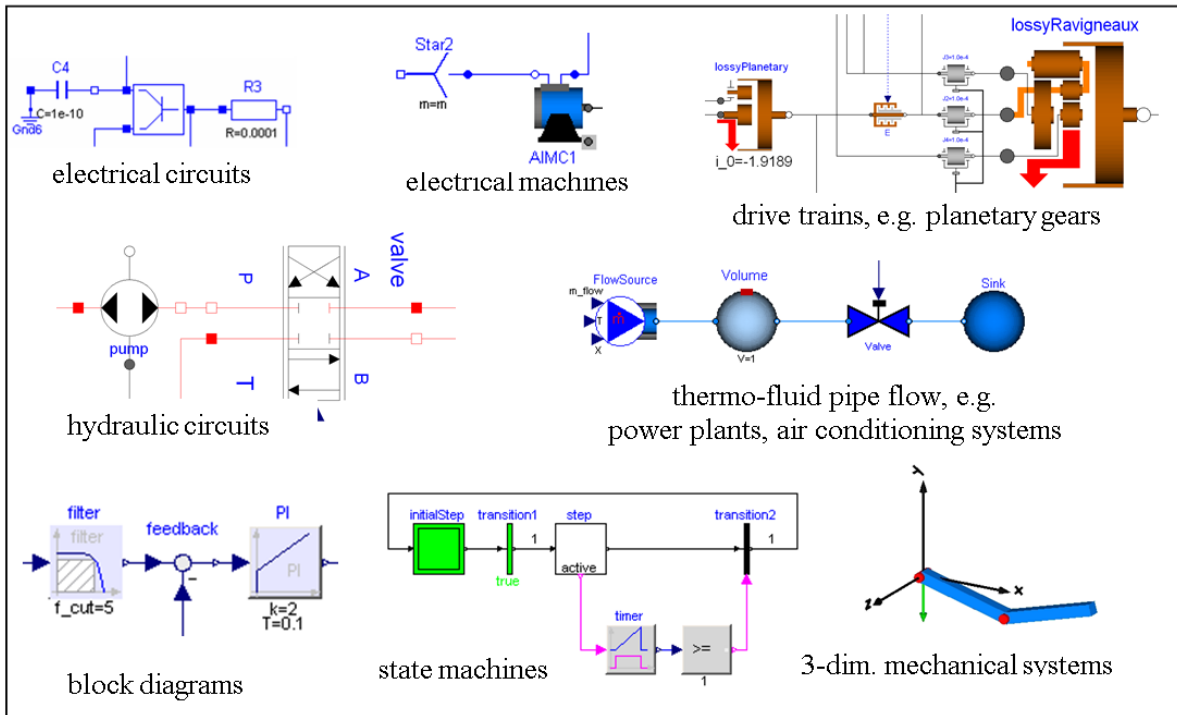


Figure 3.1 Examples of several object diagrams on Modelica. [19]

A useful feature of the Modelica language is that many libraries, or packages, are available. Modelica Libraries contains a large set of models regarding several domains, giving the user a wide choice of pre-defined components to use for his modeling work. Particularly, a very complete library is the open source Modelica Standard Library (MSL) [20], containing about 1280 model components and 910 functions from many domains.

Many modeling and simulation environments for the implementation of models in Modelica language are available, either commercial or free of charge. The ones used in this thesis work are OpenModelica and Dymola, two of the most widespread. OpenModelica is an open source software developed by the Open Source Modelica Consortium (OMSC), freely available for use, intended for research, teaching and industrial usage. Instead, Dymola is a commercial modeling environment developed by Dassault Systèmes, with a Modelica translator able to perform all necessary symbolic transformations for large systems (> 100'000 equations) [21].

## 3.2. Description of the GETTHEM code for the HCPB PHTS

### 3.2.1 Introduction to the GETTHEM code

The simulations carried out for this thesis work are performed on a model based on the General Tokamak Thermal-hydraulic Model (GETTHEM) code for the HCPB BB cooling loops [22,23]. The GETTHEM code, as anticipated in chapter 1, is a global, system-level dynamic code for the thermal-hydraulic modeling of the PHTS and BoP of a tokamak. It has been developed at Politecnico di Torino (NEMO group, DENERG) within the framework of the PCD of the EU DEMO supported by the EUROfusion Consortium, using the Modelica language, which allows a modular architecture for the model as requested for this stage of the EU DEMO design. Together with the thermal-hydraulic part, this code also contains a model for the solid structures made of EUROFER97, useful to compute the distribution of the temperature reached in the solid, to make sure it does not exceed the upper limit for the material.

The GETTHEM code is focused on two of the four concept candidates for the EU DEMO BB: the HCPB, whose model will be discussed later, and the WCLL, whose model is described in [24]. For the latter, particular care must be paid to both the liquid breeder inside the BZ, performing an accurate estimate on the MHD pressure losses, and the cooling flow of liquid water, which could undergo a phase change in the case of a severe thermal transient, leading to a deterioration of its heat removal capability. Figure 3.2 shows a schematic view of the WCLL cooling loop model, where two branches in parallel, respectively for the FW and for the BZ, are fed inside the same cooling loop.

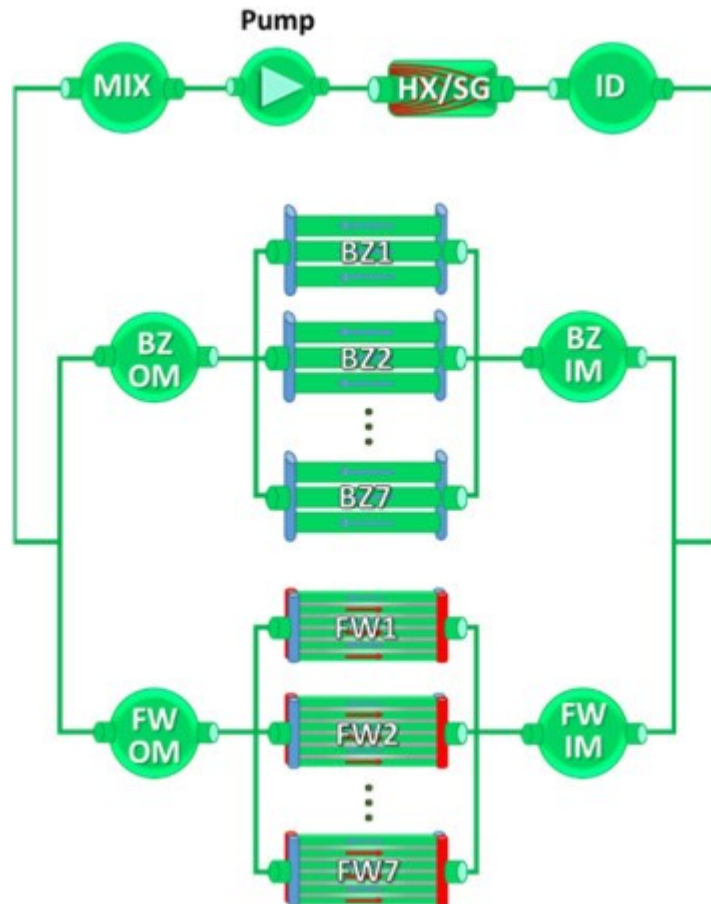


Figure 3.2: Sketch of the model for the WCLL loop (FW: First Wall object; BZ: Breeding Zone object; IM: Inlet Manifold; OM: Outlet Manifold; ID: Inlet Distributor; MIX: Mixer; HX/SG: Heat exchanger/Steam Generator) [24]

Once successfully developed, the model has been checked to see if it is indeed a suitable representation of the actual physical system. Since experimental data are not available for these new concepts of BB, the model has been validated (or, in this case, benchmarked) through a comparison with different kind of models (for instance CFD models) which, in turn, may already have been validated. The part of the code regarding the thermal-hydraulic Back Supporting Structure (BSS) of the EU DEMO HCPB has been benchmarked against previous 3D Computational Fluid Dynamics (CFD) studies in normal operating conditions (see [25]), while, in the case of an accidental release of coolant inside the VV, the model of the VV Pressure Suppression System (VVPSS) has been benchmarked from results coming from the already validated CONSEN code by ENEA [26]. Moreover, in [27] the solid model for the EUROFER97 is analyzed, where the results on the hot-spot temperatures reached in the solid are benchmarked against 3D heat transfer CFD studies performed by the HCPB design team, reported in [28].

### 3.2.2. GETTHEM code assumptions

The GETTHEM code for the HCPB cooling loop is based on a 0D/1D approach to adequately model the objects described in it: for “long” components, such as cooling channels or pipes, the mass, momentum and energy equations are discretized with 1D Finite Volumes (FV) method, whereas other components where there is no developed fluid flow were modeled as 0D objects (this is the case of manifolds, valves and circulators). The choice of FV for 1D objects is motivated by its relatively easy implementation, still maintaining a good level of detail on a system-level point of view. Each BB cooling loop features a Steam Generator (SG), which is modeled, by means of a 1D thermal pipe, as an ideal Heat eXchanger (HX), meaning that helium at the HX outlet is always at the design temperature of 300 °C. All the objects describing the components of the circuit, from circulators to simple pipes, are taken from (or are an extension of components implemented in) the Modelica library ThermoPower [30], a free and open source library developed by Politecnico di Milano for the implementation of energy systems.

In order to allow fast-running simulations, some simplifying assumptions had to be made by the developers of the code because of the large amount of cooling channels of the PHTS to be modeled (about 1700 per blanket module in the 2015 baseline design) [22, 29]. In view of this, a new Modelica library has been implemented to simplify the calculation of fluid and solid properties.

The helium coolant, in normal operating conditions, can be considered as an ideal gas. This significantly simplifies the computation of its properties: the helium specific heat is constant with no error, while the density can be simply deduced from the Ideal Gases Law, considering negligible the pressure dependence due to small pressure variations, as inversely proportional to the temperature. In addition, since the fluid velocities inside the cooling loop are much smaller than the speed of sound, helium is considered incompressible.

Still considering normal operating conditions, also for what concerns the solid structures made by EUROFER97 important simplifications were made. For instance, the thermo-physical properties of the material, such as specific heat, density and thermal conductivity, were assumed to be independent on the temperature, introducing an average error on the inputs of 8%, 0.3% and 3% respectively [29]. Also, the heat transfer coefficient between EUROFER and helium is assumed to be constant, and it is computed with the Dittus-Bölder correlation at nominal average conditions. Other phenomena can affect the heat transfer coefficient, such as flow acceleration due to heating of the fluid or coolant phase-change phenomena in the case of the WCLL blanket; however, since they would only improve the heat transfer, a conservative choice of neglecting them has been done in order to avoid slower simulation performances. In conclusion, these assumptions resulted in an overall error on the results that does not exceeds 3%, in normal operation.

However, things change if severe accidental scenarios are involved. In such cases, indeed, the fluid and the solid structures will experience severe variation from nominal operating conditions, which could lead to very high pressures and temperatures inside the BB. Such scenarios obviously invalidate the assumptions described above about solid and fluid proper-

ties. For this reason, a different approach has been adopted, by the GETTHEM code developers, to cope with this issue in the case of LOCAs; in these cases, to maintain the fast-running nature of the code, the choice was to simplify the geometry of the system (0D model for the PHTS) rather than make assumptions on the coolant and solid properties. Thus, the helium flow is modeled more in detail, using the ideal gas model from the Modelica Standard Library, with NASA coefficients, for its properties.

### 3.2.3. GETTHEM code equations

In this section the equations implemented in the GETTHEM code will be presented (but only the ones referring to the HCPB cooling loop model, since that is of interest in this thesis work) for both the fluid and solid objects, specifying the terms that cancel out in view of the assumptions made.

Concerning the helium part of the objects modeled as 1D, which are basically the cooling channels, the equations involved are the conservation of mass, momentum and energy. Since these components are modeled with FVs, the equations refer to each fluid volume  $i$ :

$$A \cdot l_i \cdot \frac{d\rho_i}{dt} = \dot{m}_{in,i} - \dot{m}_{out,i} \quad (3.1)$$

$$\frac{l_i}{A} \cdot \frac{d\dot{m}_i}{dt} = p_{out,i} - p_{in,i} + \Delta p_{friction,i} + \Delta p_{loc} \quad (3.2)$$

$$A \cdot l_i \cdot \rho_i \cdot c_{v,i} \cdot \frac{dT_i}{dt} + \dot{m}_{out,i} h_{out,i} - \dot{m}_{in,i} h_{in,i} = \dot{Q}_{m \rightarrow f,i} \quad (3.3)$$

where subscripts in/out stand for inlet/outlet,  $\dot{m}$  is the mass flow rate,  $p$  is the pressure,  $T$  is the temperature,  $\Delta p_{loc}$  are the localized pressure drops,  $\Delta p_{friction}$  are the pressure drops by friction along the channels,  $h$  is the specific enthalpy,  $\dot{Q}_{m \rightarrow f,i}$  is the power transferred to the helium,  $A$  and  $l$  are, respectively, the cross-sectional area and length of the channel,  $\rho$  is the fluid's density and, finally,  $c_v$  is the specific heat. The time-dependent term of eq. (3.1) can be simplified thanks to the assumption of incompressibility discussed above, the time-dependent term of eq. (3.2), instead, cancels out because of the mass flow rate is constant in the case of normal operating conditions, while the one in eq. (3.3) is neglected because of the quite large difference between the heat capacity of helium with respect to the one of EUROFER.

In normal operating conditions, pressure losses (appearing in equation (3.2)) are computed with a simplified expression, in order to allow much faster solutions. They are obtained with a simple linear expression, as following:

$$\Delta p_{friction/loc} = \Delta p_{nom} \cdot \frac{\dot{m}}{\dot{m}_{nom}} \quad (3.4)$$

where  $\dot{m}_{nom}$  is the nominal mass flow rate and  $\Delta p_{nom}$  is the nominal pressure drop inside the component. As reported in [22], the error induced by this simplification is always smaller than 5% during nominal operation. However, this is not true in the case of an accidental transient, such as a LOFA. In view of this, the model used for this thesis work computes the pressure

losses with the more suitable Darcy-Weisbach equation, using for the friction factor a correlation specifically developed for the FW channels (presented in chapter 4, section 4.1.1.). The pressure loss with Darcy-Weisbach equation is computed as:

$$\Delta p_{friction,DW} = f_D \cdot \frac{L}{D} \cdot \frac{\rho u^2}{2} \quad (3.5)$$

where  $f_D$  is the Darcy friction factor,  $L$  is the pipe length,  $D$  is the hydraulic diameter and  $u$  is the fluid flow average velocity.

As mentioned above, components like manifolds, heat exchangers and circulators are modeled as 0D objects. In this case, mass and energy conservation equations are solved:

$$V \cdot \frac{d\rho}{dt} = \dot{m}_{in} - \dot{m}_{out} \quad (3.6)$$

$$V \cdot \frac{d(\rho e)}{dt} = \dot{m}_{in} h_{in} - \dot{m}_{out} h_{out} + \dot{Q}_{m \rightarrow f,i} \quad (3.7)$$

where  $e$  is the internal energy of the fluid and  $V$  is the volume of the component. In this case too, the mass balance equation can be simplified by removing the time dependent term (on the LHS) due to the incompressibility of the flow.

Solid objects, made of EUROFER97, are thermally coupled with the 1D fluid objects describing the FW cooling channels; thus, 1D FV energy equation is solved as following:

$$A_m \cdot l_i \cdot \rho_m \cdot c_m \cdot \frac{dT_{m,i}}{dt} = \dot{Q}_{in,i} - \dot{Q}_{m \rightarrow f,i} \quad (3.8)$$

where subscript  $m$  refers to the EUROFER and  $\dot{Q}_{in,i}$  is the power entering the volume. The power transferred to the fluid, instead, is computed taking into account the heat transfer coefficient between solid and fluid, according to:

$$\dot{Q}_{m \rightarrow f,i} = \Omega \cdot l_i \cdot HTC \cdot (T_{m,i} - T_i) \quad (3.9)$$

where  $HTC$  is the heat transfer coefficient and  $\Omega$  is the heated perimeter. Since the solid model is described by FVs, the temperature  $T_{m,i}$  computed by the code is obviously an average temperature inside each volume  $i$ . This means that, using this model, we can find the FV of the BB in which, on average, the solid material reaches the highest temperatures, but no information about the value and location of the hot-spot temperature can be deduced; this could negatively affect the analysis in border-line cases, where the FV average temperature is below the upper limit for the material, while in reality there is an hot-spot that exceeds it. For EUROFER this upper limit is 550°C: over this temperature, a severe loss of its creep strength is observed [31]. However, in [22] is presented a method that postprocesses the GETTHEM results to reconstruct the hot-spot temperature, by simply applying a peaking factor determined by looking at detailed temperature distributions obtained by 3D CFD analysis (described in [28]).

### 3.2.4. GETTHEM model components

The HCPB BB GETTHEM model is made of different modules. The Breeding Module (BM) object has inside of it a model for the FW, a model for the BZ, a model for the cap, which is the rooftop of the BM, and models for the inlet/outlet manifolds. The tungsten armor that covers the FW, instead, has been neglected, due to the small effect it would have on the maximum temperature (less than 1%). Similarly, also the NMM and breeder material pebble bed layers are not modeled, as, in view of the increase of computational costs and complexity of the model, the effect on the results would not have been significant for the scope of the model [29].

The manifolds are modeled as simple 0D objects, according to equations (3.6) and (3.7), because, due to their geometry and to the presence of many inlets and outlets, the helium flow inside of them does not fully develop. The only input for these objects is the manifold volume, since heat loads and pressure losses can be neglected.

Since the GETTHEM code has been developed following what, back then, was the latest EU DEMO reference design, namely the DEMO BL2015, the BZ object was originally based on the metallic Cooling Plates (CPs) concept, rather than the latest fuel pin concept. Figure 3.3 shows a sketch of the CP object.  $\text{Li}_4\text{SiO}_4$  and Be pebble beds layers between adjacent CPs are neglected, so there is no heat transfer between one plate and another.

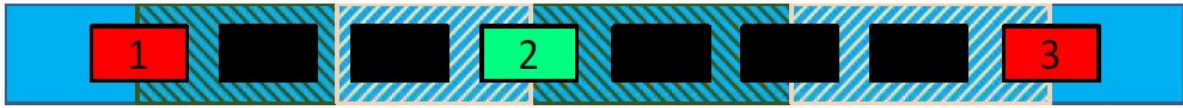


Figure 3.3: Cross-sectional view of a CP. The division of solid wall objects between adjacent channels is highlighted [29]

While the two caps and the BZ components are cooled in parallel, for the FW two different cooling schemes were modeled: an Integrated (HCPB-I) scheme, in which the coolant flow is initially distributed to the FW by the circulator, and then collected and redistributed towards the CPs, and a Separated (HCPB-S) scheme, where the FW has two additional cooling loops independent from the ones dedicated to the BZ. Figures 3.4 and 3.5 below show the BM objects for both cooling schemes. This thesis work uses a model (described later in this chapter) with an hydraulic scheme similar to the HCPB-I, with the FW objects connected in series to the BZ, although it has a simplified BZ object without caps.

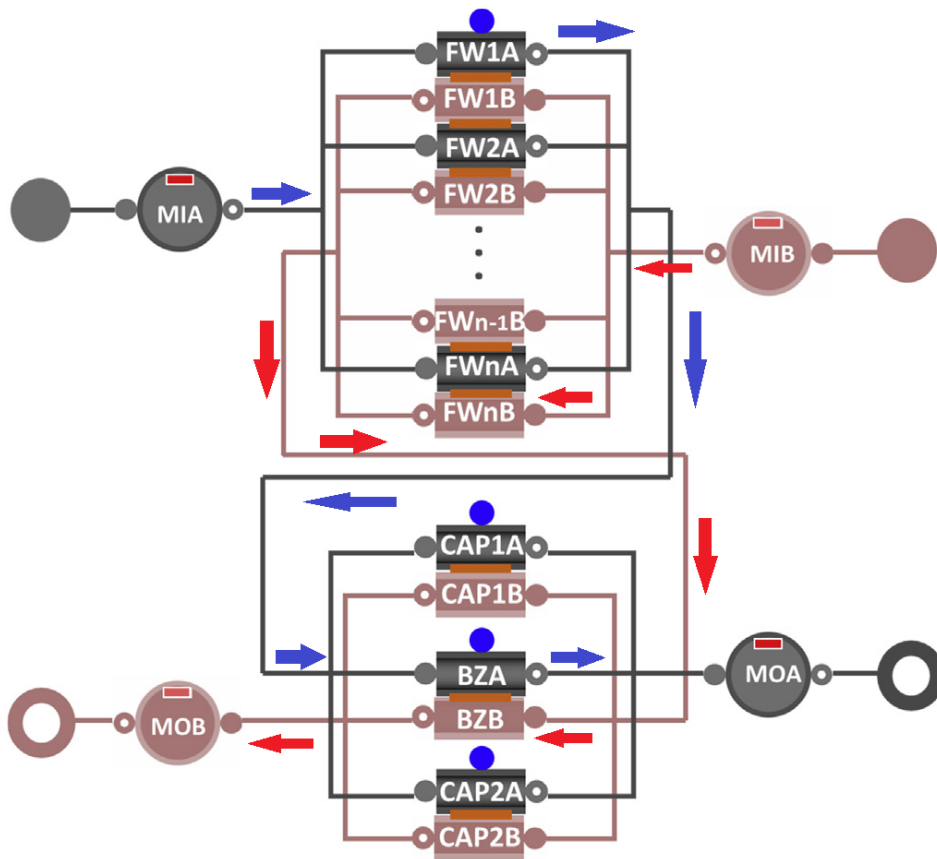


Figure 3.4: BM object for the HCPB-I cooling scheme (adapted from [23]).

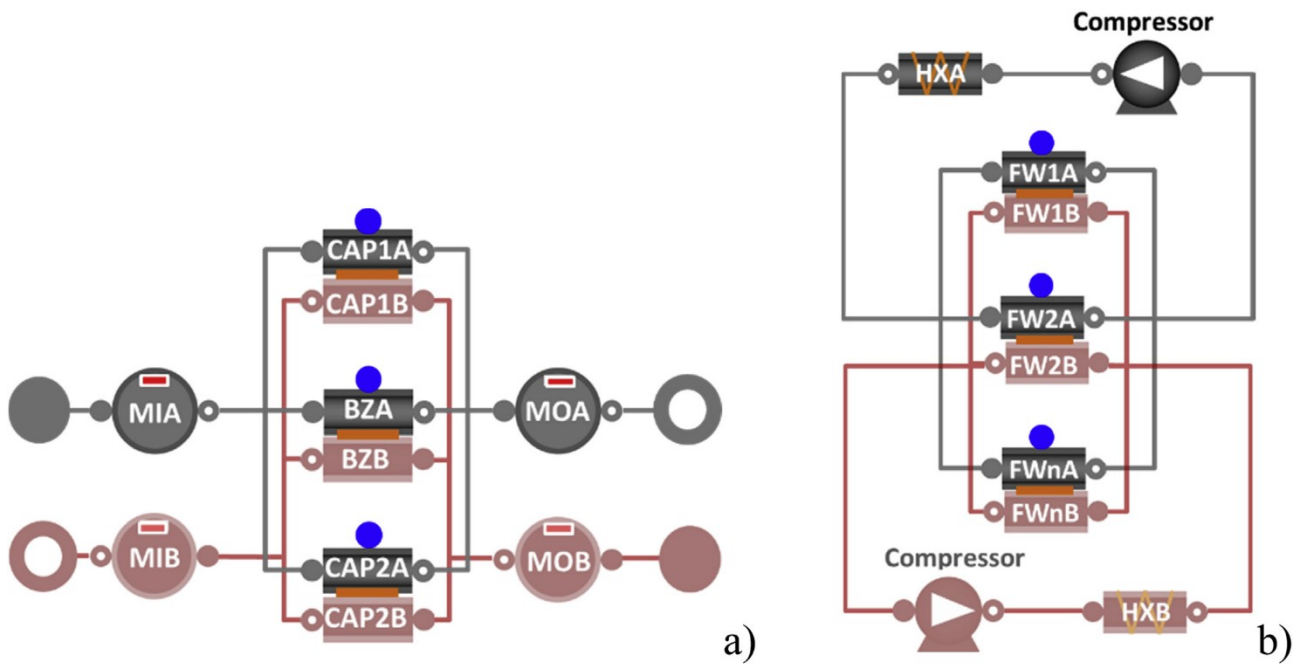


Figure 3.5: BM object for the HCPB-S cooling scheme: a) BZ and caps cooling loops; b) FW cooling loop, with ex-vessel components (heat exchanger and circulator) [23].

Figure 3.4 shows a FW object, composed by many FW square channels connected to each other thanks to connectors; each channel is thermally coupled with his neighboring channels, according to a counter current flow scheme. A single FW channel, showed more in detail in figure 3.6, consists in three channels connected in series: there is a front part, exposed to the plasma, and two side parts which run radially inside the blanket. Each one of the three channels is modeled as a 1D flow object with connectors for the thermal coupling with neighboring channels and connectors for power inputs. In particular, all the three parts are heated by a volumetric heat load, due to nuclear reactions inside the solid structures, and by conduction from the BZ, while only the front part is heated also by the plasma surface load on its plasma facing side. The bends between front and side parts are taken into consideration only as 0D localized pressure drops.

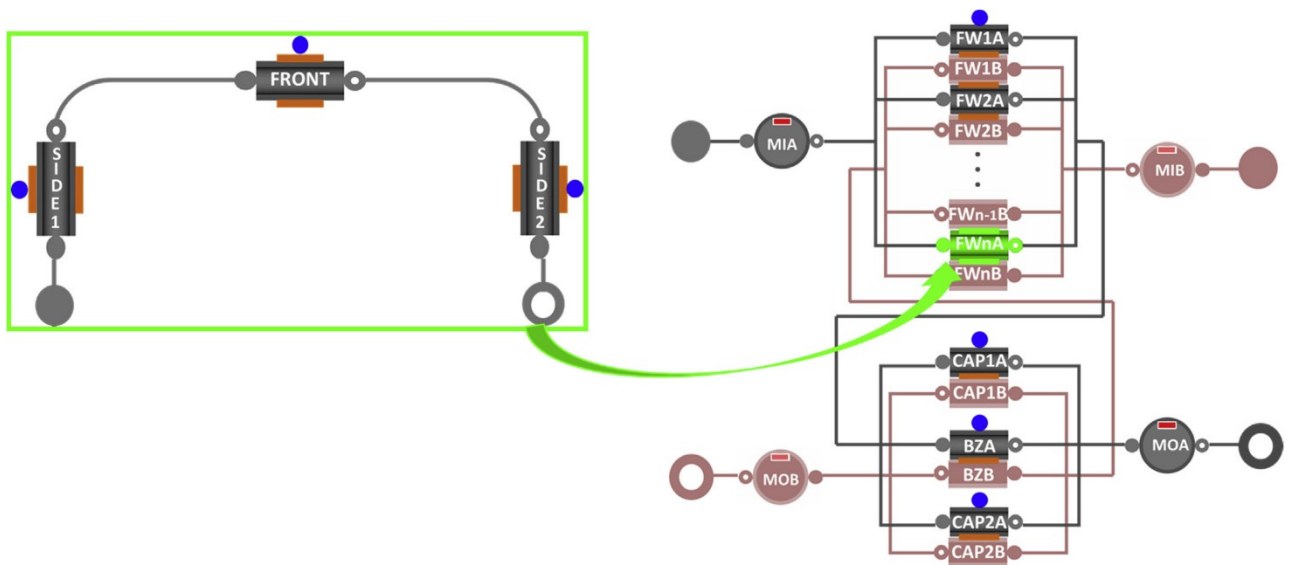


Figure 3.6: schematic view of a FW channel object; the orange rectangles are the connectors for thermal coupling with neighboring channels, and blue circles are the heat loads input connectors.[23]

As for the CP model, also FW solid structures are modeled as lumped 1D walls of the cooling channel. In particular, the EUROFER volume between two adjacent channels is split into two halves, each one of them is cooled by the helium flowing in the closest channel. Thus, as shown in figure 3.7, each square channel is surrounded by two solid models, each one discretized as a 1D FV object, where connectors are there to allow thermal coupling with the channel above, for the wall's upper half, and with the channel below, for the wall's lower half.

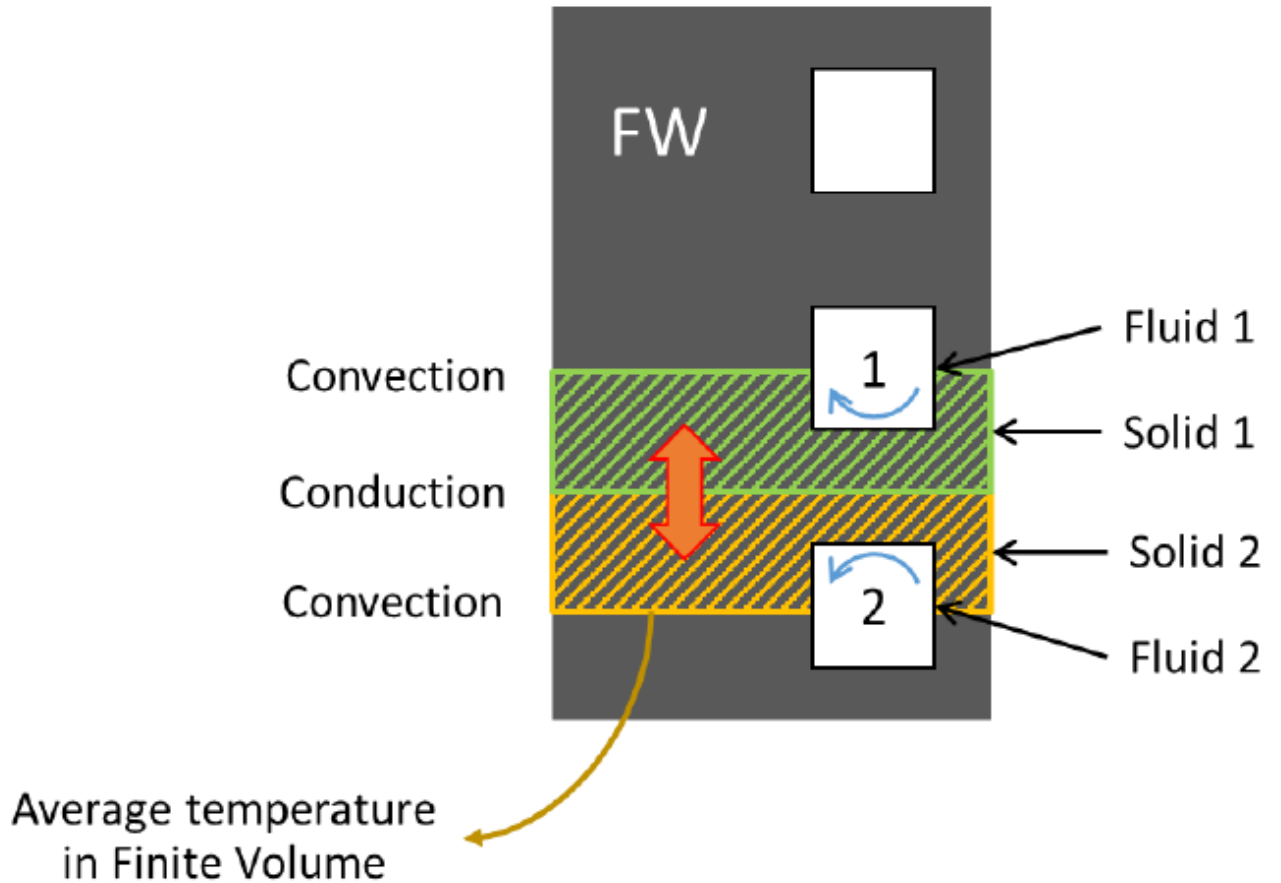


Figure 3.7: FW solid object: interface between neighboring channels; heat transfer mechanisms between solid- solid and solid-fluid are highlighted. [22]

In each solid volume, equations (3.8) and (3.9) are solved, and the wall thermal conductance is computed as  $k_m/l_{\perp,m}$ .  $k_m$  is the thermal conductivity of EUROFER, while  $l_{\perp,m}$  is the length perpendicular to the helium flow, in the direction of the coupling between two solid volumes. The wall heat capacity is written as  $c_m V_m \rho_m$ , where the quantities appearing in the expression are, respectively, the specific heat, the volume of the FV and the density of the solid. Finally, equation (3.5) is used to compute the actual pressure drop inside each channel, giving as input the nominal values of mass flow rate and pressure drop. Table 3.1 summarizes the input parameters for the FW object.

Table 3.1: Input parameters for the FW object (adpted from [22]).

<b>Name</b>	<b>Description</b>	<b>Type</b>	<b>Unit</b>
<b>Nch</b>	Number of cooling channels	Scalar	-
<b>Nv</b>	Number of FVs in each part of each channel	Scalar	-
<b>dpnom</b>	Nominal pressure drop	Scalar	Pa
<b>wnom</b>	Nominal mass flow rate	Vector (Nch elements)	kg/s

<b>lambda</b>	Heat transfer coefficient	Scalar	W/(m <sup>2</sup> K)
<b>Ls</b>	Length of the side part of each channel	Vector (Nch elements)	M
<b>Lf</b>	Length of the front part of each channel	Vector (Nch elements)	M
<b>Gs</b>	Thermal conductance of side channels' wall	Vector (Nch-1 elements)	W/K
<b>Gf</b>	Thermal conductance of front channels' wall	Vector (Nch-1 elements)	W/K
<b>A</b>	Cross sectional area of the channel	Vector (Nch elements)	m <sup>2</sup>
<b>Cm,s</b>	Heat capacity of side channels' wall	Vector (Nch elements)	J/K
<b>Cm,f</b>	Heat capacity of front channels' wall	Vector (Nch elements)	J/K

The input power  $\dot{Q}_{in,i}$  entering each solid FV, due to nuclear reactions in the solid or heat flux coming from the plasma, represents the thermal driver for the FW model. Starting from the total heat load of the BB, it is distributed to the FW object, in terms of Watts, through a time-dependent 2D array made of (Nch,  $3 \times Nv$ ) elements.

Once defined the main objects, the complete GETTHEM model for the HCPB PHTS is built by adequately assembling together all the objects. Among the FW cooling options, the one used also for this thesis work is the Integrated HCPB: figure 3.8 shows the system-level GETTHEM HCPB model for the PHTS, featuring the HCPB-I cooling scheme. In this case, two loops (red and blue in figure 3.8) feeds, with a counter current flow scheme, 7 BMs each; the twin circuits are coupled at the BM level, and BMs are connected in parallel between the inlet and outlet manifolds, which link the BB with the ex-vessel part of the loop. The latter is simply made by an ideal HX (simply modeled as a 1D fluid channel), doing the job of what in the actual system is a steam generator<sup>1</sup>, and a circulator, whose model is taken from the aforementioned ThermoPower library.

<sup>1</sup> Since the model is focused mainly on the thermal hydraulic behavior of the BB, a detailed model for the steam generator is unnecessary.

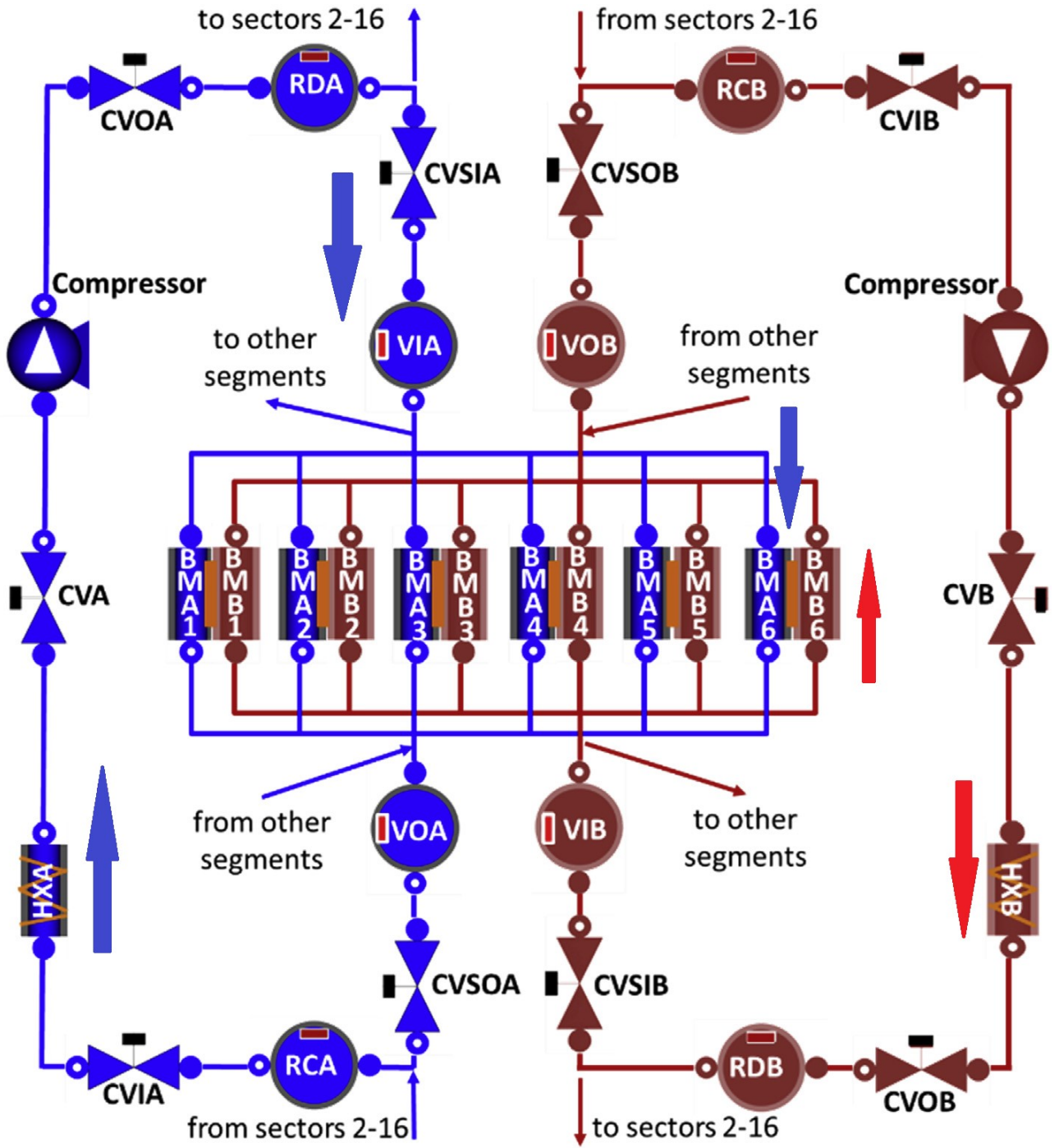


Figure 3.8: View of the GETTHEM HCPB cooling model. The blue and red arrows highlight the counter-current flow path between the twin circuits at the BM level (adapted from [23]).

### 3.3. Description of the model used for this thesis work

The scope of this thesis work is to analyze parametrically the effect and possible mitigations of a LOFA accident, with a model that allows fast-running simulations of the thermal-hydraulic behavior of the HCPB BB PHTS. In view of this, the model used for the simulation is widely based on the GETTHEM HCPB model (HCPB-I cooling scheme option), with some adjustments and simplifications to better adapt to the analysis of a LOFA and, at the same time, further reducing the computational cost of the simulations.

The main part of the model is the FW object: being the closest component to the plasma, the FW is the region more affected by an accidental scenario such as a LOFA, experiencing, in its solid structures, the largest temperature increase. To this aim, the FW channel object developed for the GETTHEM code (see figure 3.6) is used, because of its good level of detail for the fluid channel (divided into front and side parts) and the EUROFER97 walls surrounding it, both modeled with 1D FVs objects.

Regarding the BZ, the CP model was obsolete due to the changes apported with the EU DEMO BL2017 design, where radially arranged fuel pins have been introduced for the breeding zone (described in chapter 2). Hence, the fuel pins have been modeled as two 1D FV fluid objects, one for the cylindrical inner pin at the inlet and the other for the annular outer pin at the outlet, cooled by the helium flow coming from the FW channels, according to a connection in series between FW and BZ regions. In the real system, the space between inner and outlet pins is filled with  $\text{Li}_4\text{SiO}_4$  pebbles, and all the fuel element is inserted in a beryllium pebbles matrix. However, in addition to not providing metal walls to the channel (differently from the channels of the CP object), the BZ object neglects the NMM and breeder material pebbles as well; the reason behind this choice is due to the assumption that, at the expense of a more complex and computationally heavy model, the effect on the EUROFER temperature inside the FW would be low. This can also be justified by the fact that, as already mentioned above, the most critical region of the BB is the FW, therefore the model is mainly focused on its behavior, trying to keep the rest of the components as simple as reasonably possible to facilitate fast-running simulations. Nevertheless, the heat transferred from the BZ to the FW solid structures, through heat conduction, has been taken into account. As a matter of fact, the 8% of the volume load generated inside the BZ is given as an input power term for the FW solid volumes.

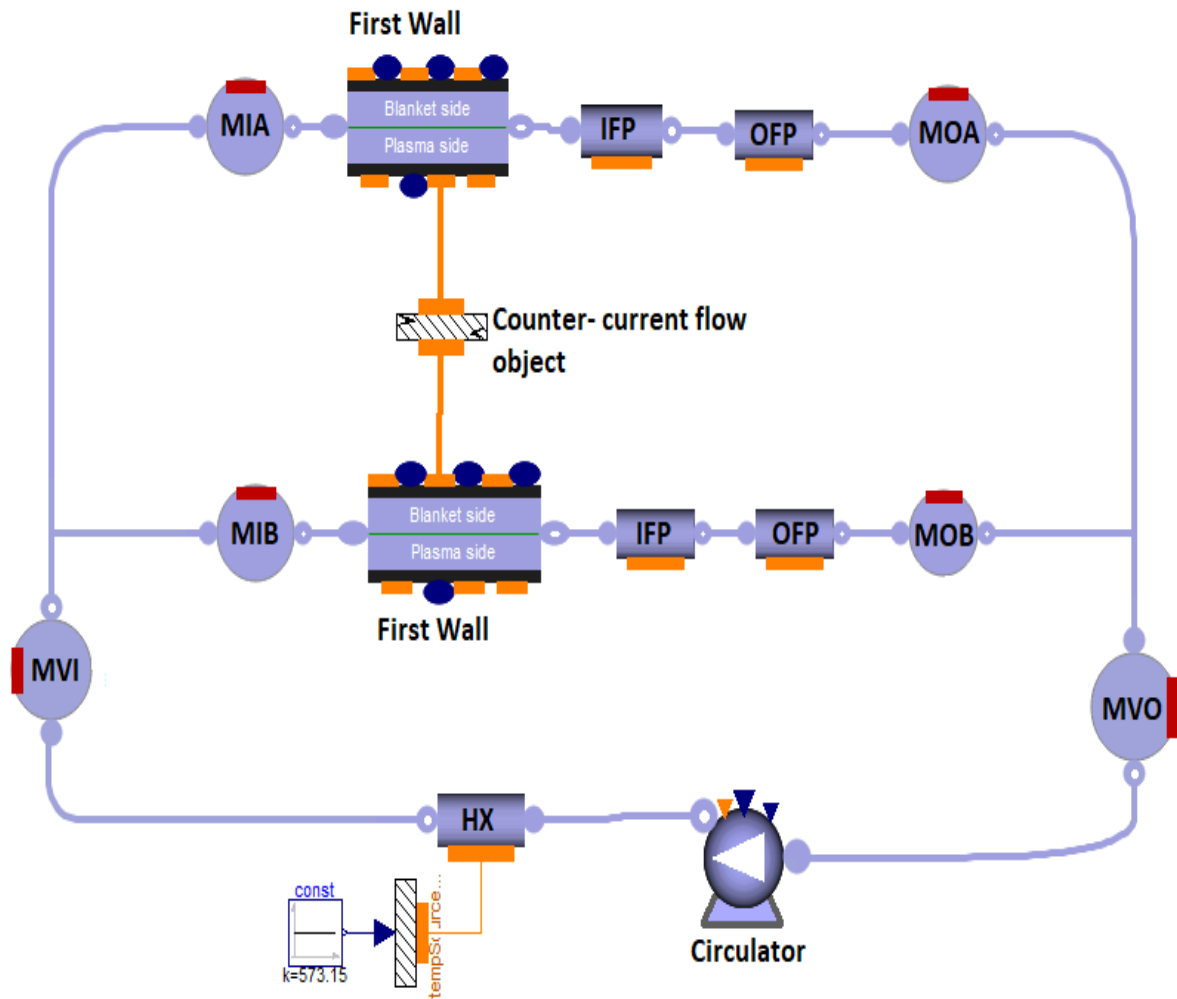


Figure 3.9: Sketch of the Dymola diagram view of the HCPB cooling loop model; IFP/OFP: Inner/Outer Fuel Pin; HX: Heat eXchanger; MVI/MVO: Inlet/Outlet Mixing Volume; MI/MO: Inlet/Outlet Manifold; A/B: branches A and B.

In figure 3.9 is reported a simplified sketch of the model’s diagram view produced, showing the main components of the model and their integration inside the cooling loop. The lower branch represents the ex-vessel part of the cooling loop: it features two plenum objects (MVI/MVO) which redistribute and collect helium to/from the BB, a circulator, and an HX. The circulator object, updated from the ThermoPower Fan model, has two important connectors used for the simulations: one for the input value of the angular velocity of the rotor, and the other one for the input number of circulators in parallel. The HX, instead, is a simple ThermoPower flow1DFV object, where the heat port is connected to a temperature source fixed at the value of 300°C (which is the design inlet coolant temperature of the BB).

The cooling train (i.e., heat exchanger and circulator) then feeds the BB, which is modeled by two identical branches (A and B in figure 3.9) connected in parallel. Similarly to the twin circuits of the GETTHEM model shown in figure 3.8, these two branches are needed to easily couple neighboring FW channels with a counter current flow scheme, by means of a ThermoPower object called CounterCurrentFV. In figure 3.9 only one of these objects is shown, but in the actual model there is one for each couple of FW thermal ports (for instance, the inlet-side channel walls of channel 1 are connected to the outlet-side channel walls of

channel 2 thanks to two CounterCurrentFV objects, and so on for the others). Also, this component is a 1D FV element that has the same number of volumes of the channels it is connected to.

Finally, while the complete HCPB GETTHEM model includes an entire BB segment (which was made of 6 instances of the BM object, according to the previous MMS design of the blanket), the model used in this work is made only by 8 subsequent FW channels, divided among the 2 FW objects and contained in the same BB segment (which, according to the latest DEMO BL2017-v2, follows the SMS architecture). A reason behind this choice is to have the possibility to perform extremely fast-running simulations, which lasted no more than few minutes each, allowing to simulate parametrically different scenarios with a limited computational cost. However, the results of the simulations can be extended to the whole tokamak; in fact, the nature of the LOFA accident scenarios considered is such that the consequences (i.e., the variations of temperature, pressure, mass flow etc.) of such accident are homogeneous on the FW channels involved. For instance, if a trip of a circulator occurs, it will affect the mass flow rate (and, therefore, also the heat transfer between helium and EUROFER) of different FW channels in the same way, since they are all fed in parallel by the same circulators. Hence, it is possible to analyze the effect on different poloidal regions by simply varying the input data regarding geometry and heat loads. An exception is represented by the scenario of a LOFA due to a channel obstruction; in this case the accident is localized, and obviously the consequences are more relevant near the obstruction. However, the results (see next chapter) show that the effect of the accident is uniformly distributed among the other channels, thanks to the large thermal conductivity of the EUROFER solid structures.

# Chapter 4

## 4. Simulation scenarios and results

### 4.1. Introduction

The model described in section 3.3, based on the GETTHEM code for the HCPB BB cooling loop, is used to simulate the thermal-hydraulic behavior of the BB FW under the accidental scenario of a LOFA. As the name suggests, a *Loss of Flow Accident* is a transient situation where the cooling flow (which is gaseous helium in this specific case) is partially or, worse, totally compromised, endangering the heat removal from the in-vessel solid structures of EUROFER97.

It is clear that the severity of the accident depends on the Initiating Event (IE) occurred; the worst case is represented by the trip of both the circulators of a single cooling loop, leading to a so-called total LOFA, where there is a complete loss of the circulating power, while milder flow reductions happen in the case of a single circulator trip or, even milder, in the case of obstruction of one or more FW channels. However, these last two cases are not to be underestimated since a late detection of the accident, and consequently a late intervention of the mitigation system (i.e., plasma shutdown), could still cause a dangerous overheating inside the FW and lead to failure of solid structures.

The simulations carried out are focused on the three scenarios mentioned above:

- *total LOFA*: initiated by a loss of off-site power or by a trip of both circulators, this scenario is simulated by gradually decreasing toward zero the angular velocity at which the ThermoPower Fan object works;
- *partial LOFA*: initiated by the trip of one of the two circulators, it is simulated by including in the model two Fan objects connected in parallel at from time zero, and then, at the time chosen for the onset of the accident, reduce the number of circulators to one (thanks to a dedicated input connector) in order to simulate the failure of one of them;
- *single FW channel obstruction*: this scenario, which is also a partial LOFA, is implemented by adding a new FW channel, thermally coupled to the first of the eight channels already modeled, connected in parallel to the others according to a counter-current flow scheme. This additional channel is put in series with a valve (whose ob-

ject is taken from the ThermoPower library); by simply closing the valve, either partially or completely, it is possible to simulate an obstruction in the channel.

Moreover, each scenario is simulated according to two different hypotheses regarding the mitigation system:

1. *Case I*: the accident is not detected, or the mitigation system fails to intervene. This situation is the most threatening as the plasma is not shut down; the power coming from fusion reactions will still heat up the BB solid structures which, due to the accident, are no longer appropriately cooled by the helium flow, leading to a severe temperature increase;
2. *Case II*: this time the loss of flow is detected, and the plasma is immediately shut down. In this case the power input is limited to the decay heat inside the solid volumes (which, in the model, is accounted for by the 2% of the total volumetric heat load), balancing the negative effect on the heat removal caused by the helium flow reduction.

### 4.1.1. Input data

Before going into detail on the different scenarios simulated, it is necessary to define the input data used for the model implementation.

Since during a LOFA the system will undergo significant temperature and pressure variations, helium and EUROFER97 thermophysical properties cannot be simplified as constants. Helium properties are simply taken from the ideal gas model from the Modelica Standard Library, with NASA coefficients, as it was for the HCPB GETTHEM model for a LOCA (mentioned previously in section 3.2.2). EUROFER97 properties, instead, come from the library “MaterialProperties” implemented inside the GETTHEM model for the EU DEMO reactor: here, density, heat conductivity and specific heat capacity of EUROFER97 are expressed as polynomial functions of the temperature inside the solid. These are empirical expressions obtained from experimental data collected by several research groups from all over the world during the last years (in [33], the experimental procedure and the results regarding the thermal, electrical and magnetic properties of EUROFER97 are presented). Table 4.1 presents the thermophysical properties of the material in a range of temperatures from 20 to 700 °C, from the material properties handbook on EUROFER97 [34].

Table 4.1: EUROFER97 thermophysical properties in the range of temperatures between 20 and 700 °C (from [34]).

$T [^{\circ}\text{C}]$	$\rho \left[ \frac{\text{kg}}{\text{m}^3} \right]$	$c_p \left[ \frac{\text{J}}{\text{kg K}} \right]$	$\lambda \left[ \frac{\text{W}}{\text{m K}} \right]$
20	7750	448	31.5
100	7753	460	32.2
150	--	477	--
200	7713	494	32.7

250	--	510	--
300	7685	527	33.2
350	--	544	--
400	7655	565	33.3
450	--	586	--
500	7625	611	32.8
550	--	644	--
600	7594	682	32.3
650	--	728	--
700	--	866	44.8

Geometrical data for the FW object are the ones used for the HCPB GETTHEM model for DEMO nominal operating conditions. Remember that the FW object models square cross-section cooling channel, divided in two side parts and a plasma-facing part, which are surrounded by EUROFER97 solid walls; hence, the dimension of the channel (cross-section side and length) and the thickness of the walls should be defined. For the inlet and outlet fuel pin channels, instead, data have been taken from the 2019 Final Report on the HCPB design [15]. In table 4.2 the geometrical data used for the simulations are summarized, including the inlet and outlet manifold total volumes, which, in the model, have been scaled down coherently with the choice of modeling only eight FW channels.

Table 4.2: HCPB BB Geometrical data; first wall and manifolds data are taken from [23], while fuel pins data from [15]

<b><i>First Wall</i></b>	
Length of the side parts [mm]	649.6
Length of the front part [mm]	1120.5
Channel cross section side [mm]	13.5
Cross section area [mm <sup>2</sup> ]	13.5 × 13.5 (square cross section)
Wall thickness (plasma facing side) [mm]	2.625
Wall thickness (blanket facing side) [mm]	5.375
Number of nodes for the fluid thermal variables [-]	5
Number of FVs on the wall interface [-]	4
<b><i>Fuel pins</i></b>	
Length of the fuel pin [mm]	800

Inlet pin diameter [mm]	16
Inlet cross section area [mm <sup>2</sup> ]	$\pi \times 16^2$
Outlet pin inner diameter [mm]	66
Outlet pin outer diameter [mm]	70
Outlet cross section area [mm <sup>2</sup> ]	$\pi \times (70 - 66)^2$
<b>Inlet/Outlet manifolds</b>	
Inlet volume [m <sup>3</sup> ]	0.171
Outlet volume [m <sup>3</sup> ]	0.0713

For the FW object, different correlations are used to compute the Heat Transfer Coefficient (HTC) and the Fanning friction factor, due to the fact that, while the inner surface of the channels in the side parts is smooth, in the plasma-facing wall of the front side the channel is considered to be ribbed to improve the heat transfer with the solid (as explained in [23]). For this reason, two different correlations for the Nusselt number are used, which are obtained in [23] from the data in [35, 36] For the side channel parts and for the non-plasma-facing wall of the front channel part, the Nusselt correlation for smooth FW ducts is:

$$Nu_{smooth} = 0.334 \cdot Pr^{0.4} \cdot Re^{0.556} \quad (1)$$

where Pr and Re are the Prandtl and Reynolds dimensionless numbers, respectively.

For the ribbed plasma-facing wall of the front channel part, instead, the Nusselt number is computed as:

$$Nu_{ribbed} = 0.05533 \cdot Re^{0.749} \quad (2)$$

Finally, from the definition of the Nusselt number, the HTC is computed as:

$$HTC = \frac{k}{D_{hyd}} \cdot Nu \quad (3)$$

where  $k$  is the heat conductivity and  $D_{hyd}$  is the hydraulic diameter, which in the case of a square channel coincides with the square side length.

Also for the calculation of the Fanning friction factor, two different correlations are used; in the ribbed front part of the channel the correlation for the friction factor is obtained, again, by the data in [35, 36], and it is:

$$f_{ribbed} = 0.1122 \cdot Re^{-0.1854} \quad (2)$$

For smooth side channels, instead, the Fanning friction factor correlation used is the Blasius one, which can be found in [37].

## 4.2. LOFA scenarios

As already mentioned previously, the EU DEMO reactor will operate with a pulsed regime. This is due to the nature of the plasma current, which, thanks to the transformer principle, is induced by an increasing monotonic electric current flowing in the CS; since this current cannot be increased indefinitely, this means that the machine must have a pulsed operation.

DEMO operation, as far as currently envisaged, should consist of a 2-hours-long burning plasma phase followed by 40 minutes of dwell time, for a total of 9600 seconds each period. Concerning the simulations, it follows that the heat load input, delivered to the FW object solid walls, must be provided during the plasma burning phase only. In figure 4.1 the heat load pulsed shape is plotted.

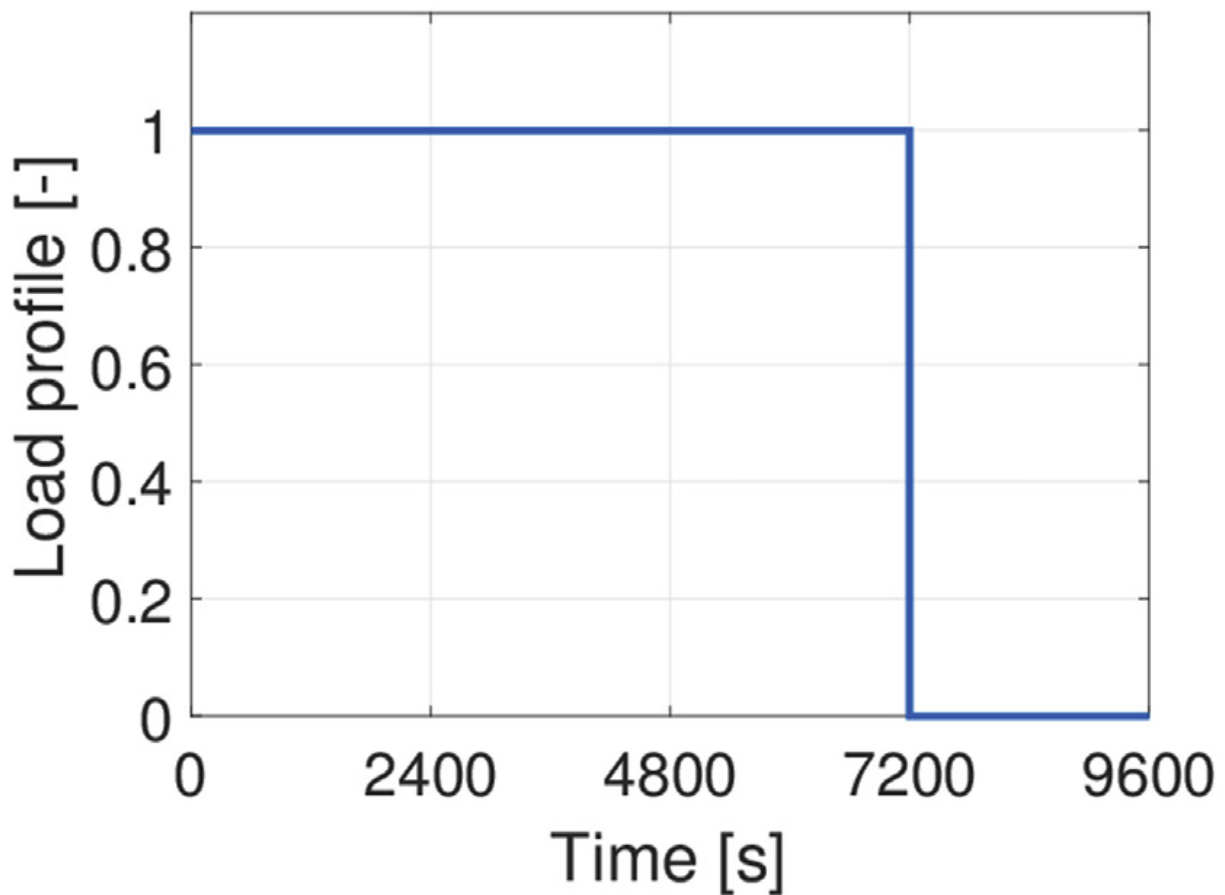


Figure 4.1: Heat load pulsed profile (1 period) applied to the FW object solid walls. [23]

In figure, the heat load goes to zero during the dwell phase; in reality, this is true only for the heat flux hitting the plasma facing wall, while a small fraction of the volumetric heat generation inside the solid structures still survives, due to the decay heat. The latter, in the model, is assumed to be equal to the 2% of the total volumetric heat generation inside EU-ROFER.

## 4.2.1. Normal operating conditions

Before simulating an accidental scenario, it is useful to show what is the thermal hydraulic behavior of the cooling loop in normal operating conditions, in order to better assess the severity of an accidental scenario by comparing it with the nominal pulsed operation of the reactor.

Hence, the model is now simulated with a load profile as shown in figure 4.1, without the intervention of the mitigation system (plasma shutdown), and with the circulators continuously providing the nominal circulating power to the helium flow, guaranteeing an adequate BB cooling during a whole period of 9600 seconds (plasma burn and dwell time).

Figure 3.9 shows that the model of the BB cooling loop features two parallel branches for the in-vessel components, for the reasons already discussed in section 3.3. The two branches are exactly equal to each other, concerning both their architecture and the drivers they are subjected to (i.e., the input heat loads in the solid structures), hence the results obtained by simulating this model are the same for both the FW objects. In view of this, the results plotted from here on are referred to one FW object only, to keep the figures more comprehensible.

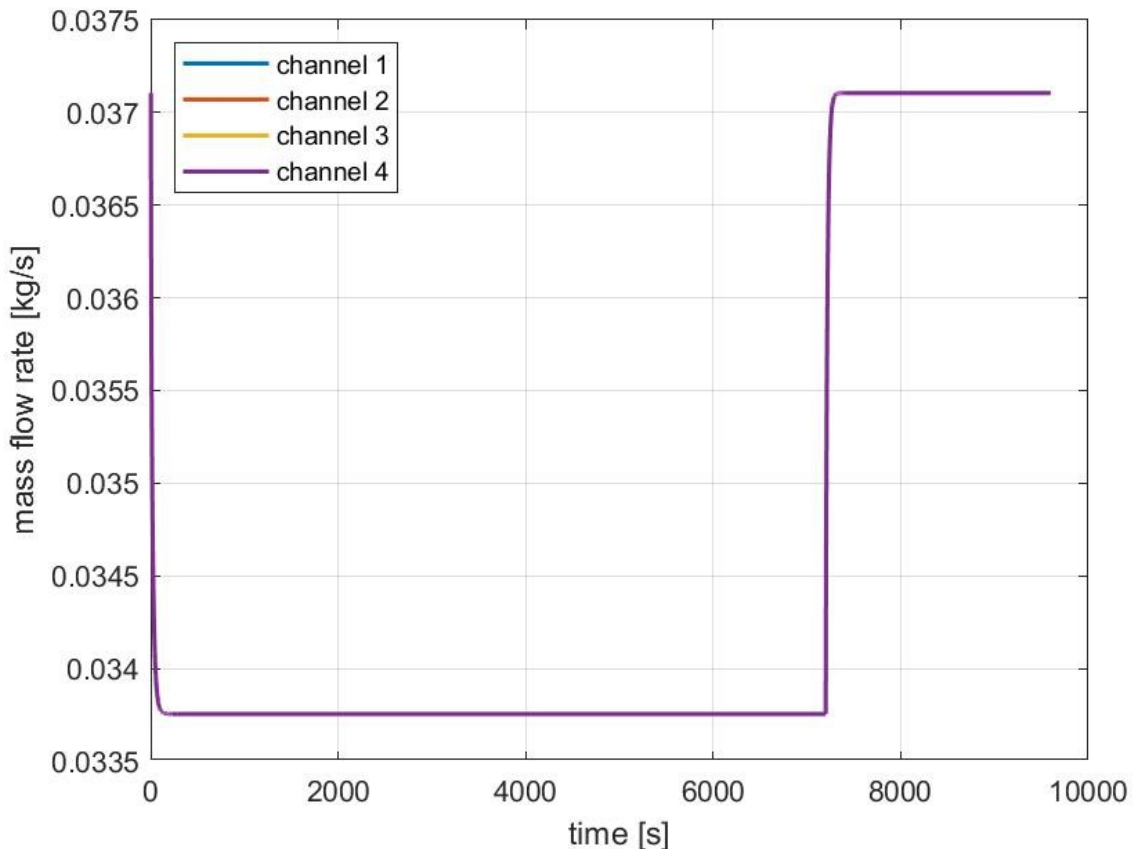


Figure 4.2: Helium mass flow rate time evolution in the front part of each FW channel; Normal Operating Conditions (NOC).

In figure 4.2 above, the mass flow rates inside the four different FW channels are highlighted. The results plotted refers to the mass flow rate in the front side but, due to the conservation of the mass, it is the same in the other FW channel portions (i.e., the side parts). The initial condition for the input power is set equal to zero; when the simulation of the model starts, the power is applied, and, as a consequence, the raise of the temperature (and, hence, the change of the density) causes the system to move to a new stationary operating point within a hundred seconds. When the new operating point is reached, the mass flow rate in each FW channel settles at the value of  $33.76 \text{ g/s}$  throughout the entire plasma burn phase. When the plasma is shut off, after 7200 s, the mass flow rate rapidly increases reaching a new stationary value of  $37.11 \text{ g/s}$ ; this increase is a consequence of the loss of the plasma heating, which induces an increase in the helium density (due to the lower temperatures) and, hence, a greater mass flow rate. Moreover, the curves referring to the four different FW channel overlaps one another, meaning that the total mass flow rate redistributes uniformly between the channels. This result was in line with expectations, since the channels are connected in parallel and have the same geometry.

The cold helium coolant entering the FW, flows through the inlet side, front side and outlet side of the channel in series, removing heat from the solid structures along its path, and exits as hot helium. In figure 4.3 below, the helium temperature along the FW is shown.

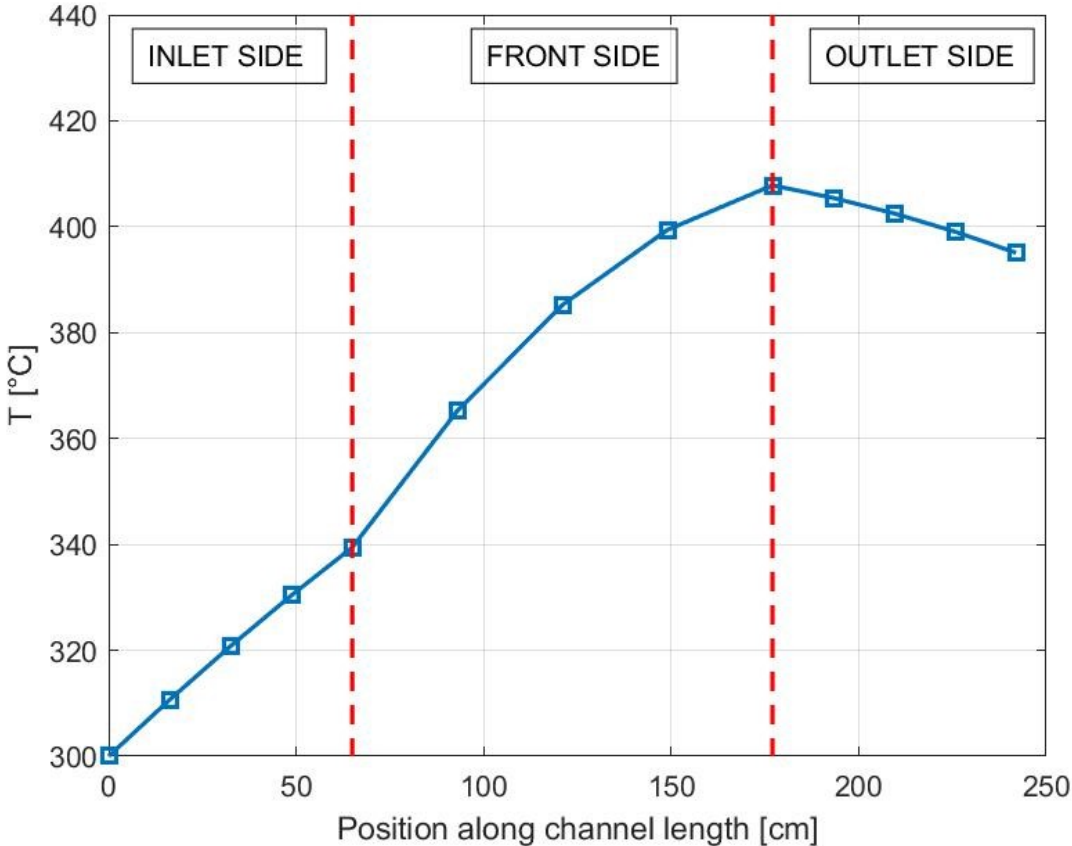


Figure 4.3: Helium temperature distribution along the FW channel length at time  $t=350 \text{ s}$  (in NOC); the squares represent the values computed in each fluid node; Inlet/Front/Outlet sides are separated by dashed red lines.

The temperatures plotted refers to the first channel, however they are the same also for the other three channels in parallel since the mass flow rates, geometry and thermal drivers are identical.

Looking at the figure, a first peculiarity is immediately noticeable: while one could expect a continuous temperature increase along the path, helium actually cools down along the outlet side of the channel (even though only slightly w.r.t. the overall temperature increase in the first two parts of the channel). This counterintuitive behavior is due to the counter-current flow scheme between neighboring channels; as a matter of fact, the outlet side walls of a channel are thermally coupled with the walls belonging to the inlet part of the two neighboring channels, where helium, and as a consequence the walls too, are still “cold”. For this reason, the outlet side solid walls are actually at a lower temperature with respect to the helium flowing inside them, thus the heat is transferred from the coolant to the solid.

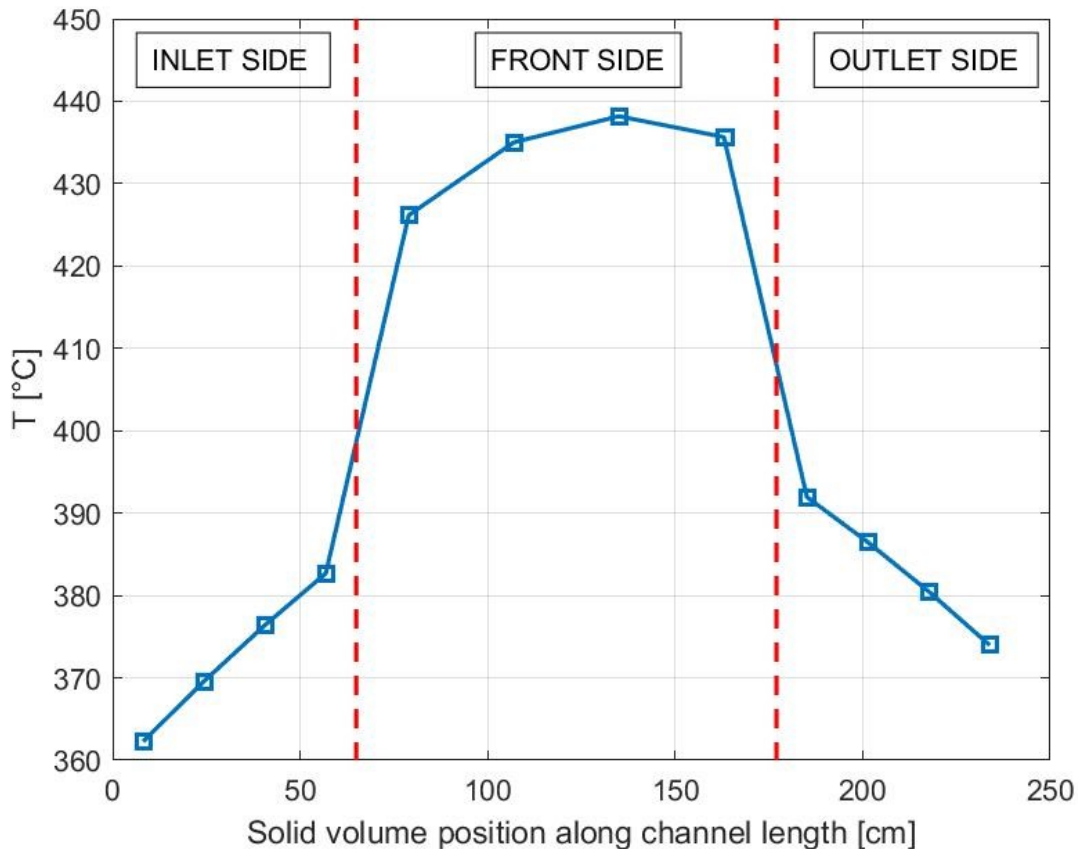


Figure 4.4: EUROFER97 temperature distribution along the FW channel length at time  $t=350$  s (in NOC); squares represent the value computed in each solid volume; Inlet/Front/Outlet sides are separated by dashed red lines.

Figure 4.4 above shows the solid wall temperature evolution along the FW channel length. In particular, it refers to plasma-facing side wall, since it is the most critical one in terms of maximum temperature reached in it. Also in this case, the temperature along the outlet side is gradually decreasing, for the same reasons discussed above.

Both graphs for helium and EUROFER97 (figures 4.3 and 4.4) are taken at a fixed time value of 350 seconds, during the plasma burn phase, when the system is in steady condi-

tions until the beginning of the dwell time. However, the shape of the temperatures along the FW channel is qualitatively similar also during transients. Made this premise, it can be seen that both helium and EUROFER reach the highest temperatures (and also the highest  $\Delta T$ ) in the front part, where the heat flux coming from the plasma plays a major role, and also the volumetric heat generation is greater than the one inside the side parts of the channel. Since this is true also during a LOFA, from now on the discussion will be focused on the results regarding the front part of the channel only.

Helium has a temperature increase inside the inlet side channel of about 40 °C, and then reaches its maximum temperature of 407.8 °C at the end of the front part of the channel; in the solid walls, instead, the maximum temperature of 438.2 °C is computed in the last but one volume of the front part, and a fast  $\Delta T$  is observable between inlet side and front side of the FW channel. This maximum temperature computed in the solid is far below the upper limit for EUROFER97 of 550 °C. Moreover, the inversion of the heat transfer in the outlet side part is clear looking at figures 4.3 and 4.4, since the helium temperature is always greater than the solid one in that region.

The time evolution of the temperature in the FW (helium and solid structures) is the opposite to the one already seen for the mass flow rate in figure 4.2.: it has its maximum value during the plasma burn phase and then, after the plasma shut down, rapidly settles at a temperature slightly higher than 300 °C (which is the HX outlet temperature) because of the residual decay heat in the solid.

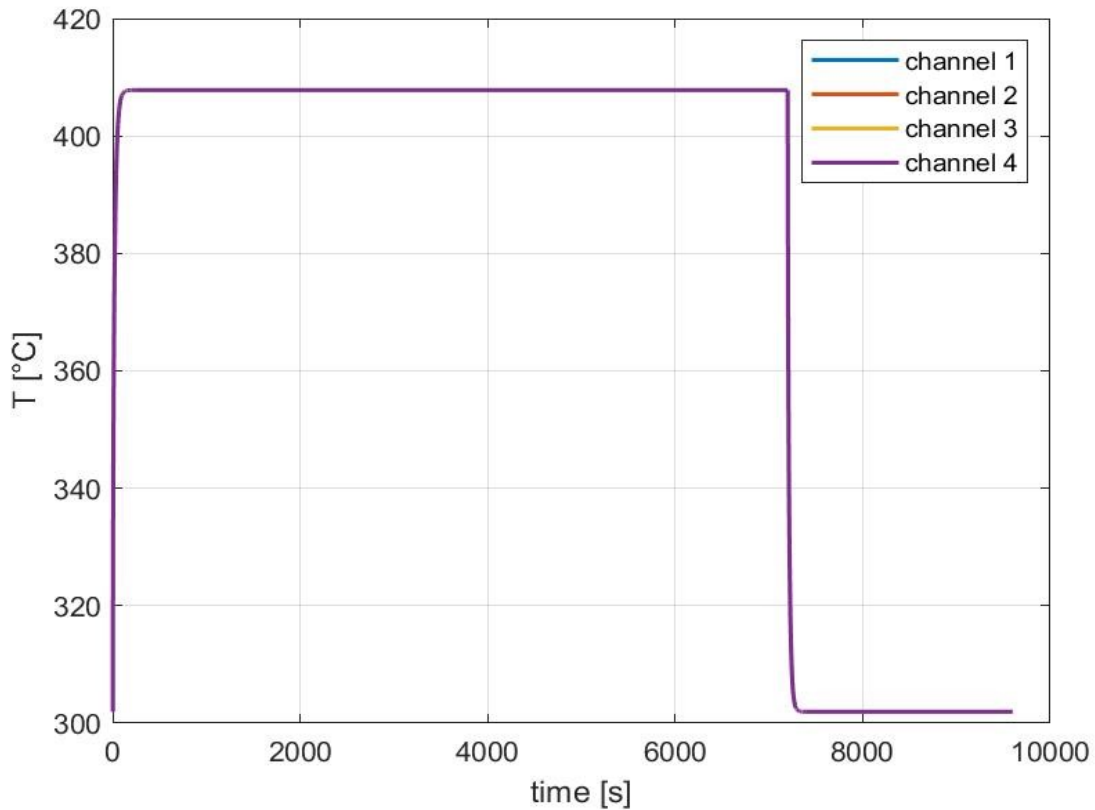


Figure 4.5: Temperature evolution in time (9600 s period) of the helium in the 5<sup>th</sup> node of the front part (NOC).

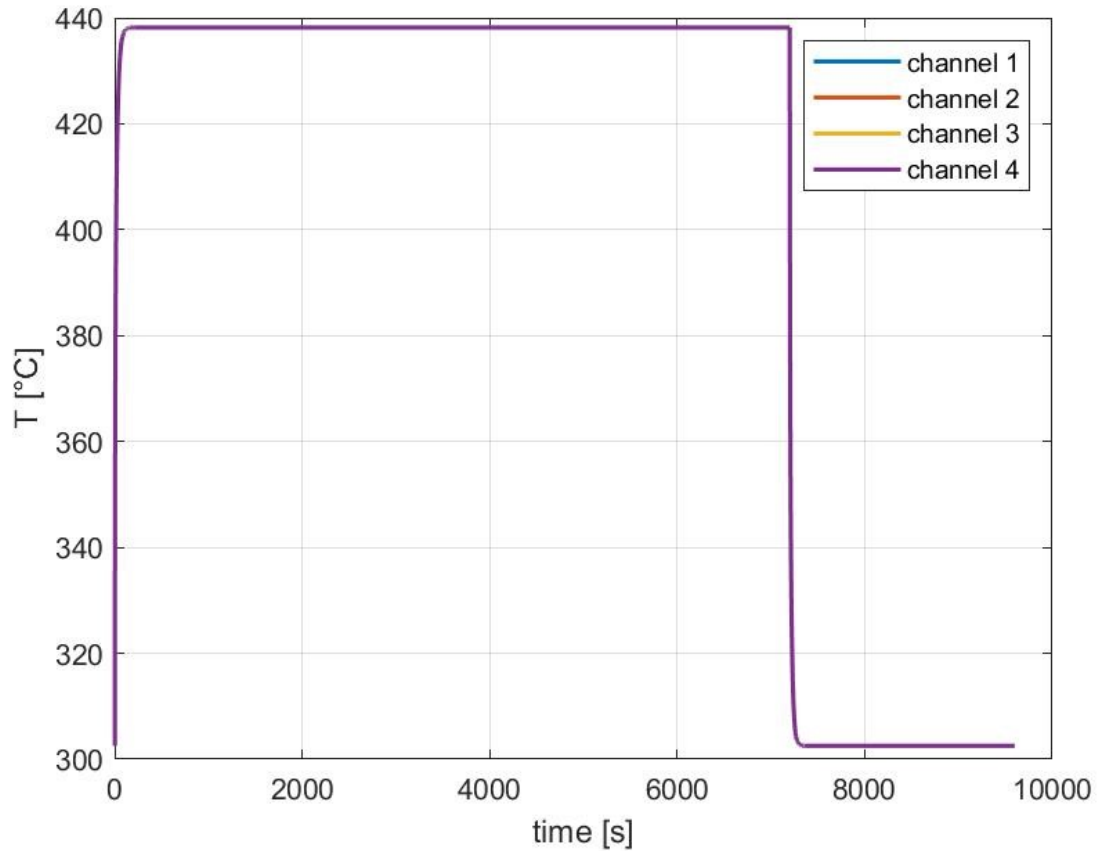


Figure 4.6: Temperature evolution in time (9600 s period) of EUROFER97 in the 3<sup>rd</sup> volume of the front part (NOC).

Figures 4.5 and 4.6 show the temperature evolution during a whole period in the most critical fluid node and solid volume, respectively, of the FW channel front part. For the same reasons already discussed, the temperature at a fixed location in different channels is exactly the same (in fact, in the two plots above, curves referring to different channels perfectly overlap each other). In view of this, it would be more interesting to plot the temperature time evolution of the different fluid nodes/solid volumes at a fixed channel, knowing that results for the other channels will be the same. In figures 4.7 and 4.8, the temperature time-evolution in channel 1 is plotted, where different curves account for the different fluid nodes (helium) or solid volumes (EUROFER97) of the front channel part.

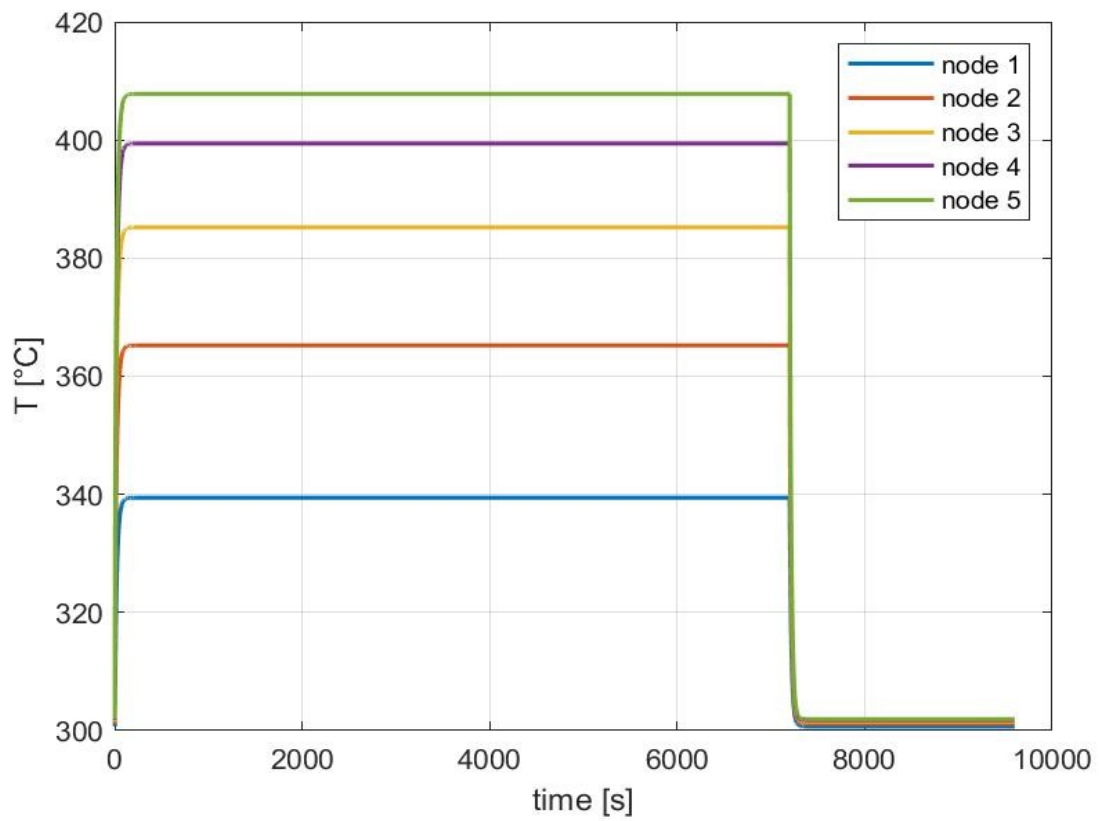


Figure 4.7: Channel 1 helium temperature evolution; each curve represents a different fluid node of the front part (NOC).

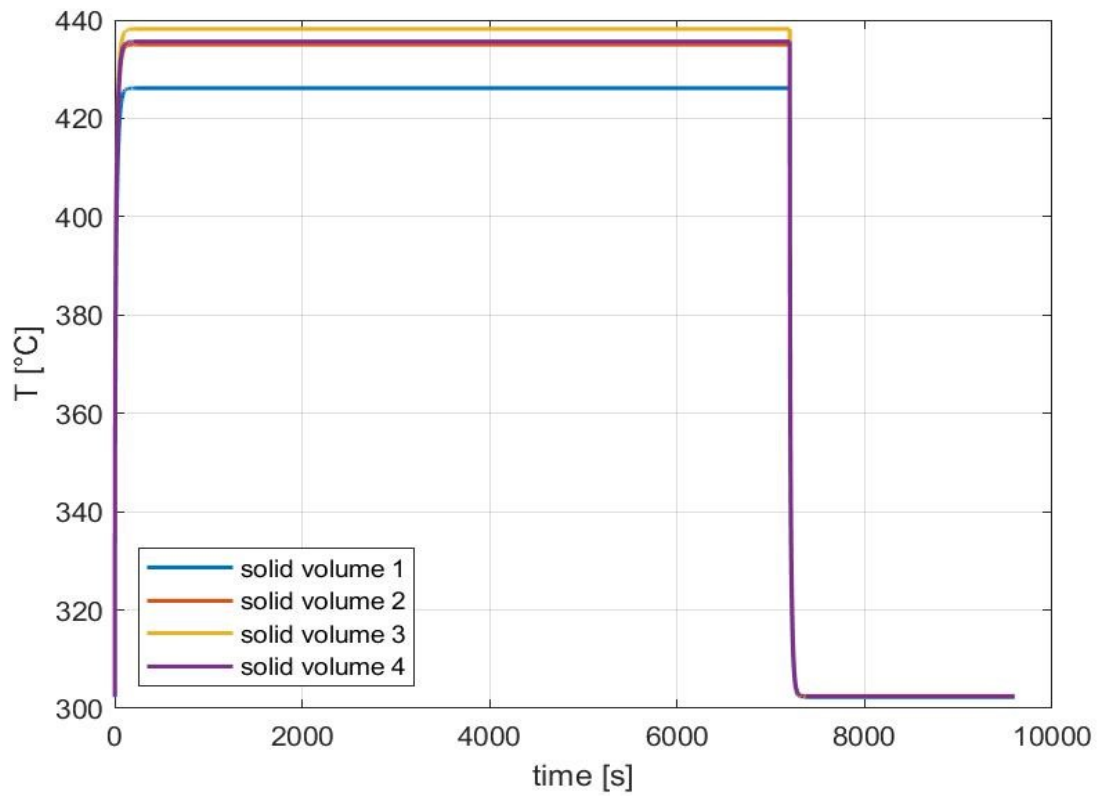


Figure 4.8: Channel 1 EUROFER temperature evolution; each curve represents a different FV of the front part (NOC).

The plots above represent the time evolution of the temperatures in the nodes/solid volumes of the front part; during the plasma burn phase (until 7200 s) the considerations that can be made are the same of the ones made for the temperature distribution along the channel at time 350 s, plotted in figures 4.3 and 4.4. Once the power is switched off, the temperatures drop near the value of 300 °C, imposed by the HX.

## **4.2.2. Total LOFA**

To simulate a total LOFA inside the cooling circuit, a loss of the whole circulating power is needed. In the model this is obtained by gradually lower toward zero the angular velocity of the blades of the circulator, which is assumed to take 120 s to stop. Actually, the ThermoPower object for the circulator is not suited to work at mass flow rates close to zero: for this reason, to simulate the trip of this component, a set of valves has been introduced in order to have the helium to bypass the BB (which is the whole point of the analysis) while still passing through the circulator. However, a small fraction of the mass flow rate (approximately the 6% of the total) is still forced through the BB, which can be seen as the fraction of coolant still circulating inside the pipes thanks to natural circulation.

Also, despite in the real system a cooling loop foresees two circulators, in the model for a total LOFA only one circulator is used, in order to keep the model as simple as possible. Of course, the characteristic curve of the circulator has been adjusted in such a way that elaborates the entire mass flow rate of the cooling loop alone.

As anticipated, the model has been simulated both with the intervention of the mitigation system and without it. The onset of the LOFA accident, as for the other scenarios, has been fixed after 2000 s from the beginning of the pulse (during the plasma burn phase).

### **4.2.2.1. Case I: no intervention of the mitigation system**

In this scenario, the negative effect of the loss of flow is not balanced by the mitigation system, consisting in the emergency shutdown of the plasma, which fails to intervene. The (almost) complete loss of circulating power during a total LOFA, in these conditions, make this the most severe scenario possible.

When the circulators trip at time 2000 s, the mass flow rate inside the FW starts decreasing rapidly and the thermal power coming from the power is not removed anymore by the coolant (fig. 4.9 shows the mass flow rate time evolution). This causes an immediate and uncontrolled overheating inside the blanket, inevitably leading to structural failures and eventually to the melting of solid structures in the most critical spots. The mass flow rate in each FW channel, after the accident, drops to about 1 g/s.

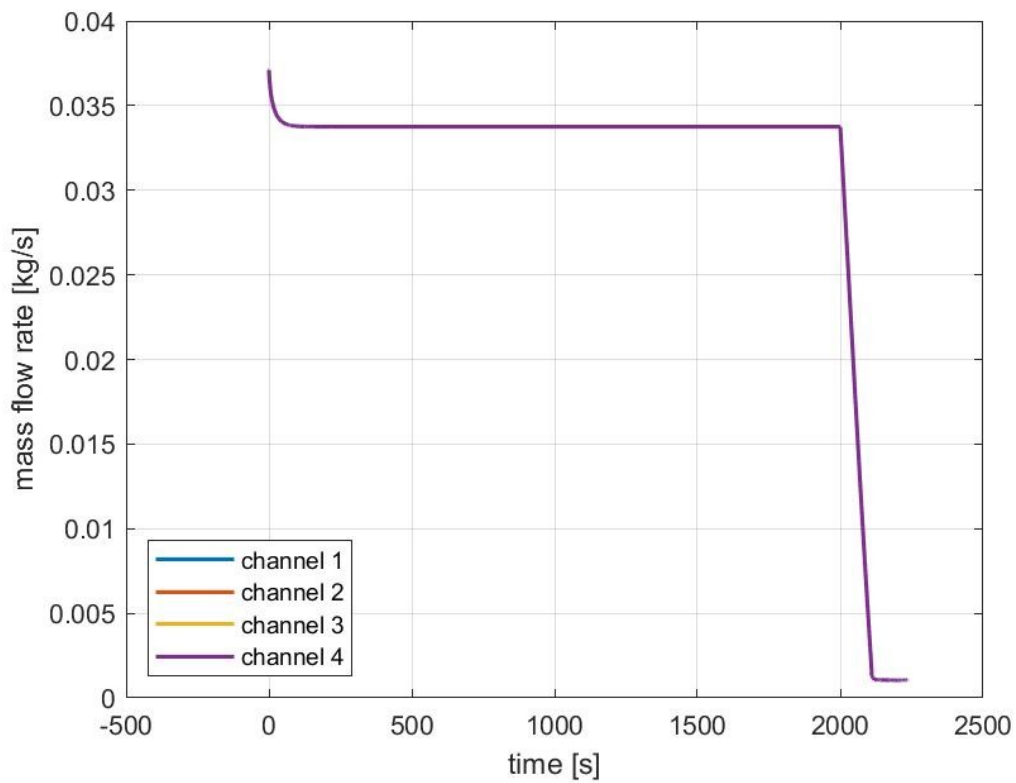


Figure 4.9: Helium mass flow rate time evolution in the front part of each FW channel; case of a total LOFA without plasma shutdown.

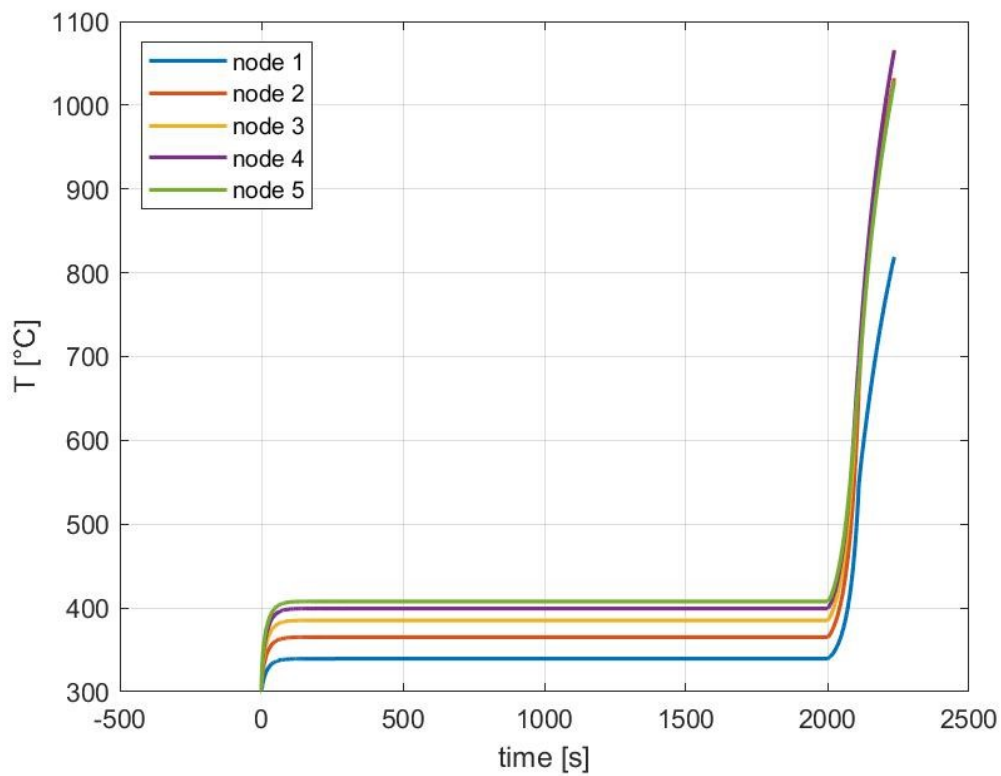


Figure 4.10: Helium temperature evolution in a FW channel; each curve represents a different fluid node of the front part; case of a total LOFA without plasma shutdown.

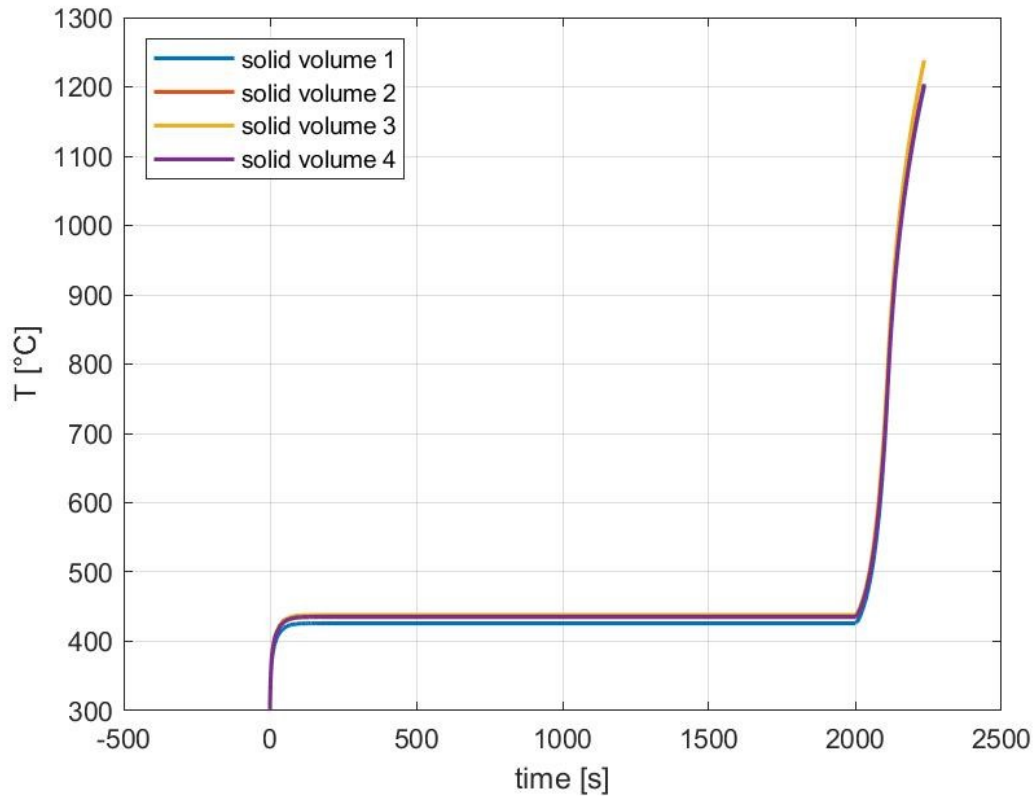


Figure 4.11: EUROFER temperature evolution in a FW channel; each curve represents a different fluid node of the front part; case of a total LOFA without plasma shutdown.

From figures 4.9, 4.10 and 4.11 it is noticeable that the curves, referred to mass flow rate, helium temperature and EUROFER temperature respectively, stop just after the loss of flow, without completing the entire period of 9600 s. The explanation to this behavior can be explained by looking at figure 4.11: the solid wall temperature inside the channel front part reaches extremely high values, above 1000 °C, exceeding EUROFER97 melting point, where its properties are not defined anymore. At this point the FW solid structures will inevitably melt, severely compromising the BB sectors involved and, among other things, shutting off the plasma. Giving that there was a complete loss of the coolant flow, and that the plasma power is still on since the automatic detection system failed, the resulting melt of the solid structures was predictable; what is interesting to see is how much time it takes, since the onset of the accident, to reach this condition. The results shows that the most critical EUROFER97 solid volume (the 3<sup>rd</sup> FV of the front part) reaches 1000 °C after 2.5 minutes and 1238 °C after nearly 4 minutes. Assuming for EUROFER97 a melting temperature equal to 1000 °C (it is a conservative assumption), this means that, in the case the automatic detection and shutdown system fails, there are 2 minutes and 30 seconds for a human to intervene before the solid structures begin to melt.

The temperature distribution along a FW channel is presented in figures 4.12 and 4.13 for helium and EUROFER97, at a fixed time corresponding to the moment when the maximum temperature is computed. The maximum temperatures computed are 1238 °C for the solid wall and 1066 °C for helium, both inside the plasma-facing channel part, but also along the side channel parts the solid walls reached temperatures up to 900 °C.

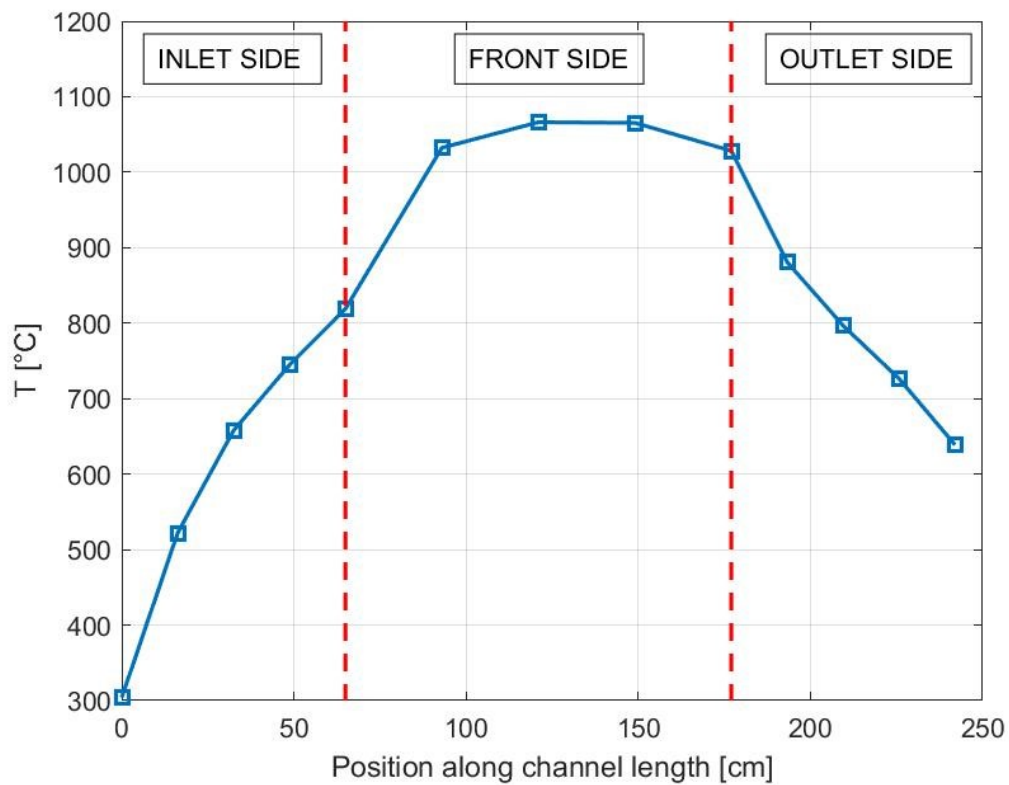


Figure 4.12: Helium temperature distribution along the FW channel length at time  $t=2461$  s; the squares represent the values computed in each fluid node; case of a total LOFA without plasma shutdown.

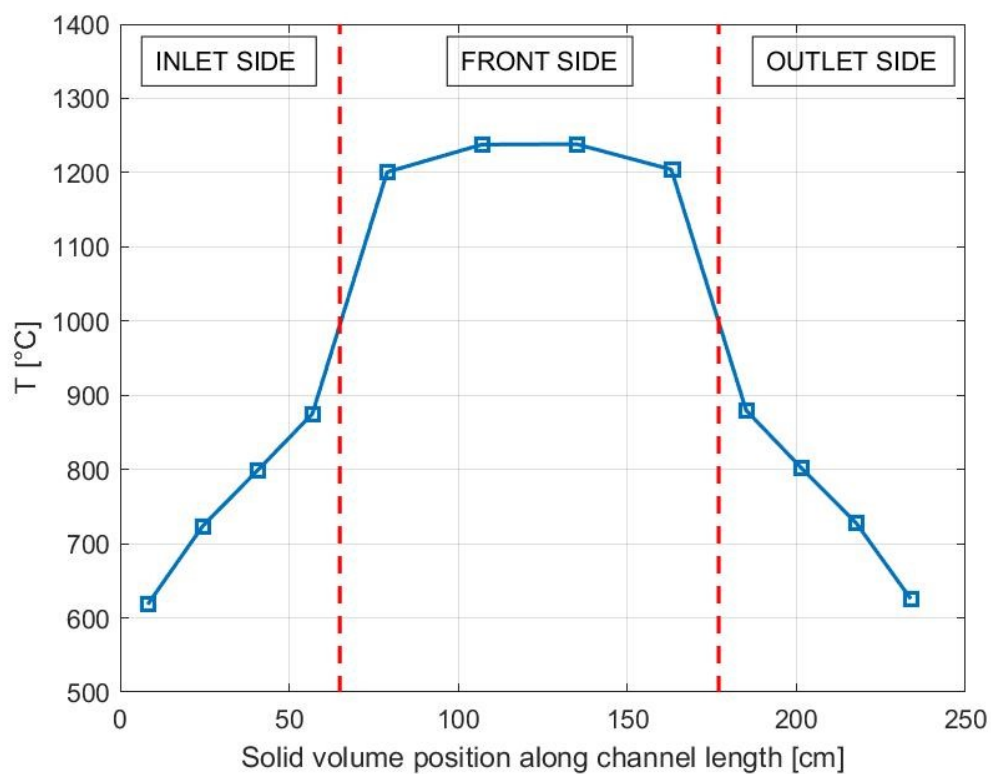


Figure 4.13: EUROFER temperature distribution along the FW channel length at time  $t=2236$  s; squares represent the value computed in each solid volume; case of a total LOFA without plasma shutdown.

### 4.2.2.2. Case II: intervention of the mitigation system

This time, the same model used for the accidental scenario of a total LOFA has been simulated by introducing the intervention of the mitigation system (i.e., emergency plasma shutdown). The shutdown of the plasma is simulated by setting the input power term referred to the heat flux on the plasma-facing wall equal to zero, and the term referred to volumetric heat generation inside EUROFER97 equal to the residual decay heat only.

This mitigation system, when triggered, prevents a further heat deposition inside the BB, allowing the solid structures of EUROFER97 to rapidly cool down. In view of this, is important to intervene before the temperature reaches hazardous values, which for EUROFER corresponds to 550 °C (loss of creep strength); for this reason, the plasma shutdown is simulated to intervene after 20, 40 and 60 seconds from the onset of the accident, to give an idea on how much delay is still allowed for the plasma shutdown intervention to stay within safety limits.

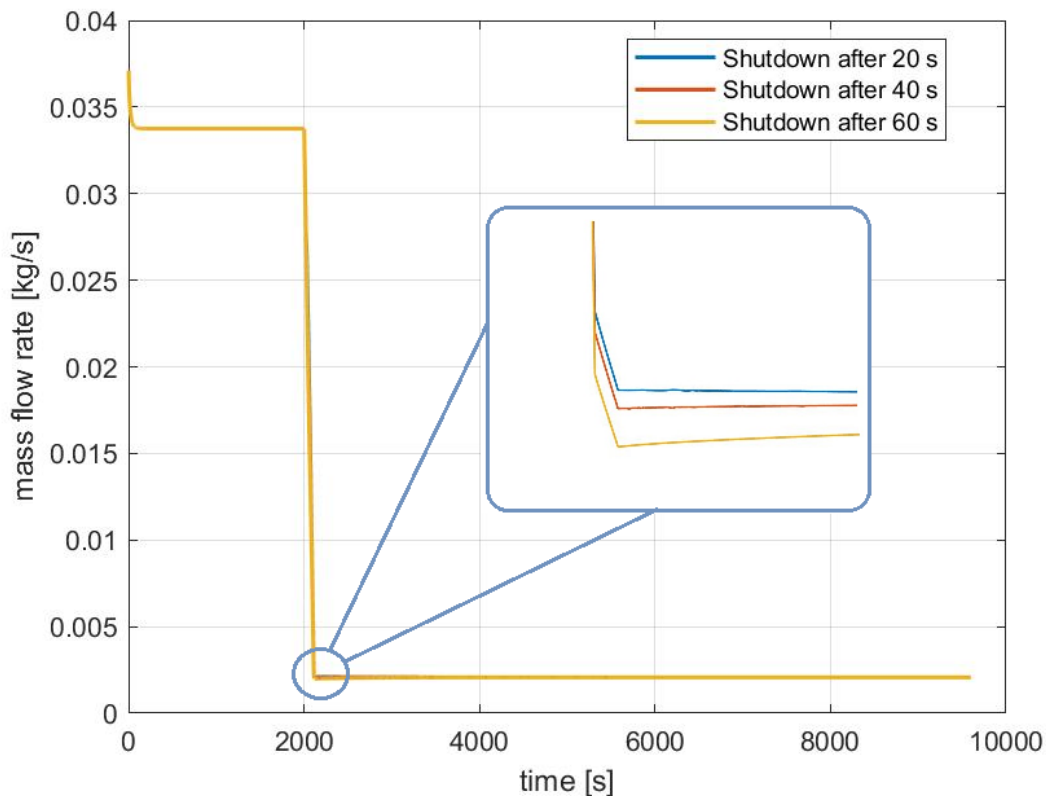
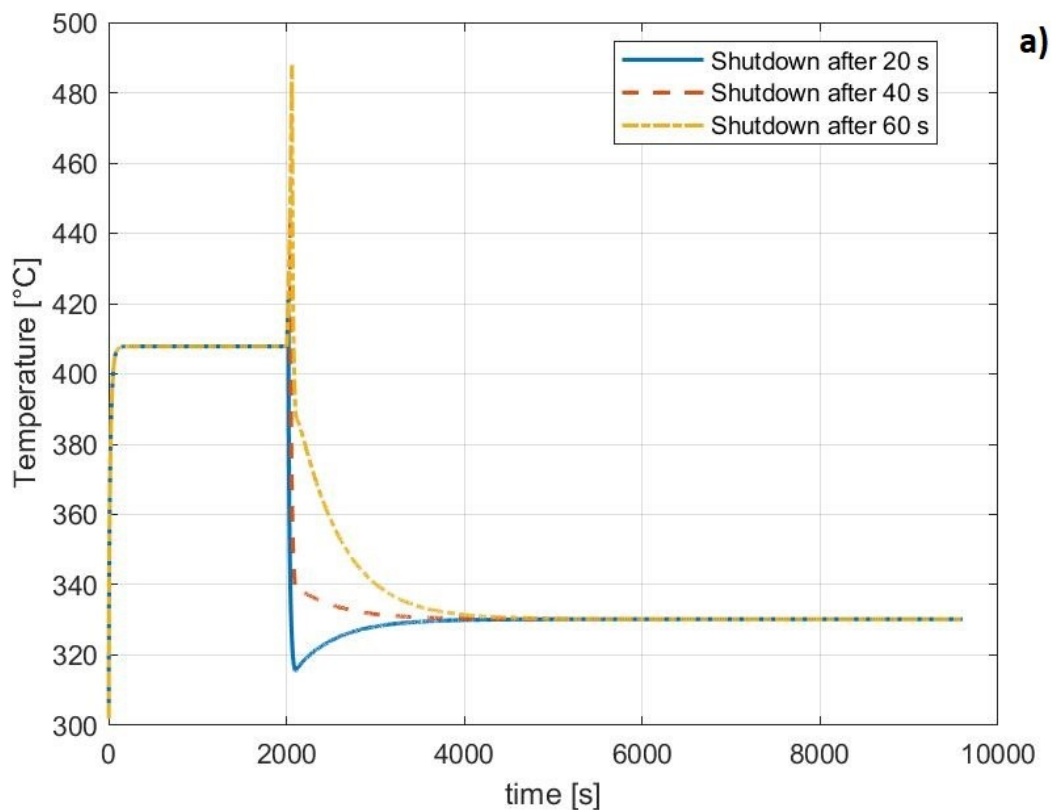


Figure 4.14: Helium mass flow rate time evolution in a FW channel.: three hypotheses on the mitigation system intervention; case of a total LOFA with plasma shutdown; in the blue box: magnified view of the curves around 2120 s.

Figure 4.14 above shows the helium mass flow rate evolution in a FW channel under the three hypotheses on the plasma shutdown. The three curves, on the 10000 s scale of the figure, seem to perfectly overlap each other, reaching all of them a steady value of 2.1 g/s soon after the complete trip of the circulators. However, a small difference, only noticeable by deeply zooming in around the time 2120 s (as in figure 4.14), is that the mass flow rates corresponding to 40 s and 60 s shutdowns take more time to reach a plateau. With respect to the case I,

when the accident is not mitigated, the helium mass flow rate settles at a higher value after the accident, due to the effect of the plasma shutdown on the density of the fluid.

For what concerns the temperatures, instead, the differences are clearer between the three cases. In figure 4.15 and 4.16 is shown the comparison between the effects of the three mitigation hypotheses on the temperature evolution in the most critical points of the fluid flow and solid. The curves present a narrow peak after the onset of the accident, with a rapid ascent and descent of the temperature, and then smoothly settle at a steady value around 330 °C for both helium and EUROER. The temperature profiles follow the trend seen for the case I until the plasma shutdown, when they drop immediately; since the overheating is so fast, a delayed intervention of the mitigation system will induce a dangerous increase of the peak temperature. In the worst case of a 60 s delayed shutdown (yellow curve in fig. 4.15 and 4.16), the solid wall experienced a  $\Delta T$  of 91°C in the most critical volume, reaching the temperature of 538 °C, just below the upper limit for EUROFER97. For the 20 s and 40 s cases, instead, the maximum temperatures computed in the solid are 453 °C and 483 °C respectively. Figure 4.17 shows the temperature distribution along the FW solid walls under the most severe hypothesis of a 60 s delayed plasma shutdown.



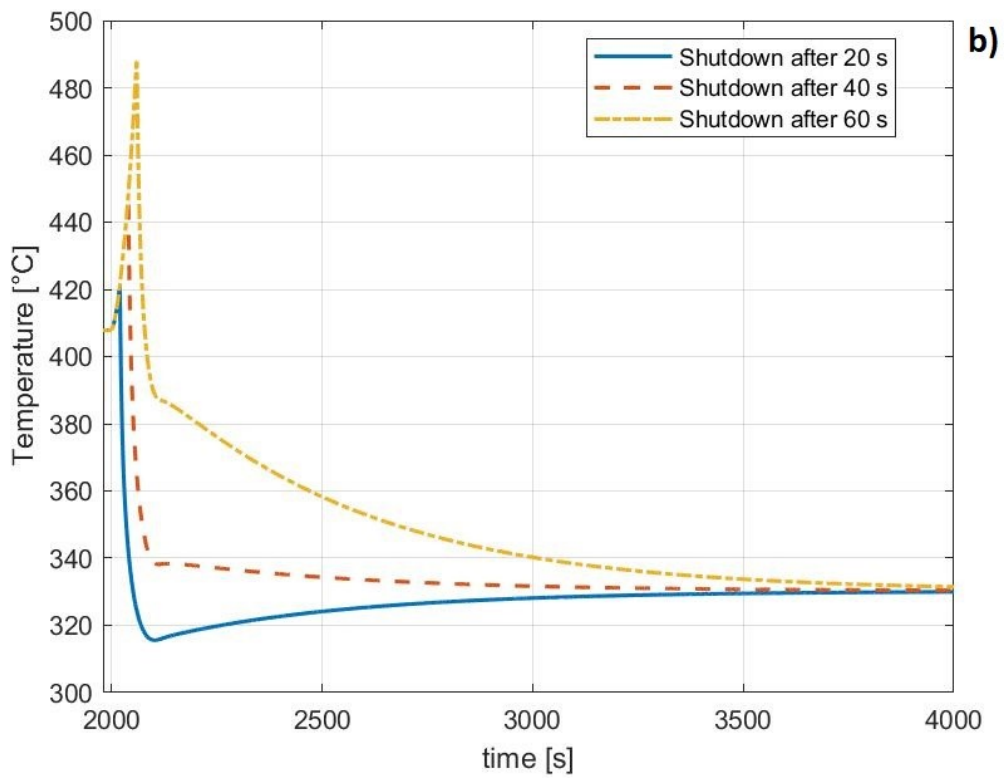
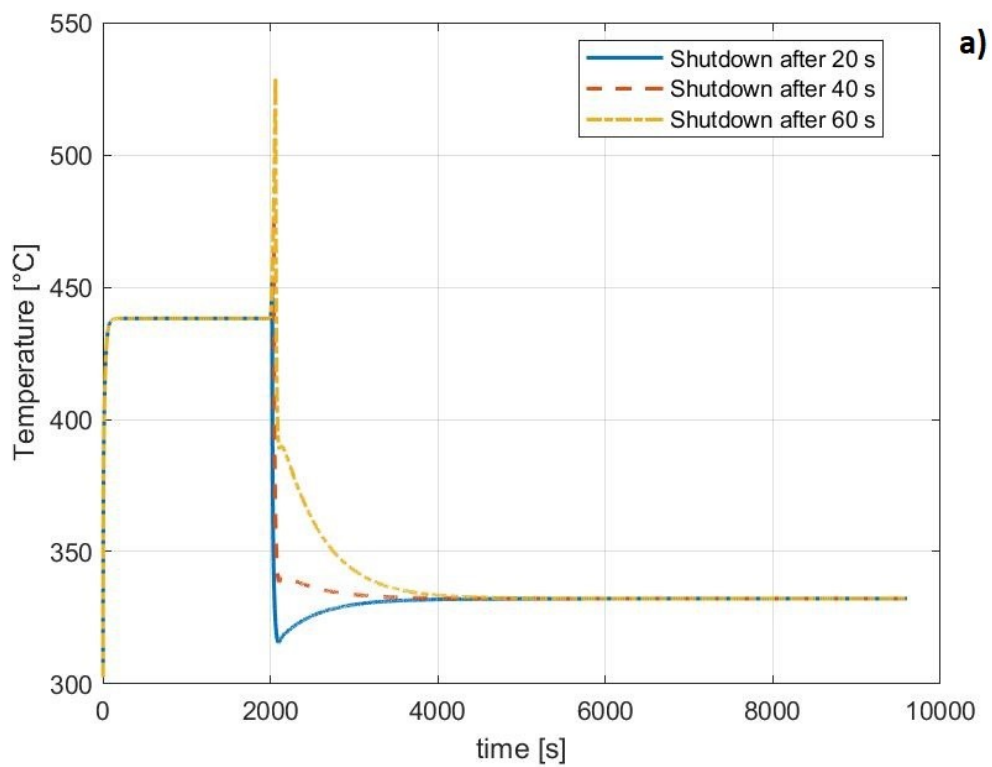


Figure 4.15: Helium temperature time evolution in the 5th node of the FW channel front part: three hypotheses on the mitigation system intervention; case of a total LOFA with plasma shutdown; a) view of the whole period, b) post-accident detail (1980 s – 4000 s).



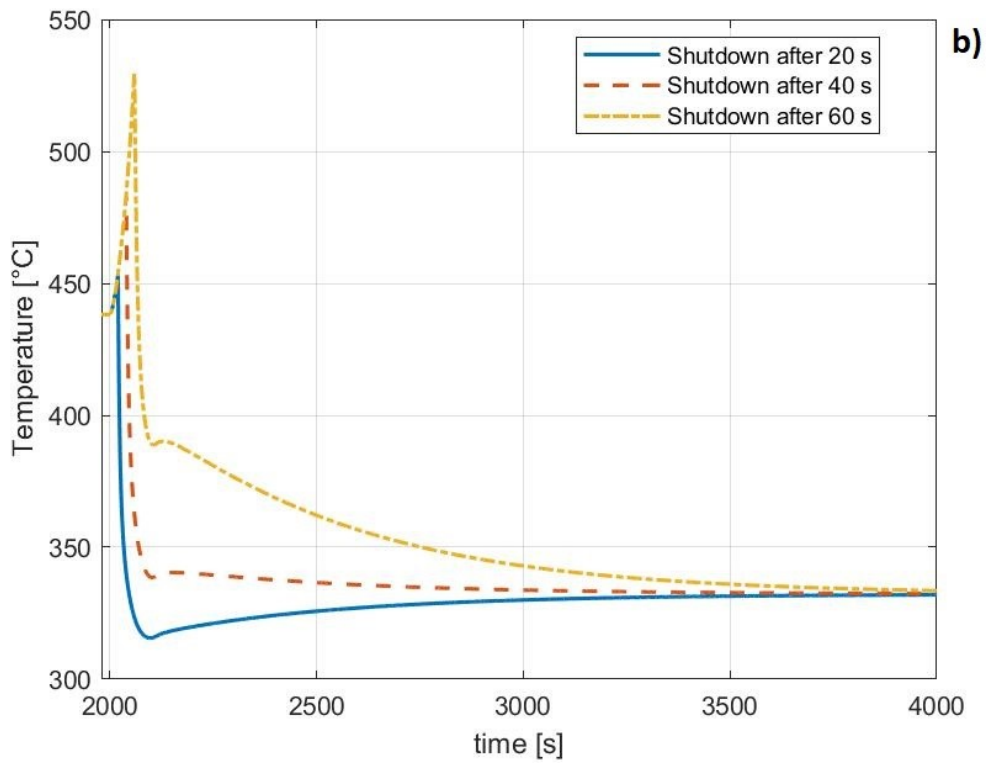


Figure 4.16: EUROFER97 temperature time evolution in the 3rd node of the FW channel front part: three hypotheses on the mitigation system intervention; case of a total LOFA with plasma shutdown; a) view of the whole period, b) post-accident detail (1980 s – 4000 s).

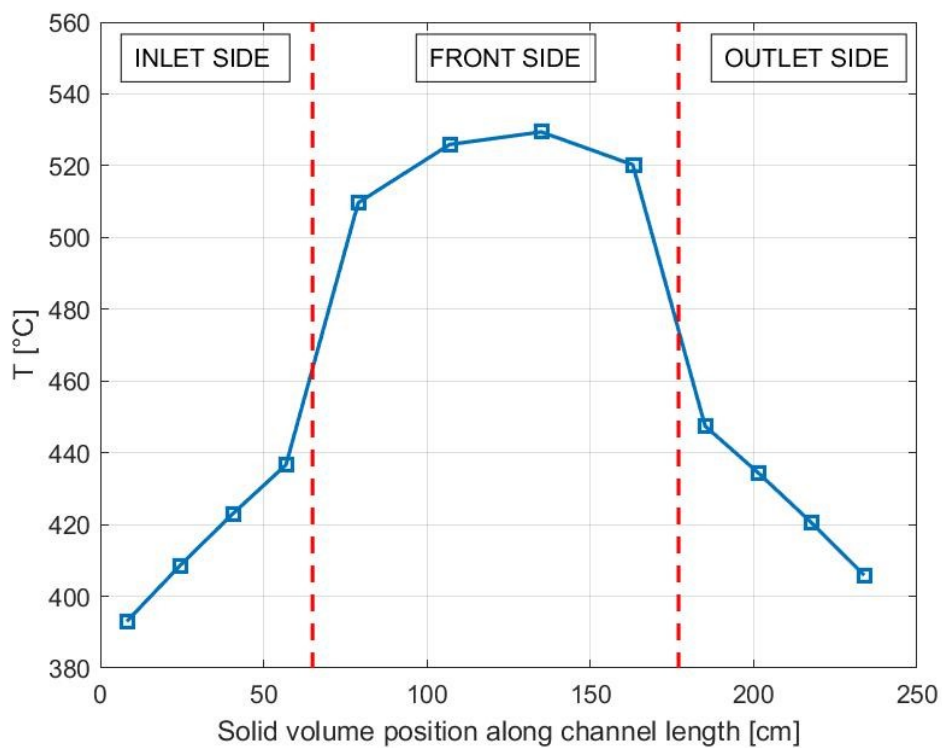


Figure 4.17: EUROFER temperature distribution along the FW channel length at time  $t=2060$  s; squares represent the value computed in each solid volume; case of a total LOFA with plasma shutdown after 60 s from the accident.

### 4.2.3. Partial LOFA: failure of one circulator

Since a PHTS cooling loop is fed by two circulators in parallel, it is interesting to see what happens inside the blanket if one of them trips, leaving the other as the only source of circulating power. Differently from the scenario simulated in section 4.2.3, where all the circulating power was lost, now the BB solid structures are still cooled by a relevant fraction of the “pre-accident” helium mass flow rate (which it is expected to drop to about a half of the normal operation value), making this scenario less severe but still needed to be carefully dealt with and promptly mitigated. Moreover, each circulator feeds the whole cooling loop, hence the effect of the accident, in this scenario too, will affect uniformly all the FW channels.

In the model, as stated above, the ThermoPower Fan object is used for the circulator. This object has an integer input connector that allows to set the number of circulators in parallel from an external integer source; in view of this, the simulations are carried on by using an integer step that switches the number of circulators from 2 to 1 when the accident is meant to occur, at time equal to 2000 s. This solution, even though simple to implement and computationally convenient, does not allow to gradually decrease the angular velocity of the defective circulator, as it was done for the total LOFA: therefore, the system switches from 2 fans to 1 instantaneously, causing an unrealistically fast decrease of the mass flow rate and, consequently, a too fast overheating of the blanket. In the case of an unmitigated LOFA this doesn't represent a huge problem, since the focus is on the new equilibrium conditions reached rather than the time taken to reach them; at contrary, when simulating the intervention of the plasma shutdown, the results obtained are inevitably most severe (in terms of maximum temperatures computed in the solid) than they actually are.

However, it must be pointed out that this assumption on the failure of the circulator is a conservative assumption; it allows to consider the worst circumstances possible (in this specific scenario) and study a suitable mitigation strategy, which will be certainly effective also in the case of an actual accident (being it less severe).

#### 4.2.3.1. Case I: no intervention of the mitigation system

When the plasma is not turned off after a partial LOFA, the BB will undergo a further heat deposition inside the solid structures, resulting in a new equilibrium condition, at higher temperatures, soon after the onset of the accident.

The mass flow rate inside each FW channel drops to 16.46 g/s after the accident, which as expected is approximately half the normal operation value of 33.76 g/s. The mass flow rate time evolution is shown in figure 4.18. At time 7200 s, as the dwell time begins, the plasma power is switched off as envisaged in normal operating conditions, and consequently the helium flow rate rises to about 20 g/s as an effect of the density change.

Temperature time evolution is plotted in figures 4.19 and 4.20 for helium and EUROFER. In this situation, helium exits the front part of the channel with a temperature almost 150 °C greater than in nominal conditions, and the solid structures are subjected, in the front channel part, to temperatures between 550 °C and 600 °C, with a maximum of 593.7 °C in the third solid volume. Therefore, the EUROFER97 upper limit of 550 °C has been exceeded, but

not by much; as a matter of fact, considering that a severe accident has happened, and it hasn't even been detected or mitigated, these results are actually less alarming as one might have expected. The side parts, instead, are safely below 550 °C, as shown in figure 4.21.

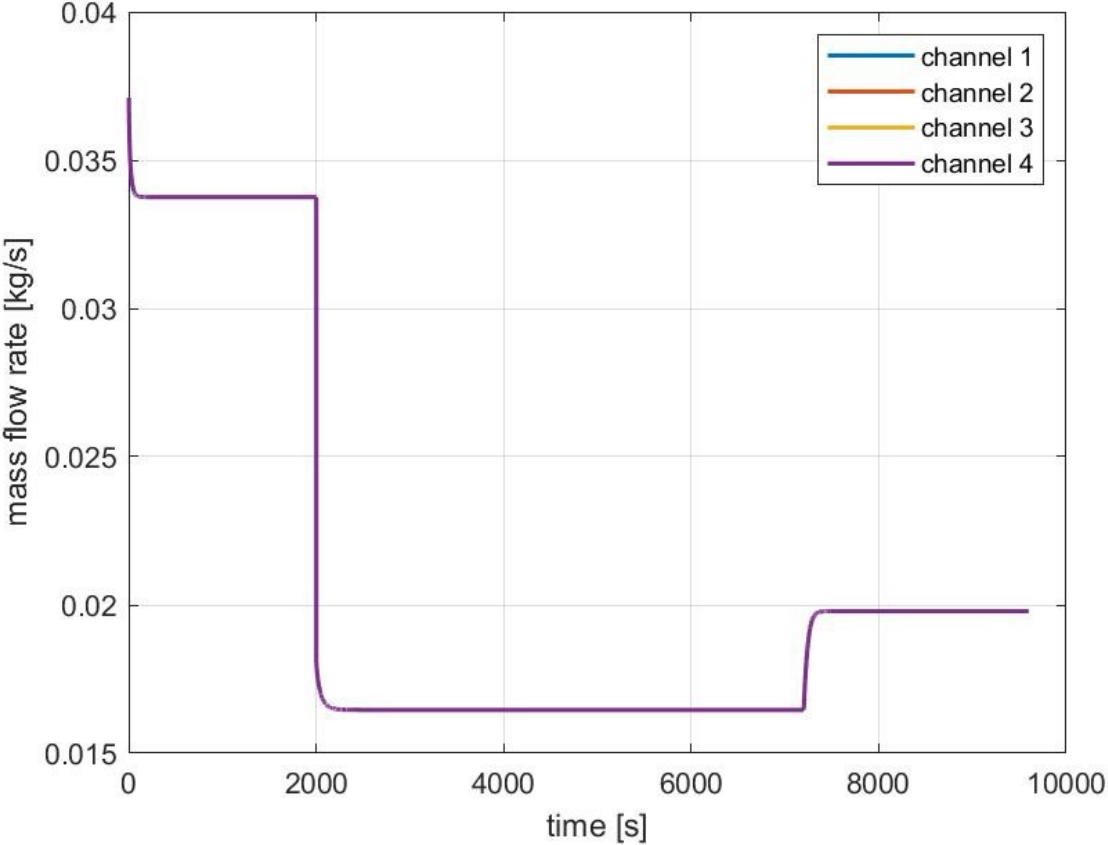


Figure 4.18: Helium mass flow rate time evolution in the front part of each FW channel; case of a partial LOFA without plasma shutdown.

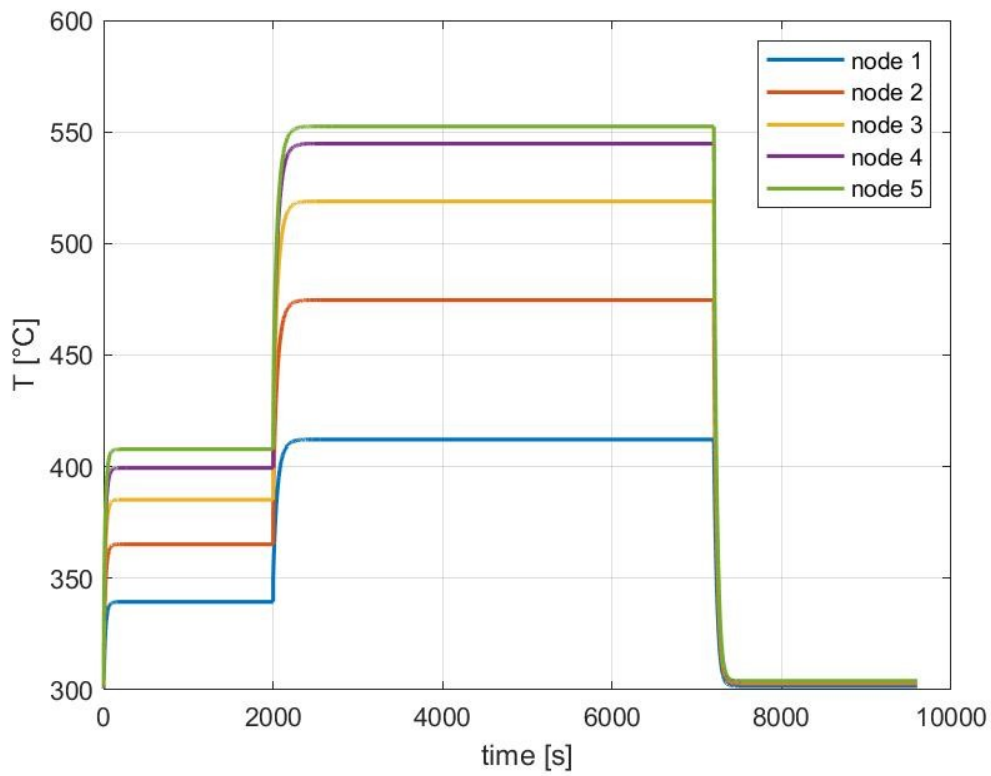


Figure 4.19: Helium temperature evolution in a FW channel; each curve represents a different fluid node of the front part; case of a partial LOFA without plasma shutdown.

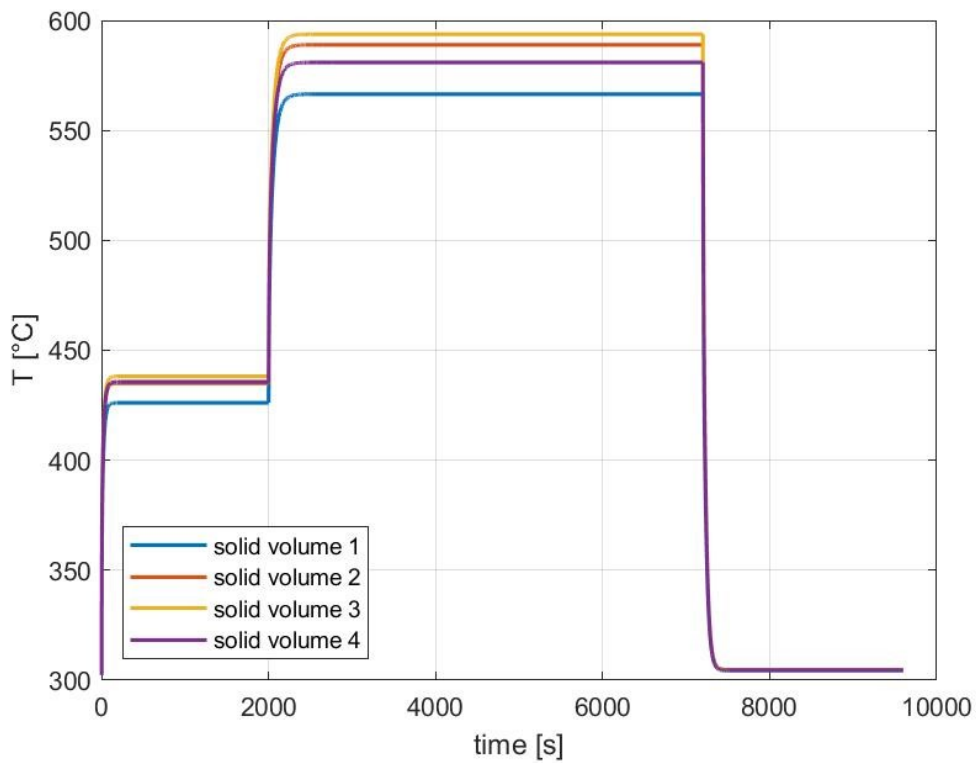


Figure 4.20: EUROFER temperature evolution in a FW channel; each curve represents a different fluid node of the front part; case of a partial LOFA without plasma shutdown.

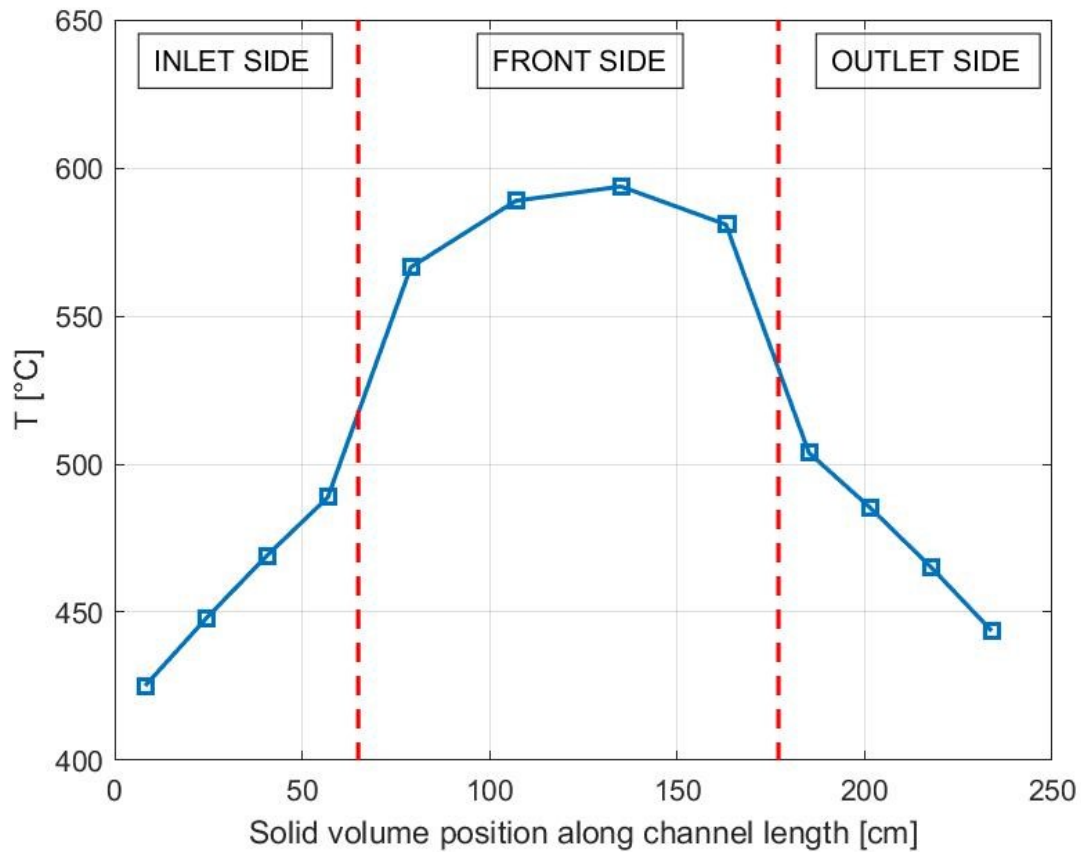


Figure 4.21: EUROFER temperature distribution along the FW channel length at time  $t=2851$  s; squares represent the value computed in each solid volume; case of a partial LOFA without plasma shutdown.

#### 4.2.3.2. Case II: intervention of the mitigation system

The mitigation system intervention is simulated under the same three hypotheses of the total LOFA scenario: the emergency plasma shutdown is actuated after 20, 40 and 60 seconds from the circulator failure.

In the following plot the results are shown. However, it should be pointed out that the peak temperatures computed are affected by the approximation made on the failure of the circulator, as explained in the introduction of section 4.2.3.

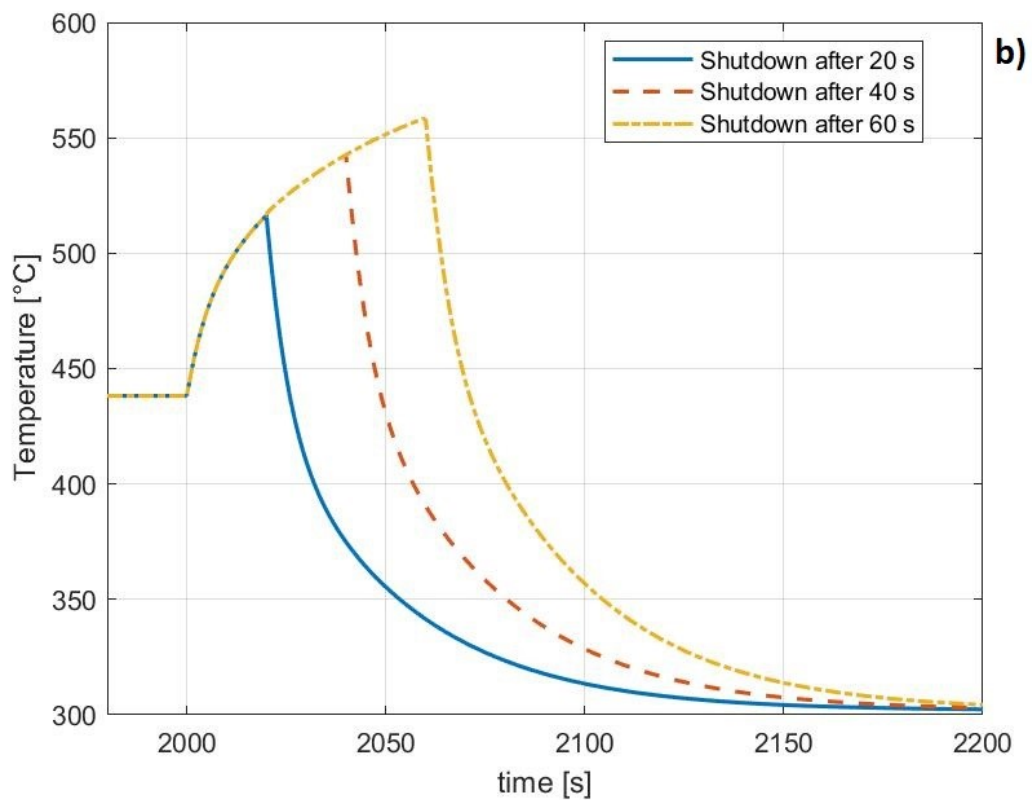
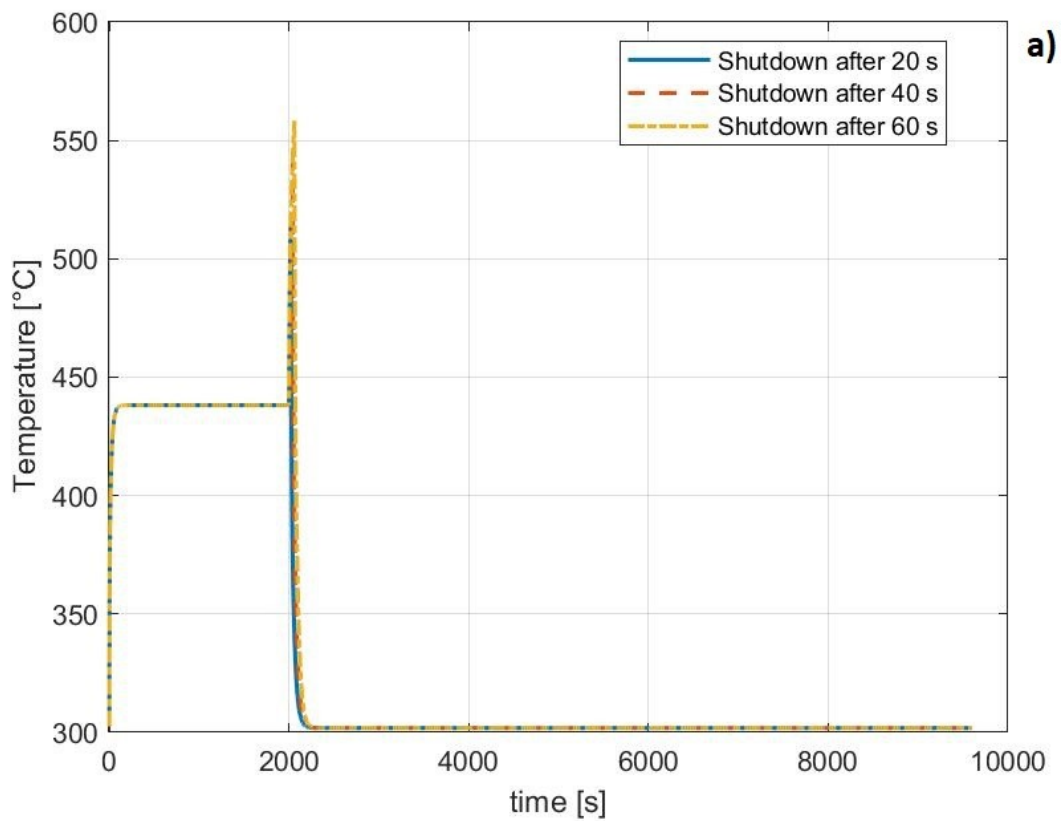


Figure 4.22: EUROFER97 temperature time evolution in the 3rd node of the FW channel front part: three hypotheses on the mitigation system intervention; case of a partial LOFA with plasma shutdown; a) view of the whole period, b) post-accident detail (1980 s – 2200 s).

The maximum temperature computed in the most critical solid volume of the FW is 588 °C for the 60 s shutdown hypothesis, while 542 °C and 516 °C are computed for the 40 s and 20 s hypotheses, respectively. Therefore, under the unlikely assumption that the circulator stops instantaneously instead of gradually, a 60 seconds-delayed emergency plasma shutdown would cause the temperatures to rise above 550 °C for some instants, in three solid volumes of the front part (see figure 4.23).

However, considered that the results obtained for a mitigated total LOFA (section 4.2.2.2) highlighted that, even with a 60 s delayed plasma shutdown, the solid temperature is kept under safety limits, then it is safe to say that also in the case of a less severe accident as a partial LOFA (with an appropriate assumption on the circulator failure) this must be true.

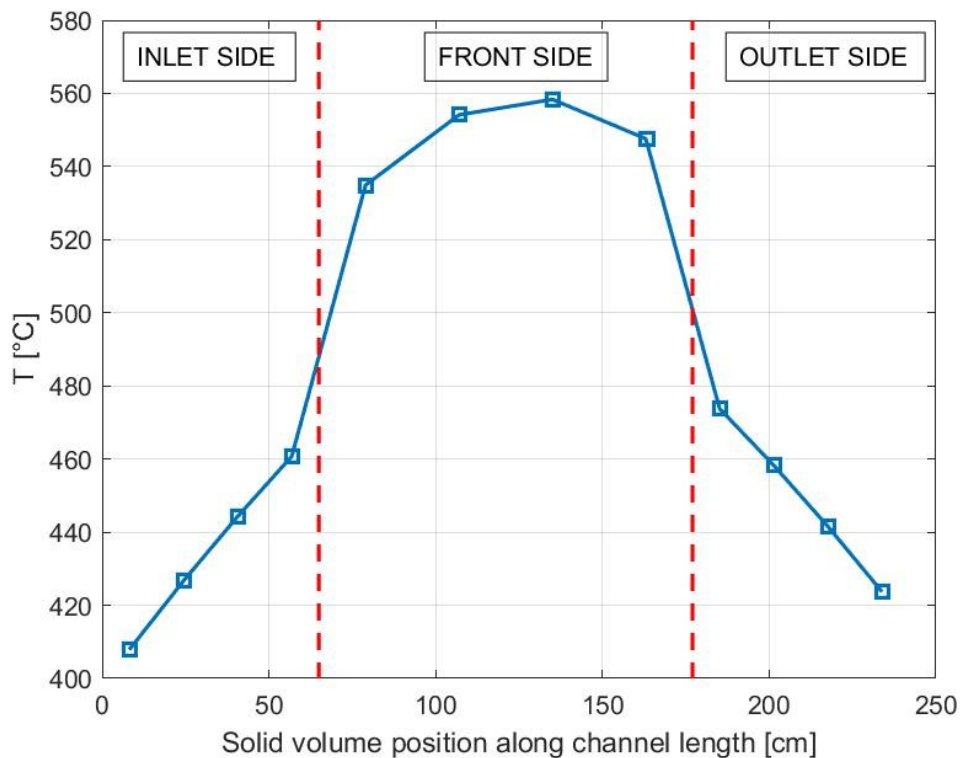


Figure 4.23: EUROFER temperature distribution along the FW channel length at time  $t=2060$  s; squares represent the value computed in each solid volume; case of a partial LOFA with plasma shutdown after 60 s.

#### **4.2.4. Obstruction of a FW channel**

The last scenario simulated for this thesis work focuses on the accidental obstruction of a single FW channel, which produces a localized heat deposition in the solid walls surrounding the said channel. This situation is not expected to represent a severe threat to the thermo-mechanical resistance of the EUROFER97 structures (because of the mild temperature increase expected), but a relevant temperature difference between the damaged channel and the others could still bring thermal stress issues. Moreover, it is interesting to see how the overheating of the obstructed channel is attenuated by the neighboring channels.

For this scenario, the model has been adjusted by adding a third in-vessel hydraulic-branch, in parallel with the others and with the same counter current cooling scheme. This new branch features the same objects as the other two, with the difference that the FW object models one channel instead of four. In addition, a valve is placed at the inlet of the branch in order to simulate the obstruction; by closing the valve, the mass flow rate in the obstructed channel gradually reduces and it is redistributed between the other channels. The valve has closed up to the 99.5 % of its wide-open position, leaving just a small fraction of the mass flow rate still flowing in the channel.

As usual, the model has been simulated in both cases with and without the intervention of the mitigation system.

### 4.2.4.1. Case I: no intervention of the mitigation system

Here the results in the case of the unmitigated LOFA accident are presented. With respect to the two scenarios showed in previous sections, now it is interesting to compare the results for different channels since the nature of the accident is localized in a specific poloidal location and not uniformly distributed for the entire segment.

In figure 4.24 the mass flow rate evolution in different channels is shown. The green dashed line represents the obstructed channel: at time 2000 s, the channel is almost entirely shut and the mass flow rate drops to 2 g/s (starting from about 33 g/s before the accident). The loss of mass flow rate in one channel is uniformly distributed among the others, which see an increase of 3 g/s each.

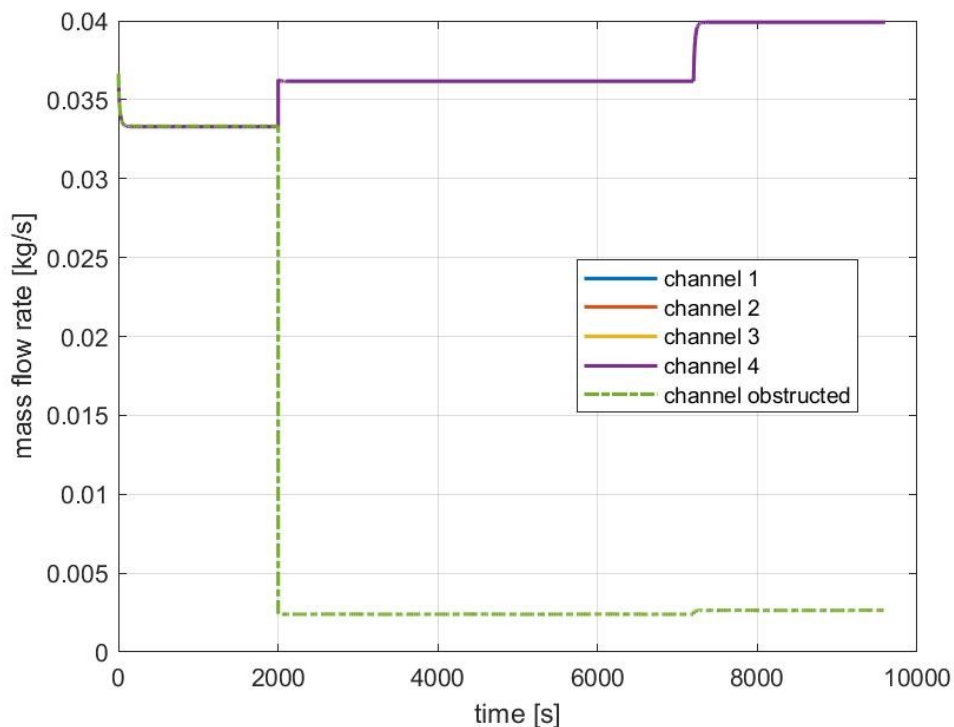


Figure 4.24: Helium mass flow rate time evolution in the front part of each FW channel; case of a channel obstruction without plasma shutdown.

Also for the temperatures, results shows that the effect of the accident is uniformly distributed among the non-obstructed channels. In fact, the post-accident temperature reached by EUROFER97 walls in channel 1, the nearest one to the obstructed channel, is the same of the one reached in channel 4, the farthest one; this is due to the good heat conduction properties of EUROFER97. Figures 4.25 and 4.26 show the temperature evolution of helium and EUROFER97 in the most critical fluid node and solid volume of the FW front channel part. In figure 4.25 an initial and short term decrease of the helium temperature is highlighted, after the accident, followed by a sudden increase of a few Celsius degrees. This initial behavior is a consequence of the mass flow rate increase in the unobstructed channels, and it is more tangible if looking at the other fluid nodes (discussed later in this section).

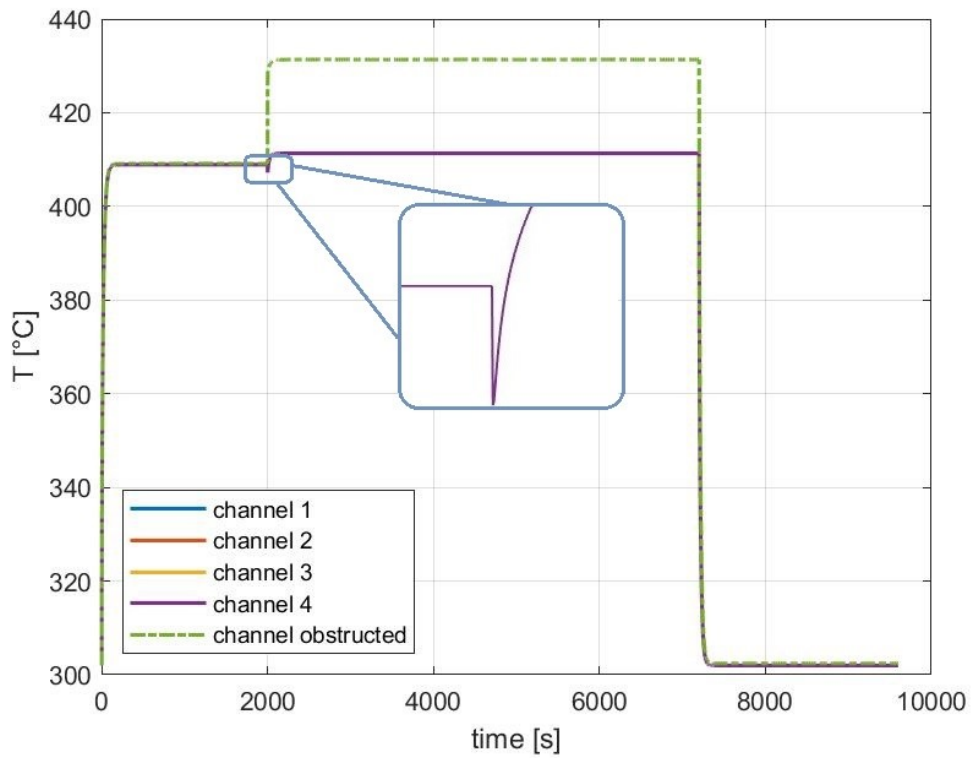


Figure 4.25: Temperature evolution in time of helium in the 5th node of the FW front channel part; case of a channel obstruction without plasma shutdown; in the blue box: magnified view of the channel 4 curve around 2000 s.

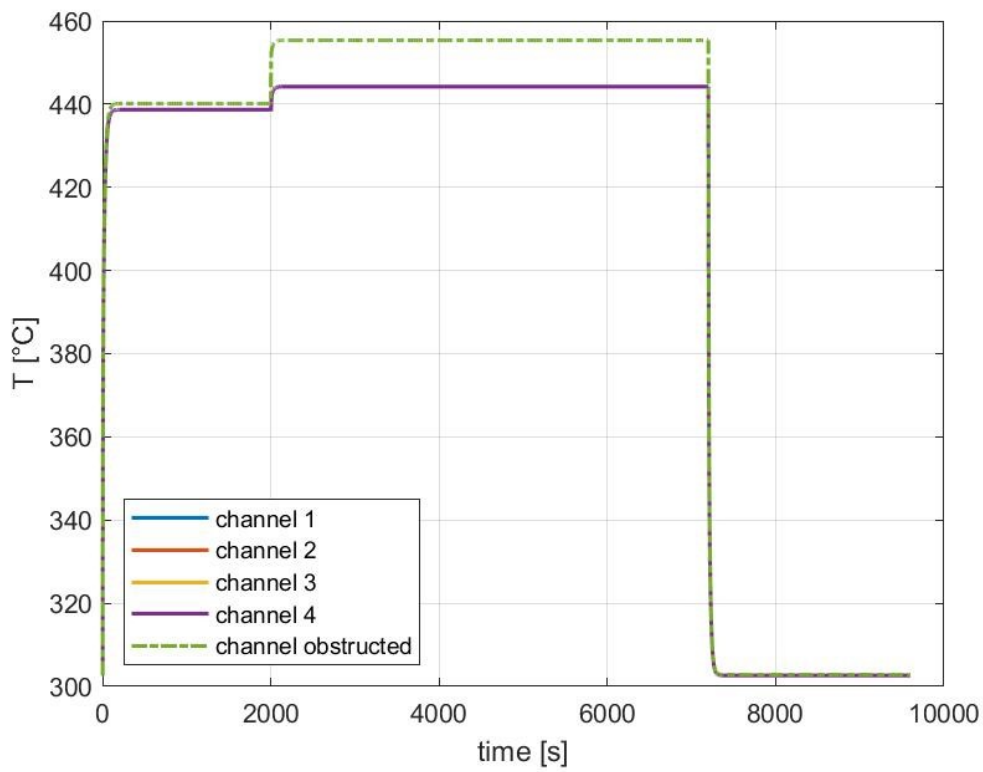


Figure 4.26: Temperature evolution in time of EUROFER97 in the 3rd solid volume of the FW front channel part; case of a channel obstruction without plasma shutdown.

The solid walls of the obstructed channel suffer a temperature increase of 15 °C, reaching the maximum temperature of 455.6 °C in the 3<sup>rd</sup> volume of the front channel part, as usual. On the other hand, a mild  $\Delta T$  of 6 °C is computed in the other channels. Moreover, as anticipated above while commenting on fig. 4.25, a peculiar behavior is noticeable if looking at the helium temperature evolution in all the different nodes of a FW channel's front part (figure 4.27). In the first three fluid nodes the temperature actually decreases after the accident, while only in the 4<sup>th</sup> and 5<sup>th</sup> node it starts increasing; this trend is explained by the fact that, as mentioned above, the mass flow rate in the unobstructed channels slightly increases, resulting in a lower average temperature of the fluid. However, along the flow path, the negative effect due to the overheating in the solid walls of the obstructed channel overcomes this mass flow rate positive effect, hence helium exits the front part with a higher temperature than before the accident.

Also, the comparison between the temperature distributions along the obstructed channel and its neighboring channel is shown in figure 4.28. Both distributions refer to a fixed time in which the maximum temperature has been computed, that is about 200 s after the accident when a new equilibrium is established. Of course, the walls surrounding the obstructed channel experience the largest  $\Delta T$ , but the accident is well mitigated by the neighboring channels: the maximum temperature is far below the upper boundary for EUROFER97, and, in the unobstructed channels, temperatures remain close to the normal operation values.

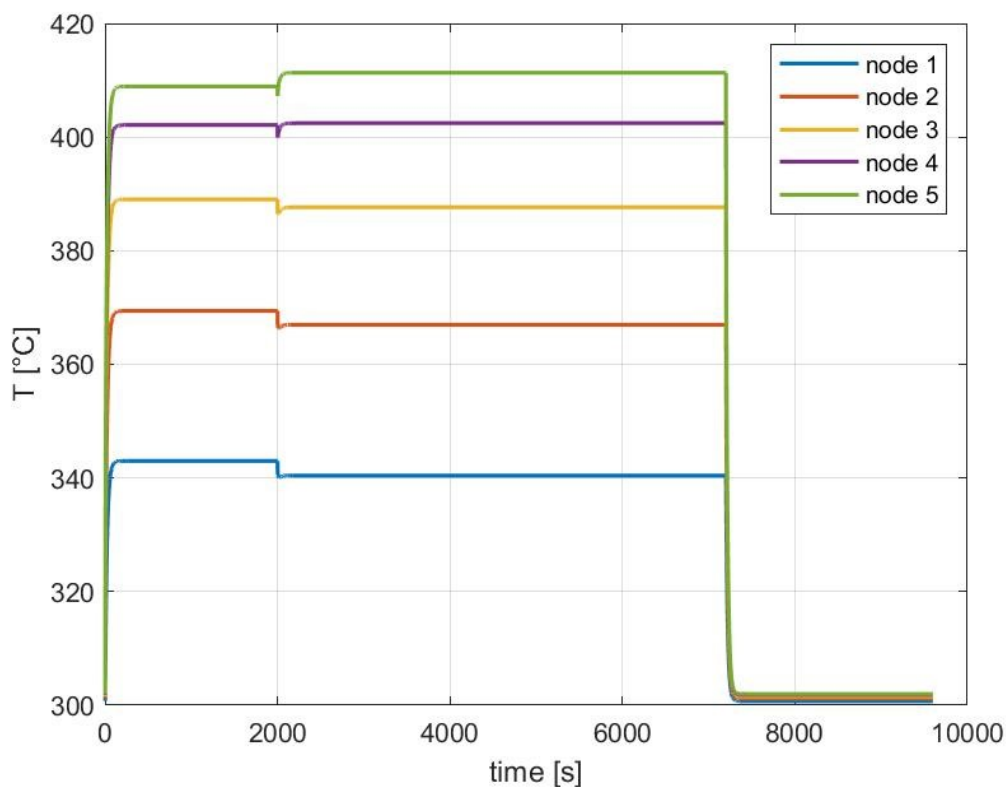


Figure 4.27: Helium temperature evolution in a non-obstructed FW channel; each curve represents a different fluid node of the front part; case of a channel obstruction without plasma shutdown.

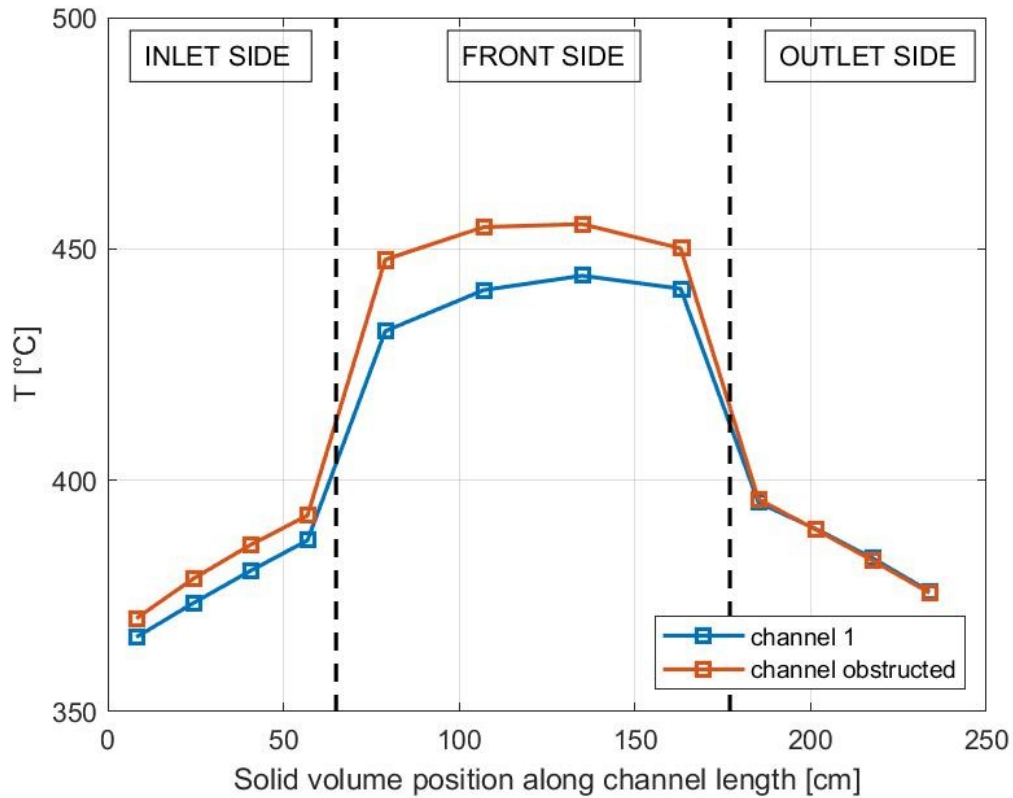


Figure 4.28: EUROFER temperature distribution along channel 1 (blue line) and the obstructed channel (red line); squares represent the value computed in each solid volume; case of a channel obstruction without plasma shutdown.

#### 4.2.4.2. Case II: intervention of the mitigation system

Case I described in the previous section showed that, in the case of a single FW channel obstruction, the resulting heat deposition in the solid walls is effectively removed by the helium still flowing inside the neighboring channels, with only a mild temperature increase widely within safety limits. However, it could still be required to activate the emergency plasma shutdown to investigate the causes of the obstruction and avoid any risks for the integrity of the FW channels close to the obstructed one.

The three usual hypotheses on mitigation system intervention are considered, with the plasma shutdown triggered after 20, 40 and 60 seconds since the accident. As it can be seen in figure 4.29, the maximum temperature reached in the obstructed channel walls is almost the same for the three different hypotheses, going from 454.1 °C to 455.2 °C for the 20 and 60 seconds delayed shutdown cases, respectively (1 °C difference only). That is because the new equilibrium after the accident is reached in a very short time (very fast transient), so that after 20 seconds the maximum temperature has gone up by 13.9 °C compared to the total 15.2 °C temperature increase computed in case I. In figure 4.30 the temperature distribution in the obstructed channel and in channel 1 are compared under the hypothesis of a 60 seconds delayed intervention of the emergency plasma shutdown. As expected, with respect to case I (see figure 4.28) differences are nearly imperceptible, for the reason already discussed above.

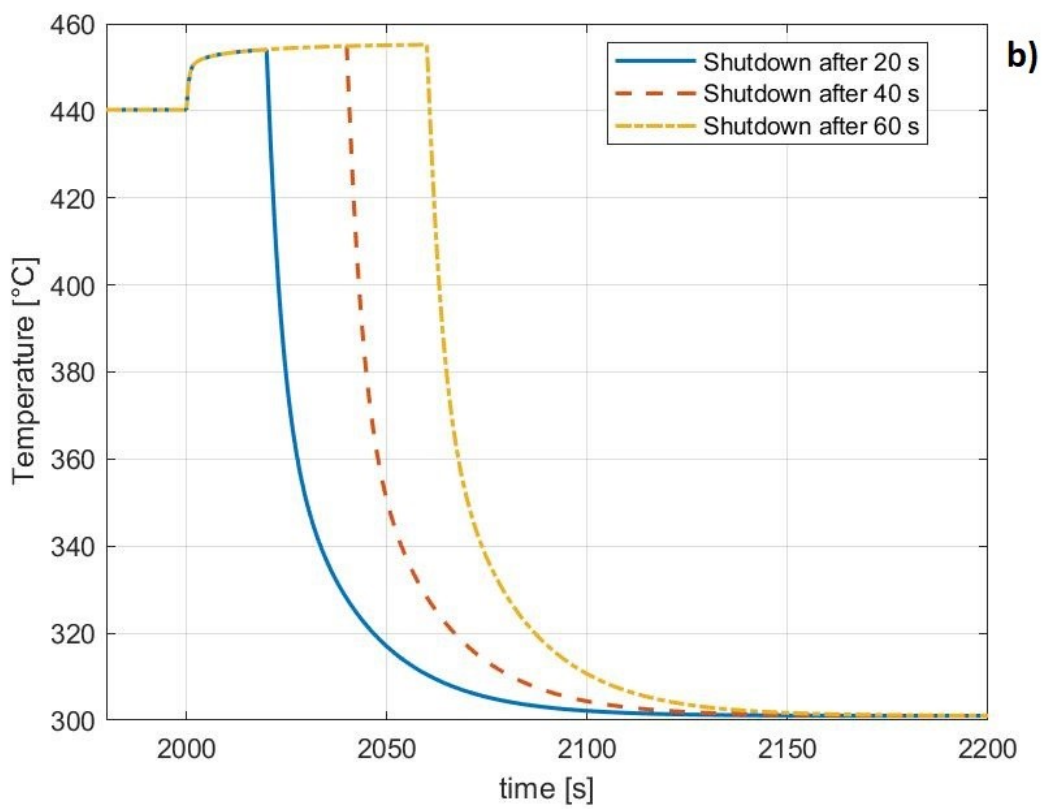
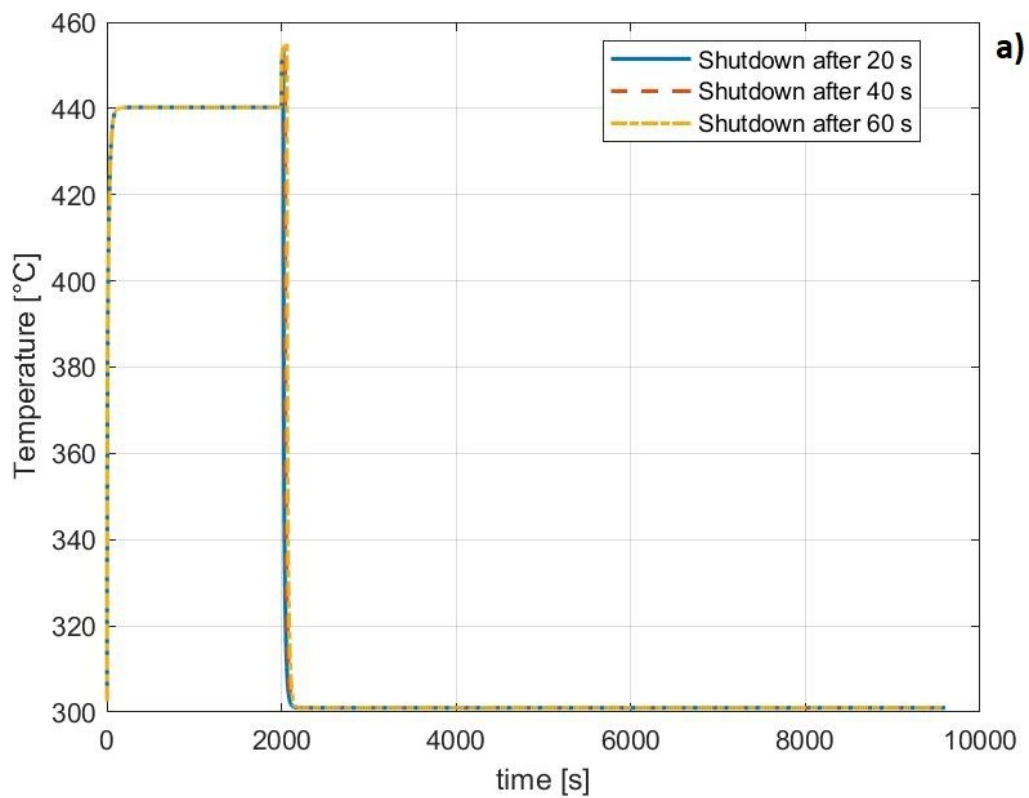


Figure 4.29: EUROFER97 temperature time evolution in the 3rd node of the obstructed channel front part: three hypotheses on the mitigation system intervention; case of a channel obstruction with plasma shutdown; a) view of the whole period, b) post-accident detail (1980 s – 2200 s).

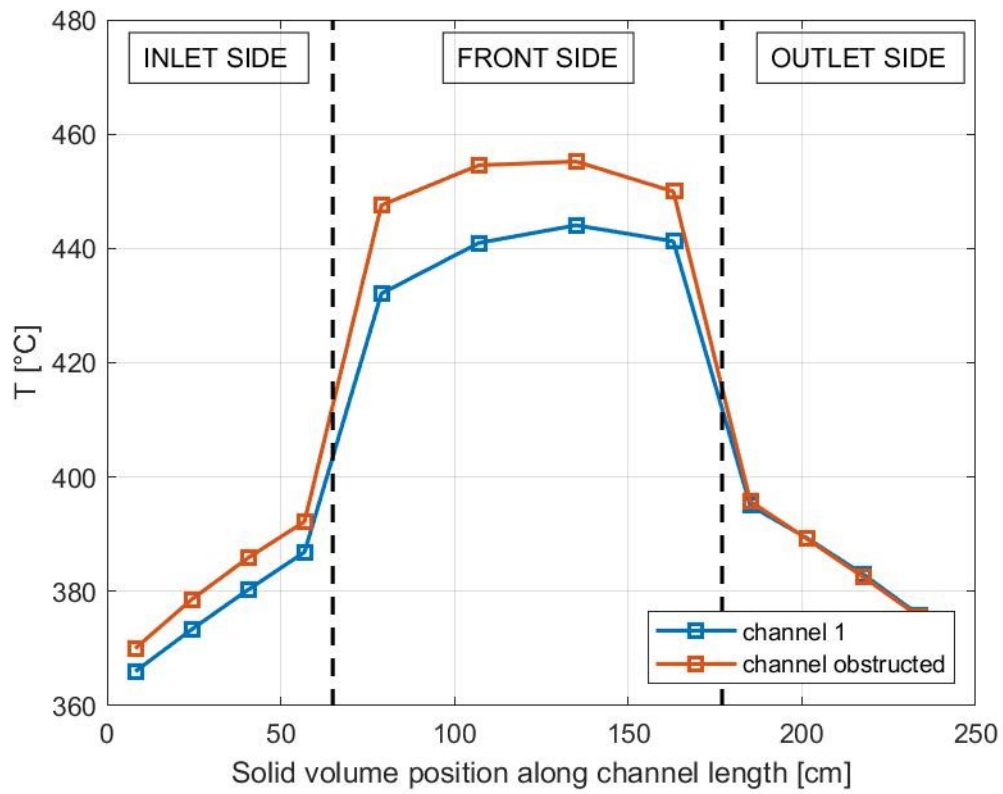


Figure 4.30: EUROFER temperature distribution along channel 1 (blue line) and the obstructed channel (red line); squares represent the value computed in each solid volume; case of a channel obstruction with plasma shutdown after 60 s.

# Chapter 5

## 5. Conclusions

This thesis work presented a preliminary system-level analysis of the global thermal-hydraulic behavior of the EU DEMO tokamak PHTS, under the accidental scenario of a LO-FA. In particular, the latest design of the HCPB concept of the BB was considered, focusing on the temperatures reached inside the solid walls of the FW channels during the accidental transient, and evaluating different hypotheses on the emergency plasma shutdown intervention.

To perform this analysis, a model based on the GETTHEM code (developed at Politecnico di Torino) for the HCPB PHTS has been used. The idea was to develop a simple and intuitive model, which allows fast-running simulations to get global results on the dynamic behavior of the HCPB BB, useful to provide feedbacks on the most critical regions where further detailed analyses are needed. To this aim, Modelica has been chosen as the modeling language, because of its objected-oriented nature, useful to easily build complex systems in a modular architecture, its dynamic nature, and its user-friendly interface. The model consists of a closed loop where an ex-vessel cooling train, made of one/two circulators and a heat exchanger, feeds two parallel branches of the BB object. Each branch is made of a FW object, which models 4 FW channels, each of them divided in two side parts and one plasma-facing part, connected in series with two instances of the fuel pin object, one for the cylindrical inner pin and the other for the annular outer pin. These two branches are thermally coupled at the FW object level according to a counter-current flow scheme. The objects describing the components of the system are modeled with a 0D/1D approach: all the components where the coolant flow is not fully developed are modeled as 0D object, while for long components, such as channels and the HX, the mass, momentum and energy conservation equations are discretized with the 1D FVs method.

The accidental situation of a loss of the coolant flow has been simulated, resulting in different extents of the severity of the accident depending on the initiating event involved, and on the hypotheses made on the mitigation system. For the latter, two cases have been taken into account: case I, the most severe condition when the accident is not automatically detected and mitigated, meaning that the plasma power still heats up the BB after the accident; case II, the accident is properly detected, and the plasma shutdown system is triggered to attenuate the negative effects of the loss of coolant flow in the cooling loop. Moreover, case II has been simulated under the assumptions that the emergency plasma shutdown intervenes 20, 40 and 60 seconds after the accident, in order to assess the effectiveness of the mitigation intervention in the case of delayed detections of the accident.

The first scenario simulated regarded a total LOFA due to the simultaneous trip of both circulators of the cooling loop, which, in turn, might have been caused by a loss of off-site power. This was the most severe scenario analyzed, since the whole circulating power has been gradually turned off and the mass flow rate inside each FW channel dropped from 33.8 g/s to about 1 g/s, almost completely compromising the heat removal from the BB solid structures. For the case I, the temperatures rapidly reached values above 1000 °C exceeding the EUROFER97 melting point, reason why the simulation stopped 236 seconds after the accident (when a maximum temperature of 1238 °C was computed), long before the scheduled end-time. The reaching of the material's melting point, in such a situation, was expected; the interesting result, instead, is that the melting point temperature, assumed around 1000 °C, is reached after two and a half minutes, which is enough time for the operators on duty in the control room to manually trigger the emergency plasma shutdown. Concerning case II, instead, results showed that, even with a 60 seconds-delayed intervention of the emergency plasma shutdown, the FW solid wall temperatures are within safety limits. As a matter of fact, a maximum temperature of 538 °C has been computed in the solid, below the upper limit of 550 °C set for EUROFER97 operation.

The second scenario consisted in the failure of one of the two circulators of the cooling loop, resulting in a 50 % reduction of the mass flow rate in each FW channel, approximately. In case I, when the emergency shutdown system fails, the system reached a new thermal equilibrium at higher temperatures; in particular, in the plasma-facing walls of the FW channels, temperatures between 550 °C and 600 °C have been computed. Considering the severity of the accident and the failure of the mitigation system, these results are actually reassuring, being the maximum temperatures only slightly above 550 °C and far below the material melting point temperature. Moreover, this scenario has been simulated with the conservative assumption that the circulator stops instantaneously when the accident occurs, hence the mass flow rate reduction is not gradual as it was for the first scenario. This assumption affected the results in the case of the emergency plasma shutdown intervention, because of the unlikely fast temperature increase involved. As a matter of fact, in the case of a 60 seconds-delayed intervention, the EUROFER97 FW channel walls reached a maximum temperature of 588 °C, which is very close to the value of 593 °C computed in the unmitigated case; however, the 40 seconds delay hypothesis has proven to be successful to stay within the material safety limits, with a maximum temperature of 542 °C in the front channel part.

Finally, the accidental obstruction of a single FW channel has been simulated. Differently from previous scenarios, in this situation the loss of coolant flow (and, as a consequence, the additional heat deposition) is not uniformly distributed among the channels but it is localized to the obstructed channel. Results showed that the overheating in the obstructed channel solid walls is well mitigated by the helium flowing inside the other channels, thanks to the good heat conductivity of EUROFER97; the latter is also the reason why the effects of the accident are uniform on the unobstructed channels, whether they are close or far from the obstructed one. In case I, a 15 °C temperature increase has been computed after the accident in the damaged channel solid walls, while the neighboring channels suffered only a mild 6 °C overheating. Moreover, the emergency plasma shutdown had no relevant effects on the maximum temperatures reached compared to the unmitigated scenario, but it still can be useful to

avoid any thermal stress issues due to the temperature difference between the obstructed channels and its neighboring channels.

# References

- [1] A. J. H. Donné, W. Morris, X. Litaudon, C. Hidalgo, D. McDonald, H. Zohm, E. Diegele, A.Möslang, K. Nordlund, G. Federici et al., “European research roadmap to the realisation of fusion energy”, EUROfusion Consortium, ISBN 978-3-00-061152-0, 2018.
- [2] G. Federici, C. Bachmann, L. Barucca, W. Biel, L. Boccaccini, R. Brown, C. Bustreo, S. Ciattaglia, F. Cismondi et al., “DEMO design activity in Europe: Progress and updates”, Fusion Engineering and Design, Volume 136, Part A, November 2018, Pages 729-741.
- [3] F. Romanelli, et al., Fusion Electricity—A Roadmap to the Realisation of Fusion Energy, European Fusion Development Agreement (EFDA), (2012) ISBN 978–3–00–040720–8T.
- [4] C. Bachmann, S. Ciattaglia, F. Cismondi, T. Eade, G. Federici, U. Fischer, T. Franke et al., “Overview over DEMO design integration challenges and their impact on component design concepts”, Fusion Engineering and Design, 2018, Volume 136, Pages 87-95.
- [5] L. Barucca, S. Ciattaglia, M. Chantant, A. Del Nevo, W. Hering, E. Martelli, I. Moscato,” Status of EU DEMO heat transport and power conversion systems”, Fusion Engineering and Design 136 (2018) 1557–1566.
- [6] ITER project website, Superconducting Magnets. Available: <https://www.iter.org/mach/Magnets>.
- [7] ITER project website, Cryostat. Available: <https://www.iter.org/mach/Cryostat>.
- [8] R.R. Parker, “Design of in-vessel components for ITER”, Volume 36, Issue 1, April 1997, Pages 33-48.
- [9] Sharma R.G. (2021) Superconducting Magnets in Fusion Reactors. In: Superconductivity. Springer Series in Materials Science, vol 214. Springer, Cham. [https://doi.org/10.1007/978-3-030-75672-7\\_11](https://doi.org/10.1007/978-3-030-75672-7_11)
- [10] Ugo Bonavolontà, Christian Bachmann, Domenico Coccoresse, Giuseppe Di Gironimo, Vito Imbriani et al., EU-DEMO divertor: Cassette design and PFCs integration at pre-conceptual stage, Fusion Engineering and Design, Volume 159, October 2020, 111784.
- [11] L. V. Boccaccini (2013) Progress in EU Blanket Technology, Fusion Science and Technology, 64:3, 615-622, DOI: 10.13182/FST13-A19160.
- [12] Yican Wu, Sümer Şahin, Comprehensive Energy Systems, chapter 3.13 Fusion Energy Production, Volume 3, 2018, Pages 538-589.
- [13] Francisco A. Hernández, Pavel Pereslavl'tsev, Guangming Zhou, Qinlan Kang, Salvatore D'Amico et al., Consolidated design of the HCPB Breeding Blanket for the pre-Conceptual Design Phase of the EU DEMO and harmonization with the ITER HCPB TBM program, Fusion Engineering and Design 157 (2020) 111614.
- [14] Francisco A. Hernández, Pavel Pereslavl'tsev, Guangming Zhou, Heiko Neuberger, Jorg Rey, Qinlan Kang, Lorenzo V. Boccaccini et al., An enhanced, near-term HCPB design as driver blanket for the EU DEMO, Fusion Engineering and Design 146 (2019) 1186–1191.
- [15] Lorenzo Virgilio Boccaccini, HCPB Design and Integration Studies 2019, Final Report 2020, EUROfusion BB-1.2.1-T006-D001.
- [16] Luciana Barucca, HCPB PHTSs DDD for WPBOP DR (Indirect Coupling) – 2020, EUROfusion, BOP-2.1-T056.

- [17] I. Moscato, “HCPB BOP - Studies in support of pre-conceptual design of the BB PHTS,” <https://idm.euro-fusion.org/?uid=2NG4VW>, 2020
- [18] P. Fritzson, Principles of object-oriented modeling and simulation with Modelica 2.2, Wiley, 2003.
- [19] Modelica Association, “Modelica® - A Unified Object-Oriented Language for Systems Modeling - Language Specification Version 3.5,” February 18, 2021. [Online]. Available: <https://modelica.org/documents/MLS.pdf>.
- [20] Modelica Association, “Modelica Language”. [Online]. Available: <https://modelica.org/modelicalanguage.html>.
- [21] Modelica Association, “Modelica Tools”. [Online]. Available: <https://modelica.org/tools.html>.
- [22] Froio, Antonio. Multi-scale thermal-hydraulic modelling for the Primary Heat Transfer System of a tokamak. Diss. PhD Thesis, 2018.
- [23] Froio, A., et al. "Dynamic thermal-hydraulic modelling of the EU DEMO HCPB breeding blanket cooling loops." Progress in Nuclear Energy 93 (2016): 116-132.
- [24] Froio, A., et al. "Dynamic thermal-hydraulic modelling of the EU DEMO WCLL breeding blanket cooling loops." Fusion Engineering and Design, Volume 124 (2017): 887-891. [Online]. Available: <https://doi.org/10.1016/j.fusengdes.2017.01.062>.
- [25] A. Bertinetti, et al. "Hydraulic modeling of a segment of the EU DEMO HCPB breeding blanket back supporting structure." Fusion Engineering and Design 136 (2018): 1186-1190.
- [26] A. Froio, et al. "Benchmark of the GETTHEM Vacuum Vessel Pressure Suppression System (VVPSS) model for a helium-cooled EU DEMO blanket." Proc. ESREL. 2017.
- [27] A. Froio, F. Cismondi, L. Savoldi and R. Zanino, "Thermal-Hydraulic Analysis of the EU DEMO Helium-Cooled Pebble Bed Breeding Blanket Using the GETTHEM Code," in IEEE Transactions on Plasma Science, vol. 46, no. 5, pp. 1436-1445, May 2018, doi: 10.1109/TPS.2018.2791678.
- [28] F. A. Hernández González, P. Pereslavtev, Q. Kang, P. Norajitra, B. Kiss, G. Nádas, and O. Bitz, “A new HCPB breeding blanket for the EU DEMO: Evolution, rationale and preliminary performances,” Fus. Eng. Des., to be published. DOI: 10.1016/j.fusengdes.2017.02.008.
- [29] Froio, Antonio; Cismondi, Fabio; Savoldi, Laura; Zanino, Roberto. Thermal-Hydraulic Analysis of the EU DEMO Helium-Cooled Pebble Bed Breeding Blanket Using the GETTHEM Code. - In: IEEE TRANSACTIONS ON PLASMA SCIENCE. - ISSN 0093-3813. - STAMPA. - 46:5(2018), pp. 1436-1445.
- [30] F. Casella and A. Leva, “Modelica open library for power plant simulation: design and experimental validation,” Proceedings of 3rd International Modelica Conference, pp. 41-50, Linköping, Sweden, 3-4 November 2003.
- [31] L. V. Boccaccini, L. Giancarli, G. Janeschitz, S. Hermsmeyer, Y. Poitevin, A. Cardella and E. Diegele, “Materials and design of the European DEMO blankets,” Journal of Nuclear Materials, Vols. 329-333, part A, pp. 148-155, 2004.
- [32] E. Rajendra Kumar and TBM Team, “Test Blanket Module: Steels & Fabrication Technologies”, Institute for Plasma Research, Bhat, GandhinagarWS&FT-08, 21st July 2008, IPR. Available: <https://slideplayer.com/slide/3900311/>

- [33] K. Mergia, N. Boukos, "Structural, thermal, electrical and magnetic properties of Eurofer 97 steel", *Journal of Nuclear Materials*, Volume 373, Issues 1–3, 2008, Pages 1-8, ISSN 0022-3115, <https://doi.org/10.1016/j.jnucmat.2007.03.267>.
- [34] F. Gillemot, E. Gaganidze, and S. Ildikó, "Material property handbook on EUROFER97 (2015-MTA)," MAT-1.2.1.02, D-2MRP77, 2016.
- [35] Arbeiter, F., Bachmann, C., Chen, Y., Ilic, M., Schlindwein, G., Schwab, F., Sieglin, B., Wenninger, R., 2016. Thermal-hydraulics of helium cooled First Wall channels and scoping investigations on performance improvement by application of ribs and mixing devices. *Fusion Eng. Des.* <http://dx.doi.org/10.1016/j.fusengdes.2016.01.008>.
- [36] Ruck, S., Arbeiter, F., 2016. Thermohydraulics of rib-roughened helium gas running cooling channels for first wall applications. *Fusion Eng. Des.* <http://dx.doi.org/10.1016/j.fusengdes.2016.01.029>.
- [37] Incropera, F., Dewitt, D., 2006. *Fundamentals of Heat and Mass Transfer*, sixth ed. John Wiley & Sons.